Dynamics of a Multi-Tethered Satellite System Near the Sun-Earth Lagrangian Point

Brian Wong

Department of Mechanical Engineering

McGill University, Montreal

August 2003

A thesis submitted to the Faculty of Graduate Studies and Research in partial fulfillment of the requirements of the degree of Master of Engineering

© Brian Wong, 2003

Library and Archives Canada

Published Heritage Branch

395 Wellington Street
Ottawa ON K1A 0N4
Canada

Bibliothèque et Archives Canada

Direction du Patrimoine de l'édition

395, rue Wellington
Ottawa ON K1A 0N4
Canada

Your file Votre référence
ISBN: 0-612-98574-1
Our file Notre référence
ISBN: 0-612-98574-1

NOTICE:
The author has granted a non-exclusive license allowing Library and Archives Canada to reproduce, publish, archive, preserve, conserve, communicate to the public by telecommunication or on the Internet, loan, distribute and sell theses worldwide, for commercial or non-commercial purposes, in microform, paper, electronic and/or any other formats.

The author retains copyright ownership and moral rights in this thesis. Neither the thesis nor substantial extracts from it may be printed or otherwise reproduced without the author's permission.

AVIS:
L'auteur a accordé une licence non exclusive permettant à la Bibliothèque et Archives Canada de reproduire, publier, archiver, sauvegarder, conserver, transmettre au public par télécommunication ou par l'Internet, prêter, distribuer et vendre des thèses partout dans le monde, à des fins commerciales ou autres, sur support microforme, papier, électronique et/ou autres formats.

L'auteur conserve la propriété du droit d'auteur et des droits moraux qui protège cette thèse. Ni la thèse ni des extraits substantiels de celle-ci ne doivent être imprimés ou autrement reproduits sans son autorisation.

In compliance with the Canadian Privacy Act some supporting forms may have been removed from this thesis.

While these forms may be included in the document page count, their removal does not represent any loss of content from the thesis.

Conformément à la loi canadienne sur la protection de la vie privée, quelques formulaires secondaires ont été enlevés de cette thèse.

Bien que ces formulaires aient inclus dans la pagination, il n'y aura aucun contenu manquant.

Canada

Acknowledgements

I wish to thank my supervisor Professor Arun Misra for this guidance and patience during the past two years. His knowledge with tethered systems in particular and astrodynamics in general are of great help in my moments of confusion.

I would also like to thank my family for allowing me to attend graduate school and for their support.

Abstract

This paper examines the dynamics of a tether connected multi-spacecraft system, arranged in a wheel-spoke configuration, in the vicinity of the L_2 Lagrangian point of the Sun-Earth system. First, the equations of motion of a N-body system are obtained and equilibrium configurations of the system are determined and small motions about one of these configurations are analyzed. Then, a numerical analysis of the free tether libration is carried out for a three-mass case when the system is near L_2 and the parent mass is assumed to be in a halo orbit of different sizes. Finally, a set of control goals are defined and a time domain state feedback control system is integrated into the numerical model. The performance of the control system is tested under different conditions.

Résumé

Ce mémoire examine la dynamique d'un système spatial composé de plusieurs satellites câblés en formation de roue-et-rayons aux alentours du point de Lagrange L_2 du couple Soleil-Terre. D'abord, les équations de mouvement et les états d'équilibre d'un système multi-corps sont dérivés, suivis d'une étude des petits mouvements au voisinage de ces points d'équilibre. Ensuite, une analyse numérique de la libration libre du câble est effectuée pour le cas d'un système à trois masses orbitant près du point L_2 où le corps central est contraint à des orbites de halo de différentes tailles. Finalement, des objectifs de contrôle sont définis et un système de contrôle par rétroaction sur le domaine temps est introduit dans le modèle numérique. Ce système de contrôle est soumis à des conditions variées et sa performance est évaluée.

Table of Contents

Table of Symbols

G	Universal Gravity Constant
D	Distance between M_1 and M_2
D_1	Distance from O to M_1
D_2	Distance from O to M_2
ε	$M_2/(M_1+M_2)$
X,Y,Z	Right hand axis centred at O
x,y,z	Right hand axis centred at L_2
N	Rate of rotation of the M_1-M_2 system
$\mathbf{R}_p$	Position vector of the parent mass relative to O
$\mathbf{R}_1$	Position vector of the parent mass relative to M_1
$\mathbf{R}_2$	Position vector of the parent mass relative to M_2
$\mathbf{r}_i$	Position vector of the i^{th} end mass relative to the parent mass
L_2	Second Lagrangian Point
X_L, Y_L	Coordinate of L_2 relative to O
x_p, y_p, z_p	Generalized coordinates of the parent mass relative to L_2
x_i, y_i, z_i	Generalized coordinates of the i^{th} end mass relative to the parent mass
θ_i	In-plane libration angle of the i^{th} and mass. Also a generalized coordinate
φ_i	Out-of-plane libration angle of the i^{th} end mass. Also a generalized coordinate
l_i	Length of the i^{th} tether
$\mathbf{V}_p$	Velocity of the parent mass
$\mathbf{V}_i$	Velocity of the i^{th} end mass

T	Kinetic energy of the tethered system
V	Potential energy of the tethered system
δ_1	$\frac{X_L+D_1}{D}$
δ_2	$\frac{X_L-D_2}{D}$
I	$D^2\left(\frac{1-\varepsilon}{\delta_1}+\frac{\varepsilon}{\delta_2}\right)$
A	$D\left(\frac{1-\varepsilon}{\delta_1^2}+\frac{\varepsilon}{\delta_2^2}\right)$
B	$\frac{1-\varepsilon}{\delta_1^3}+\frac{\varepsilon}{\delta_2^3}$
C	$\frac{1}{D}\left(\frac{1-\varepsilon}{\delta_1^4}+\frac{\varepsilon}{\delta_2^4}\right)$
f_{xp}	Control force acting on the parent mass in the **i** direction
f_{yp}	Control force acting on the parent mass in the **j** direction
f_{zp}	Control force acting on the parent mass in the **k** direction
$f_{\theta i}$	Control force acting on the i^{th} end mass perpendicular to the tether
$f_{\varphi i}$	Control force acting on the i^{th} end mass perpendicular to the tether
Q_{xp}	Generalized force for the x_p generalized coordinate
Q_{yp}	Generalized force for the y_p generalized coordinate
Q_{zp}	Generalized force for the z_p generalized coordinate
$Q_{\theta k}$	Generalized force for the θ_k generalized coordinate
$Q_{\varphi k}$	Generalized force for the φ_k generalized coordinate
θ_{ieq}	In-plane equilibrium angle of the i^{th} tether
φ_{ieq}	Out-of-plane equilibrium angle of the i^{th} tether
x_{eq}, y_{eq}, z_{eq}	Equilibrium position of the parent mass relative to L_2

η	Observation axis of the rotating tethered system
γ	Azimuth of the observation axis relative to the *X* axis
α	Elevation of the observation axis relative to the ecliptic plane

Table of Figures

Chapter 1

INTRODUCTION

1.1 Preliminary Remarks

For some applications, using a group of small satellites working together is more efficient than putting all the instruments onto one large spacecraft. An example of this is high-resolution interferometry, where formation flight allows one to establish a longer baseline and get a sharper image. However, long-term perturbations can nudge members of the formation out of position and propulsion would be required to correct the situation. Compared to free-flying formations, tether-connected satellites can remain in formation without using much fuel. In addition, the use of tethers may allow for formations that are not possible for free-flying spacecraft due to the constraints of orbital mechanics.

Space tethers have many other potential uses besides formation keeping. Atmospheric research, artificial gravity generation, orbit modification and power generation are some of the areas where tethers can find applications[1]. A large number of these applications make use of two-body systems in low Earth orbits, with some applications using three-body systems. Multi-body systems at other locations (Lagrangian points, Earth trailing orbits, planetary probes, etc) are relatively recent ideas and so far only exist on academic papers.

Besides remote sensing, scientific applications of tethered satellites include exploration of the Earth's upper atmosphere by lowering a tethered probe into the atmosphere from a space shuttle or a parent satellite. At the end of the experiment the probe could either be recovered for later use or cut loose to avoid the difficulties of tether retrieval.

Artificial gravity generation is another potential application for tether-connected bodies. Science fiction writers in the 1960s envisioned giant space stations with a rotating habitat ring; an artificial gravity field can be generated due to the centrifugal acceleration. On a much smaller scale the same effect can be achieved with two tethered bodies spinning about their combined centre of mass. The magnitude of the acceleration experienced depends on the rate of rotation of the system and the distance from the centre of mass and this acceleration is directed away from the centre of mass. This system does not have to generate 1 g to be useful. For long duration missions, even 1/3 g is sufficient to maintain the inhabitants' physical conditioning and avoid the health problems upon their arrival at a stronger gravitational field.

Power generation and orbit change applications are related. When a conducting wire is moved through the Earth's magnetic field, a current is generated. This current can be used to power a spacecraft's electronics and supplement or replace it solar panels. However, an electrodynamic force is induced that acts on the tether and its orbit rapidly decays. A returning spacecraft can make use of this force to deorbit. This electrodynamic drag principle can also be made to work in reverse by feeding a current into the wire and generate a thrust that would propel the spacecraft into a higher orbit. Using this method for gross orbit changes allows for smaller amount of fuel to be carried aboard to be used for finer manoeuvres, thereby extending the service life of the spacecraft. Other orbit modification schemes have been proposed. They include tethered slingshots and momentum exchange devices.

Tethered systems have been considered in more exotic locations such as the Lagrangian points. A spinning tethered space station, generating an artificial gravity field for its inhabitants, has been considered at L_1 of the Earth-Moon system. This station would serve as a transit point for future missions to the moon. The SPECS[2] mission proposes to put a multi-tethered satellite formation at L_2 of the Sun-Earth system. This mission, along an introduction to science behind this mission, will be discussed with more detail in the following sections as discovering the dynamics of this multi-tethered system is the main thrust of this thesis.

1.2 Infrared Astronomy

The wavelengths belonging to the infrared region of the electromagnetic spectrum stretches from about 1 micron (near infrared) to 200 microns (far infrared). This region sits between visible light and radio waves. A lot of information can be obtained in this wavelength, and several properties of the physical universe made infrared observations an important aspect of observational astronomy.

The temperature range of solid bodies in space is from 3 to 1500 Kelvin and most of the energy radiated by objects in this temperature range is in the infrared. Therefore infrared astronomy is sometimes the only way to study interstellar nebulas, protostars, brown dwarfs and everything else not hot enough to emit visible light.

Just finding an interstellar object and knowing its shape and temperature is only the first step. Knowing the chemical composition of that object is also important. Fortunately, the emission and absorption band of almost all molecules and solids are in the infrared. This allows different elements and molecules to be identified via spectrograph. With both the physical condition and the composition in hand, astronomers can model the physical processes behind the life of stars and planets. And given the current interest in planet finding, the presence of water and oxygen can be discovered via spectrography.

Looking up at the night sky, one can see patches of darkness where nothing can be seen. However, space is not as empty as it looks and interstellar dust and gas can block visible light and obscure the viewing of many important astronomical objects. It is like throwing a blanket in front of a camera. Some of the most interesting regions and events in the universe are hidden from optical view and infrared astronomy allows astronomers to visualize that the happenings in these previously unseen places as IR radiations can move through dust and gas clouds.

Infrared observations also allow one to look back in time. The general expansion of the universe shifts energy to longer wavelengths in an amount proportional to the distance between an object and its observer. Since the universe has been expanding since the Big Bang, objects formed near the beginning of time are now very far away and the energy they gave off is redshifted into the infrared region. Much of the shape and structure of the early universe would have to be learned from infrared observations.

Earth's atmosphere absorbs almost all cosmic IR radiation with the exception of a few narrow windows. The best place to do IR astronomy on the Earth is at high elevations, such as on Mouna Kea in Hawaii. Atop that extinct volcano is Britain's 3.8 meter infrared facility. The thin air at this location minimizes atmospheric distortion and absorption. But mountains on Earth only go so high. To get a truly unobstructed view one must place the telescope in space.

1.3 Interferometry

In astronomical term, resolution refers to angular resolution as measured in arc seconds. High angular resolution is the ability for an instrument to form distinct and separate objects lying close together in its field of view. An example would be seeing a binary star system a few light years away as two separate objects instead of one blob. Angular resolution is proportional to the wavelength of the radiation divided by the diameter of the telescope mirror or baseline. For a given wavelength, a longer baseline gives higher angular resolution. While building a large telescope is one way to go, various design issues limit the size of any telescope both on earth and in space. Since angular resolution depends on the length of the baseline and not on actual area of the mirror, several smaller ones placed far apart can substitute for one large mirror. This type of instrument is called an Interferometer. The effective baseline is the distance between its outermost detectors. Interferometry works by analyzing how waves interfere when they are added together. Two or more detectors are used in tandem to observe the same object at the same wavelength and at the same time. If the detected signals are in step, they combine constructively and if not they cancel each other. As the detectors track the object, a series of peaks and troughs emerges and a computer would then translate this into a high-resolution image.

1.4 Space-Based Infrared Telescopes and Interferometers

The Earth's atmosphere is opaque to most of the electromagnetic spectrum, including most of the infrared spectrum. Air molecules also tend to absorb and refract photons. Therefore, the best place to put an observatory is at high elevations, bypassing the most dynamic part of the atmosphere. The Kech Telescopes at Mauna Kea, Hawaii, is a good example. They are situated at an extinct volcano 4 km above the sea level. Ground base telescopes have several advantages such as being easier to build and upgrade. Their main mirror can be larger as well, although this is partly offset by the dimming effect of the atmosphere. As high as some of the mountains are, they are still surrounded by air. Space-based telescopes offer an unhindered view of the stars. The full electromagnetic spectrum can be observed in space, rather than the limited window available here on earth. Far-infrared astronomy, the kind needed in order to understand galaxy and star formation, can only be done in orbit. Similarly direct evidence of the existence of black holes can only be found by observation from space, as the X-rays given off by matter being ingested by a black hole cannot penetrate the atmosphere. The biggest drawback of space telescopes is the prohibiting cost of building and operating one. Building a sensitive astronomical instrument with very exact specifications is going to be expensive no matter where it is placed. Add to that the launch cost, and the threat that any single failure in any stage of the construction, launch and operating process can potentially cause the loss of the instrument and the billions invested. It is easy to understand why despite all the advantages of a space based observatory, there are only a handful currently in orbit with a few more on the drawing board.

There are several upcoming space infrared and interferometric missions. The Space Infrared Telescope Facility (SIRTF) is scheduled for launch in August 2003, to be followed by the James Webb Space Telescope roughly ten years later. Those two observatories would focus on near and mid-infrared light. The SPECS program aims to put a space-based interferometer around the second Lagrangian point of the Sun-Earth system and this telescope will focus on the far-infrared observations.

1.5 Introduction to SPECS

One proposed use of a tether-connected satellite formation is the SPECS (Submillimeter Probe of the Evolution of Cosmic Structure) project being developed by NASA's Goddard Space Flight Center. The goal of SPECS is to build a space telescope that will enable astronomers to see into the far-infrared and submillimeter wavelengths, leading to answers to fundamental questions pertaining to the formation of the first stars and the origins of galaxies. The SPECS system is set for launch in the middle of the next decade. To achieve the kind of angular resolution and photon gathering ability desired, a large telescope must be built and placed in a very cold region of space. With a proposed baseline of up to 1 km, this telescope cannot be build the conventional way even with futuristic technologies such as large inflatable structures and thin membrane-like mirrors. A tethered formation, consisting of as few as three 3-4 meter diameter mirrors operating together as an interferometer, can take the place of a massive primary mirror. These mirrors must be kept very cold in order to not swamp the faint astronomical signals with radiations emitted from other sources. Active cooling can be minimized by placing the interferometer in a cold, stable temperature environment, such as L_2 of the Sun-Earth system. The L_2 location also allows the instruments to "stare" at a target much longer than if the interferometer is placed in the Earth orbit, due to the much lower rate of rotation of the Sun-Earth system compared to objects in the Earth orbit.

1.6 Literature review of Lagrangian Point Dynamics and Halo Orbits and Overview of Past Missions

The classic restricted three-body problem deals with the motion of an object with mass m in the gravitational field of two massive primary bodies with mass $M1$ and $M2$, where m is very small compared to $M1$, $M2$. The circular restricted three-body problem is a special case where the two primary bodies are in circular orbits about their barycenter. Euler first formulated the problem in 1772 and he found three equilibrium solutions. Later on, Lagrange found another two. These five equilibrium points (Figure 1.1), where gravitational and centripetal accelerations are balanced out, are denoted by L_1 through L_5 and are called the Lagrangian or libration points. Three of these points are on a line joining $M1$ to $M2$, and the other two form equilateral triangles with these bodies in the plane of orbital motion. The collinear points, L_1, L_2 and L_3, are unstable while the triangular points, L_4 and L_5, are quasi-stable.

Motion of a single mass near a collinear Lagrangian point is a well-researched problem. After Euler and Lagrange, Moulton[3] and Poincare [4] investigated two and three-dimensional periodic solutions of the three-body problem and produced families of solutions. However, due to the computational complexity of the problem and the lack of numerical tools that are so common today, much of the work afterwards focused on planar solutions and very little work was done on the control of libration point objects.

In 1950, Arthur C. Clarke[5] suggested placing satellites at L_2 and L_4 of the Earth-Moon system to facilitate communication with colonies on the far side of the moon. Pioneering work by Colombo[6] has shown that a simple linear feedback control would work for positional stabilization. Others, such as Breakwell[7] and Farquhar[8], explored how continuous communication can be established with the far side of the moon using only one satellite. Ralph Pringle at Lockheed proposed the initial solution[9], which was unpublished. It involves a spacecraft oscillating about the L_2 point in the Earth-Moon plane. This solution proved unsatisfactory, as the spacecraft would periodically pass behind the moon. Farquhar[10] proposed an out-of-plane solution that would keep a spacecraft orbiting L_2 in view of both Earth and the inhabitants on the far side of the moon. As the in-plane motion of a libration point object has a divergent mode as well as an oscillatory mode, the initial conditions could be chosen such that only the oscillatory modes are excited and the spacecraft could be placed and maintained in a quasi-periodic orbit with very little control effort. This planar solution can be coupled with the out-of-plane motion, which is naturally harmonic. The resulting three-dimensional trajectory is called a Lissajous trajectory and it is actually more fuel efficient to hold the spacecraft in this trajectory than it is to hold it steady at the libration point. The Lissajous trajectory still was not satisfactory as it does not close and the spacecraft goes behind the moon on occasions. The reason for this is that the in-plane and out-of-plane frequencies are different. Breakwell proposed forcing those two numbers to match using a continuous controller, closing the trajectory and making the spacecraft visible from Earth at all times. This is the basic concept of a "halo orbit".

Due to the lack of computational capabilities, many of the early attempts at describing motions in the vicinity of a libration point are done with semi-analytical techniques and the search for large orbits and families of halo orbits were hampered by some complicated mathematics. In recent years, the increased computational capabilities available to researchers have enabled them to compute a range of halo/Lissajous trajectories numerically, and to develop modern techniques that incorporate dynamical system theory (DST) in support of trajectory design in three-body problem. Howell and Pernicka[10] determined Lissajous trajectories numerically, and Cielasky and Wie[11] developed a simple, iterative method for determining halo orbits. From the mid 1970s on, the topic of libration point dynamics and control expanded from a purely academic one to include engineering research in support of future Lagrangian point missions.

Although the initial interest of the space flight community was for a lunar communication station, all the missions flown thus far went around the Sun-Earth L_1 point. Starting with ISEE-3 (International Sun Earth Explorer–3)[12,13] in 1978, several missions have placed spacecraft in periodic orbits around a Lagrangian point. They include SOHO (Solar Heliospheric Observatory)[14], ACE (Advanced Composition Explorer)[15] and Genesis[16,17]. All of the above spacecraft performed or are performing extremely useful scientific functions, but only their orbital mechanics is of interest here.

From November 1978 to June 1982, the ISEE-3 spacecraft (Figure 1.2) completed 4 halo orbits around the L_1 point about 1.5 million kilometres from Earth. The primary science objective of this mission was to continuously monitor the solar wind and other events such as solar flares, and the placement of the satellite gave about an hour of advance warning before those events affect the space environment around the Earth. For operational reasons a halo orbit was chosen and the reference orbit used in this mission is described a paper written by Richardson[18]. The spacecraft employed what can be described as a tight control technique[19], in that it varies two or more components of ΔV to target a three dimensional nominal path. As ISEE-3 is the first libration point mission, fuel consumption was higher than it might have been as the ground controllers were more focused on keeping the complexity and risk to a minimum. Later missions built on the experience gained and were able to orbit L_1 using less fuel.

Fourteen years after ISEE-3, the SOHO spacecraft (Figure 1.3) was inserted into a halo orbit almost identical to the one flown by ISEE-3 on February 14th, 1996. The primary goal of SOHO is to serve as a space weather station and provide advanced warning in case of abnormal solar activities. The control strategy used for SOHO is different from that used for ISEE-3 as it just seeks to remove the unstable component of the motion and no attempt was made to control the path of the spacecraft. This technique is a form of loose control called Orbital Energy Balance[19]. As there was no reference path, SOHO was free to circle L_1 according to the natural dynamics of a libration point object and it resulted in a Lissajous trajectory. Station keeping fuel consumption was lower for SOHO than it was for ISEE-3 and a part of the saving can be attributed to the loose control technique. The average ΔV for the SOHO mission is 0.6 m/s Vs 2 m/s for ISEE-3 with each manoeuvre around 90 days apart. The spacecraft is still operational and the mission is ongoing.

The station keeping technique used in the ACE mission (Figure 1.4) is very similar to that used on the SOHO mission, differing mainly in the details. The ACE spacecraft was placed in a Lissajous trajectory in mid-December, 1997. After all the initial problems were resolved, the average ΔV for this mission was around 0.4 m/s, but each station keeping burn occurred only 58 days apart. This was due to the frequent attitude reorientations required to keep its sensors and instruments pointed in the correct direction. Each reorientation imparted some perturbation to the orbit which must be cancelled out with station keeping burns. The overall ΔV per year was comparable to SOHO, however.

The Genesis mission (Figure 1.5) was launched on August 8, 2001 and is currently in a halo orbit around the L_1 Sun-Earth libration point. The primary purpose of the mission is to capture and return to Earth a sample of the solar wind. While that in itself is very interesting, the trajectory design for this mission is definitely unique. The Genesis trajectory is the first to make use of modern dynamical systems theory. The transfer trajectory to L_1 was constructed using the stable manifold, while the free return trajectory used the unstable manifold. The halo orbit trajectory was calculated using the invariant manifold associated with the orbit. Two to four station keeping manoeuvres are planned during the halo orbit phase. The unique aspect of the Genesis trajectory is that the spacecraft automatically leaves the halo orbit without a departure burn, making use of gravitational channels of the Sun-Earth system much like an airliner makes use of the jet stream of our atmosphere. The spacecraft is scheduled to leave its halo orbit and return to the Earth sometime next year.

Several other missions currently on the drawing board will circle around the L_2 libration point of the Sun-Earth system. This location is ideal for astronomical applications, as the Sun, the Earth and the Moon are all on one side of the spacecrafts and one light shield can eliminate stray radiations from the Sun and Earth. The European Space Agency has two missions planned: FIRST and Planck. Besides SPECS, NASA's James Webb Space Telescope will also be in a halo orbit around the same libration point.

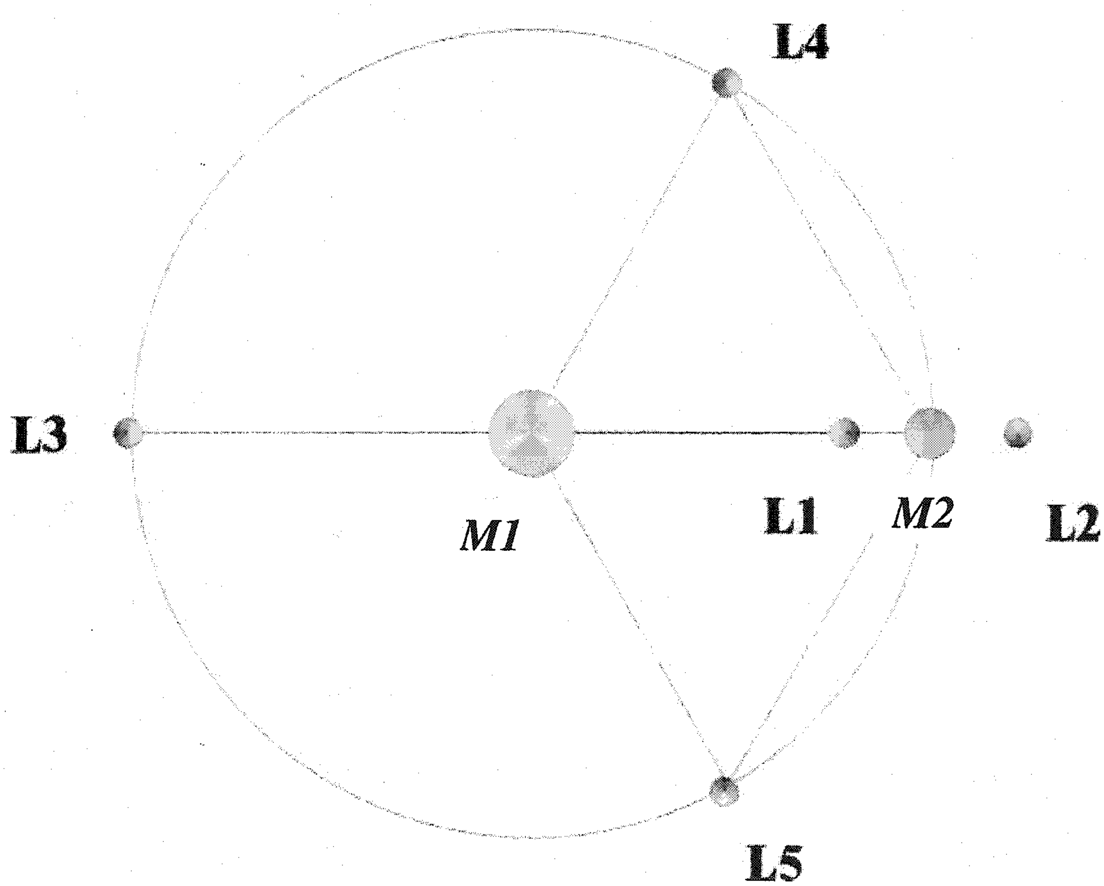

Figure 1.1 Lagrangian Points (www.paias.com/paias/home/Science/Newton/Newt8Fig4L1-L5.htm)

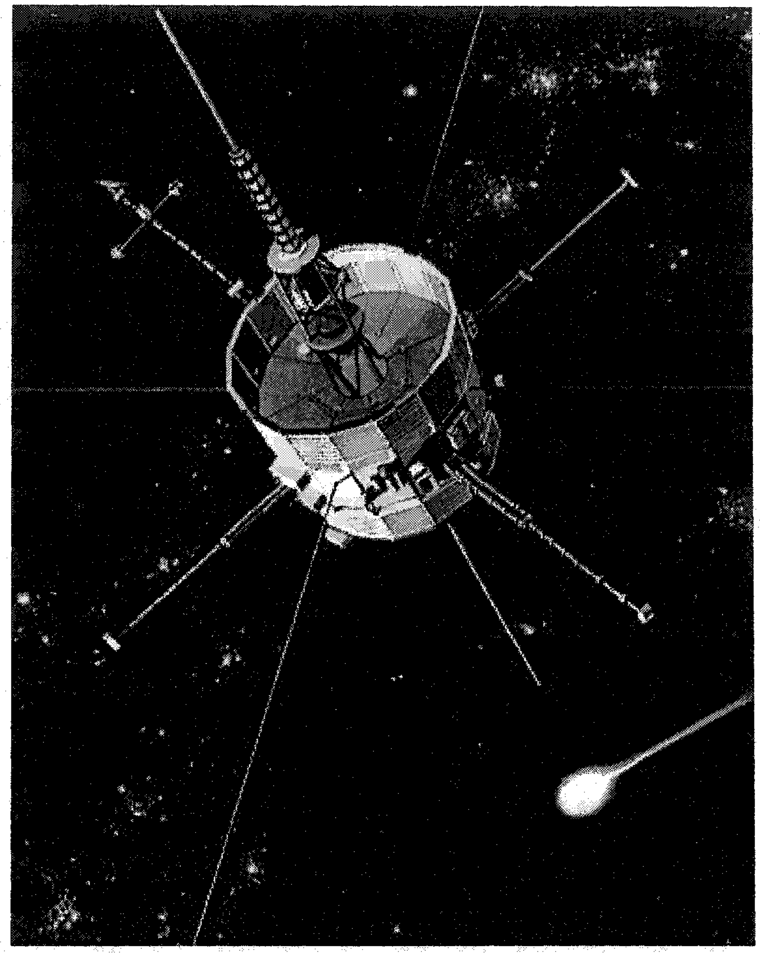

Figure 1.2 ISEE-3 Spacecraft (stardust.jpl.nasa.gov/comets/ice.html)

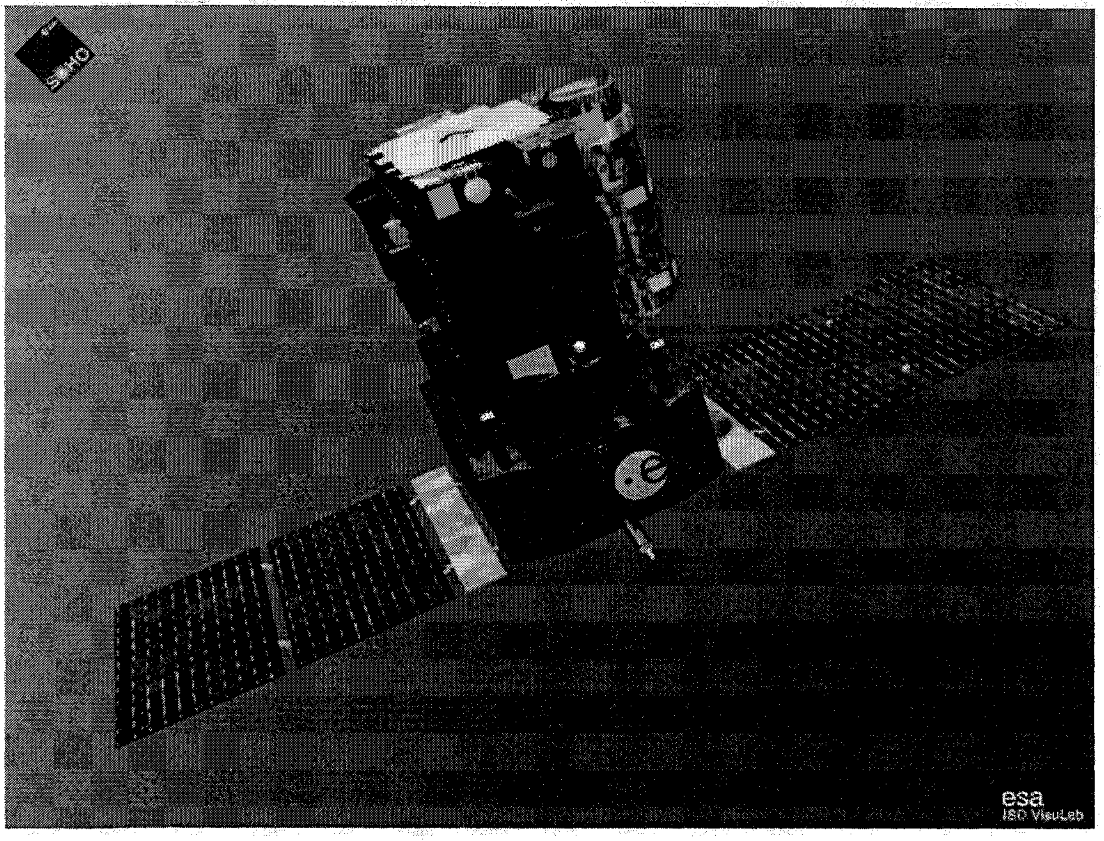

Figure 1.3 SOHO Spacecraft (sohowww.nascom.nasa.gov/)

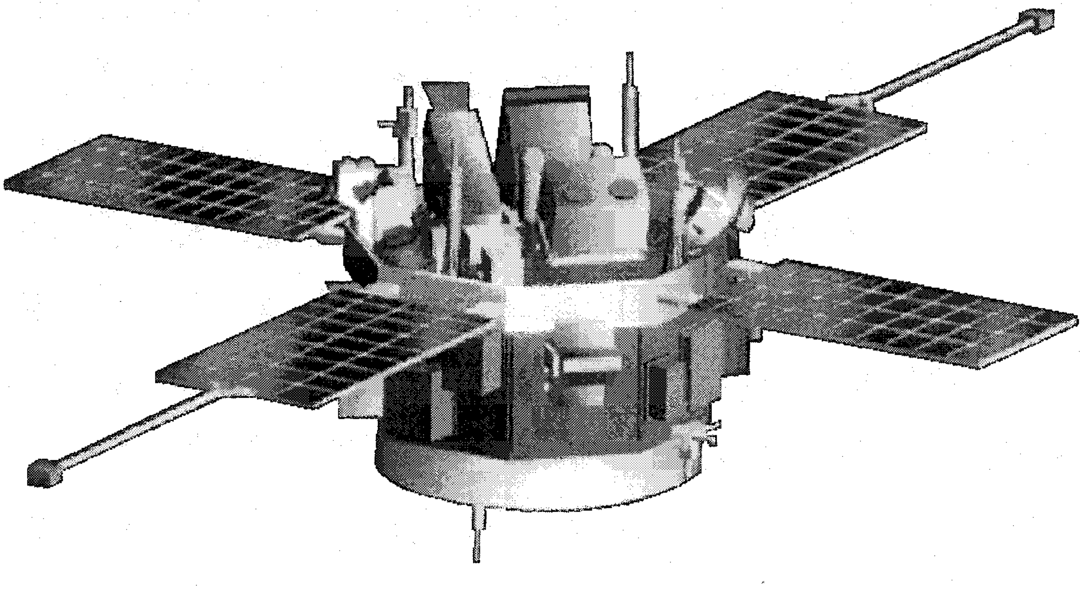

Figure 1.4 ACE Spacecraft (helios.gsfc.nasa.gov/ace_spacecraft.html)

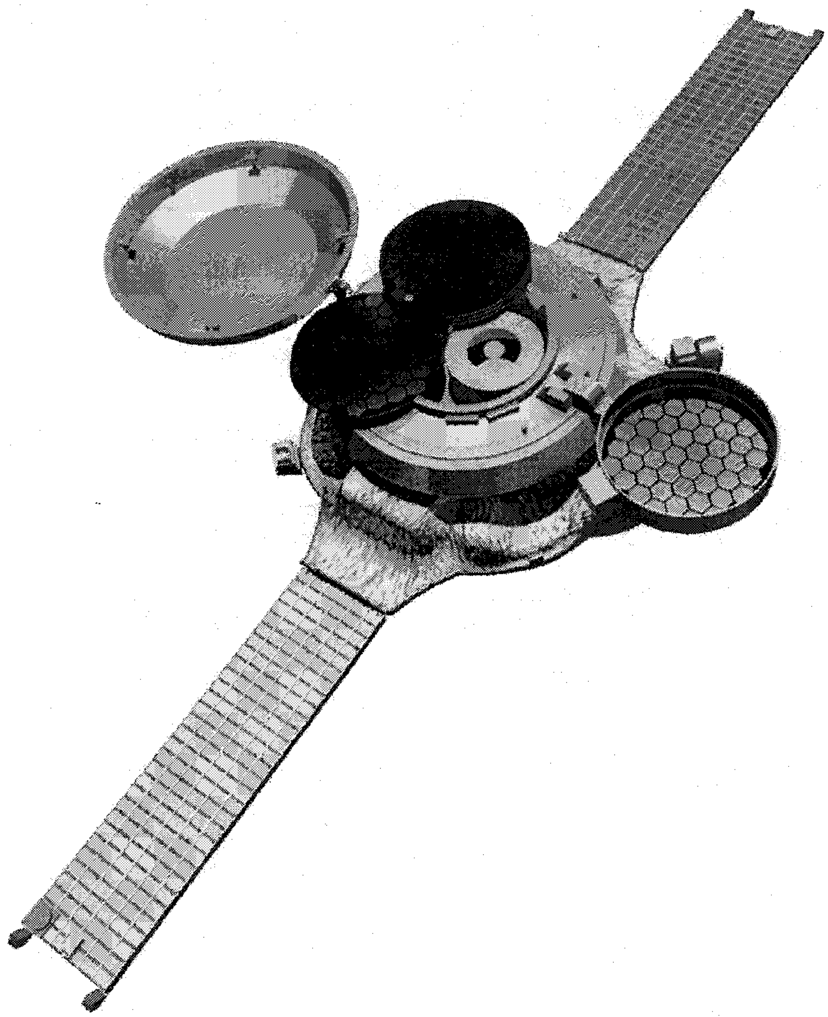

Figure 1.5 Genesis Spacecraft (www.genesismission.org/mission/scgallery.html)

1.7 Basics of Tether Dynamics

Most works are for geocentric satellites. A tether in the Earth orbit is subjected to two main forces, the gravitational force and the centrifugal inertia force. Other forces, such as aerodynamic drag, solar pressure and electrodynamic forces are much smaller in magnitude and are considered as perturbations. For a constant length tether, the balance of the gravitational force and the inertia force lead to three possible equilibrium positions; one vertical, two horizontal. The vertical equilibrium, where the tether is simply aligned along the local vertical, corresponds to a similar aligned dumbbell system and the stability of this configuration is maintained by the gravity gradient. The two horizontal equilibriums are marginally stable in theory and are unstable in practice.

The dynamics of the tether are different when its length is not constant, such when it is being deployed or retrieved. The deployment phase, where the length is increasing, is inherently stable as long as the rate of deployment is not too large. In this case, the Coriolis force acts to damp out the librations of the tether. The retrieval phase, however, is unstable as the Coriolis force now amplifies the librations. Several different types of control laws have been devised to combat this instability. These include different flavours of tension control laws, length control laws and offset control laws.

1.8 Literature review of Tether Dynamics at Lagrangian Points

As with a single mass, tethered systems are also unstable in the vicinity of L_1 and L_2. In contrast to the extensive volume of research on the dynamics and control of a single spacecraft in the vicinity of these points, the dynamics of tethered spacecraft at these locations is a relative new area of research. Most of the studies have focused on positional stability near the Lagrangian points, while a few others considered tether librations. Almost no research has been done on the dynamics and control of a tethered system in a Halo/Lissajous orbit.

There are two main approaches to analyze the dynamics of a tethered satellite at Lagrangian points. One approach is to treat each sub-satellite as an individual element with motion constraints. This is the way which Farquhar[20], and later on Gates[21], Kim, and Hall[22] approach this problem. The other method is to treat the group of tethered satellites as a system and derive the equations of motion for that system. Misra and Bellerose[23] used this technique. Each approach has its advantages and disadvantages, and which method to use will depend on the problem at hand.

As part of his research on the dynamics and control of libration point objects, Farquhar derived the equations of motion of an ideal tethered satellite located at L_2 of the Earth-Moon system using the Newtonian method. The left hand side of the resulting equations are the familiar equations describing the motions of a single body, but the right hand side is more complicated due to the tether-imposed constraints. With these equations, he analyzed the positional stability of the system and showed that it is possible to stabilize its position by changing the distance between the two end masses using a linear control law. With Farquhar's formulation, it takes a bit of effort to work in a length control algorithm as a term describing the tether is not immediately obvious. Gates used a Lagrangian approach to derive the equations of motion for an arbitrarily configured tethered system consisting of N masses and M tethers located in the vicinity of a Lagrangian point. The tether is treated as another applied force rather than as an integral part of the system. He did not explicitly consider gravitational and other environmental forces acting on the system at L_2. Instead, he treated them as generalized forces acting on each mass. The rotation of the Sun-Earth frame was also not considered in his analysis. All of those factors have significant effects on the dynamics of the parent mass and on the attitude of the system. Kim and Hall took the particle model developed by Gates and used it as a basis for the development of a nonlinear controller for a rotating triangular system. They analyzed the performance of this controller in several mission scenarios for the SPECS missions. However they also did not consider gravity and other environmental forces in their analysis and their results represents what can be achieved in the best case scenario. The element approach in general is easier to use for a diverse range of shapes, including those without a physical centre. Any change in the configuration of the system is reflected in the constraint and generalized force terms, and not in the equations of motion. This makes the element approach a very flexible method to use in the design phase of a system, when different shapes are evaluated. The downside in treating each mass individually is the large number of equations required to describe the full system, and it is more difficult to understand the tethered system as a whole. There are also no guarantees that the constraint and generalized force terms will be simple to derive or to deal with.

Misra and Bellerose[23] looked at the problem with a system approach and derived the planar equations of motion of a two-body system in the Earth-Moon system. The equations of motion were derived for the motions of the centre of mass and motions about the centre of mass. The tether was assumed to behave like a rigid rod and they worked out the equilibrium position and tether libration frequencies. They also developed a tether length control law to stabilize the centre of mass and the tether librations of the idealized tethered system at the equilibrium point and performed numerical simulations for the motion of the centre of mass near the translunar libration point. The systems approach that Misra and Bellerose took resulted in fewer equations needed to describe the system compared to the elements approach. The equations of motion need not be derived about the centre of mass, but the equations are mathematically simpler if it is. In practice, it is more useful to derive equations for and about the centre mass as that are what the ground stations are tracking. The systems approach is well suited to systems with a defined centre and it is easier to get a systems level understanding of the dynamics. In addition, the tether term is explicit in the equations of motion and tether control laws are easier to derive. There are several disadvantages to using this approach. The equations of motion are slightly more complicated, and tether tensions are harder to calculate. Changing the physical configuration of the system will require a rederivation of the equations of motion rather than just changing the constraint equations.

1.9 Reference Trajectory for Tethered Systems in Periodic Orbits

Since it takes less fuel to maintain a halo/Lissajous orbit that it does to remain static, it makes sense that the control system of the tethered formation should attempt to place and hold the system in a periodic trajectory. For small sized orbits (amplitude less than 3000 km), a first order approximation to the actual trajectory is sufficient. A first order Lissajous type reference trajectory can be described by

$$x = -A_x \sin\left(\omega_{xy} t\right) \tag{1.1}$$

$$y = -A_y \cos\left(\omega_{xy} t\right) \tag{1.2}$$

$$z = A_z \sin\left(\omega_z t\right) \tag{1.3}$$

where ω_{xy} and ω_z are respectively the nondimensional in-plane and out-of-plane frequencies of the oscillatory modes. A_x, A_y, A_z define the amplitudes of the reference trajectory for the x, y and z axis respectively. The dimensions of a halo orbit can be characterized completely by specifying A_x and expressing the other two amplitudes in terms of A_x. As mentioned previously, if $\omega_{xy} = \omega_z$, the resulting trajectory closes and is called a halo orbit. Otherwise the satellite is in a Lissajous trajectory. It should be noted that a halo orbit does not represent the natural dynamics of a body around L_2 and a Lissajous trajectory is closer to the true picture. Specifying the type of orbit, halo or Lissajous, would have a major impact in the dynamics of the tethered system and the control effort required to enforce certain behaviour. For trajectories with a large semi-major axis, additional terms are needed and the resulting shape looks more like the cross section of a pancake than an ellipse.

1.10 Objective of thesis

There are three major objectives in this work. The equations of motion of a N-body system tethered system located at L_2 Sun-Earth Lagrangian point must first be derived. The second goal is the development, implementation and verification of a detailed computer model, focusing on the 3-body case, using the previously derived equations of motion. The third objective is to analyze the control effort required in order for a spin stabilized tethered system to first remain in a halo/Lissajous orbit, and second maintain some astronomically useful configuration.

1.11 Outline of thesis

This thesis first presents the mathematical derivation of the equations of motion describing the dynamics of an N-body tethered system in chapter 2. These equations determine the effect of tether lengths, the number of masses and the mass ratios on the motion of the parent mass as well as the tether librations. Information such as stable equilibrium configurations of the tether and equilibrium positions of the parent mass can also be obtained from the equations of motion.

Chapter 3 describes the numerical results from different initial conditions. The computer model used is based on the equations derived in chapter 2. Of specific interest is the librations of the rotating tethers when the parent mass is assumed to be in a halo orbit of a certain size.

Chapter 4 discusses the setup of a proposed control system for the tethered system, both to hold it in a certain orbit and to control the librations of the tether in some useful manner. Specific attention would be paid to the amount of control effort required to hold the parent mass in a halo or a Lissajous orbit of a certain size while controlling the plane of rotation of the spinning tethers.

Chapter 5 summarizes the findings of chapters 2 to 4, and offers some concluding remarks. Some future directions of this research are also suggested.

Chapter 2

FORMULATION OF THE PROBLEM

2.1 Description of the System

The system under consideration consists of a parent mass m_p and a set of end masses $m_1, m_2 ... m_N$ moving under the gravitational influence of the Sun and the Earth (Figure 2.1). The i^{th} end mass is connected to the parent mass by a tether of length l_i. It is assumed that all the masses can be treated as point masses and that the tethers are rigid, inextensible and of negligible mass. The forces on the tethers are likely to be very small, as seen in the geocentric cases, and the elastic oscillations are should have no higher than second order effects on station keeping. Hence the tethers can be treated as rigid. It is assumed that the Sun, of mass M_1, and the Earth, of mass M_2, revolve around their common mass centre O in circular orbits. The fixed distance between M_1 and M_2 is denoted by D, while D_1 and D_2 denote the distances of the Sun and the Earth from O, respectively. It can be shown that

$$D_1 = \varepsilon D, \qquad D_2 = (1-\varepsilon)D \tag{2.1}$$

where $\varepsilon = M_2/(M_1+M_2)$.

The motions of the masses are described using a set of rotating coordinate axes $[X\ Y\ Z]$, with its origin at O and the X-axis in the direction of M_1 to M_2. The Y-axis is perpendicular to the X-axis in the plane of motion of the primary bodies and the Z-axis is along the normal to this plane. Unit vectors along the X, Y and Z axes are denoted by **i**, **j** and **k**, respectively. The axes rotate about O at a constant rate of n about the Z-axis, with

$$n = [G(M_1+M_2)/D^3]^{1/2} \tag{2.2}$$

where G is the universal gravitational constant.

Two additional sets of axes are used. The set of axes $[x\ y\ z]$ is located at the Lagrangian point of interest, L_2 in this case, and is parallel to $[X\ Y\ Z]$. The two sets of axes are related by

$$X = X_L+x \qquad Y = Y_L+y \qquad Z = z \tag{2.3}$$

where $(X_L, Y_L, 0)$ are the coordinates of the Lagrangian point of interest. This set of axis is used to describe the motion of the parent mass relative to L_2. The locations of the end masses relative to the parent mass are described using a set of spherical coordinates centred at the parent mass, which is rotating with the $[x\ y\ z]$ axes. The in-plane and out-of-plane rotation angles, θ_i and ϕ_i, are measured relative to the x, y, z axes. θ_i is measured counter-clockwise from the x-axis about the z-axis and ϕ_i is measured down from the z-axis (Figure 2.2). At any arbitrary instant, the location of an end mass relative to the parent mass can be described by

$$x_i = l_i \cos\theta_i \sin\phi_i, \qquad y_i = l_i \sin\theta_i \sin\phi_i, \qquad z_i = l_i \cos\phi_i \tag{2.4}$$

for $i = 1..N$, with N being the number of end masses and l_i as described above. The ratio of the i^{th} mass to the total mass, μ_i, is defined as $\mu_i = m_i/m_t$, where m_t is the total mass of the system.

The position vector of the parent mass m_p relative to O is denoted by $\mathbf{R}_p$, while its position vectors relative to the two primary bodies are denoted by $\mathbf{R}_1$ and $\mathbf{R}_2$

respectively. The vector $\mathbf{r}_i$ denotes the position vector of the end mass m_i relative to the parent mass. These vectors are given by

$$\mathbf{R}_p = X\mathbf{i}+Y\mathbf{j}+Z\mathbf{k} = (X_L+x_p)\mathbf{i} + (Y_L+y_p)\mathbf{j} + z_p\mathbf{k} \tag{2.5}$$

$$\mathbf{R}_1 = (D_1+X_L+x_p)\mathbf{i} + (Y_L+y_p)\mathbf{j} + z_p\mathbf{k} \tag{2.6}$$

$$\mathbf{R}_2 = (-D_2+X_L+x_p)\mathbf{i} + (Y_L+y_p)\mathbf{j} + z_p\mathbf{k} \tag{2.7}$$

$$\mathbf{r}_i = x_i\mathbf{i} + y_i\mathbf{j} + z_i\mathbf{k} \tag{2.8}$$

In this paper, the generalized coordinates for the system are x_p, y_p, z_p, θ_i, and ϕ_i for i = 1..N. The lengths of the tethers are constant. The coordinates x_p, y_p and z_p are the coordinates of the parent mass of the tethered system in the rotating frame located at the Lagrangian point, while θ_i, and ϕ_i define the orientation of the tether connected to the end mass m_i. The number of equations to be analyzed is 3+2N for a system with N end masses.

Given that this paper deals only with inextensible tethers, the choice of this particular set of generalized coordinates does not require constraint equations and leads to a simpler formulation of the dynamic equations. An alternative way of describing the system would be to select the location of the parent mass and the end masses as generalized coordinates, as described in chapter 1. This method would increase the number of required coordinates to 3N+3 while also introducing N constraint equations. The total number of unknowns would then be 3+4N and the resulting differential algebraic equations are more difficult to solve. If the tethered system is modelled using extensible tethers, the two sets of generalized coordinates would be of the equal number and the choice of the generalized coordinates would depend on the problem at hand.

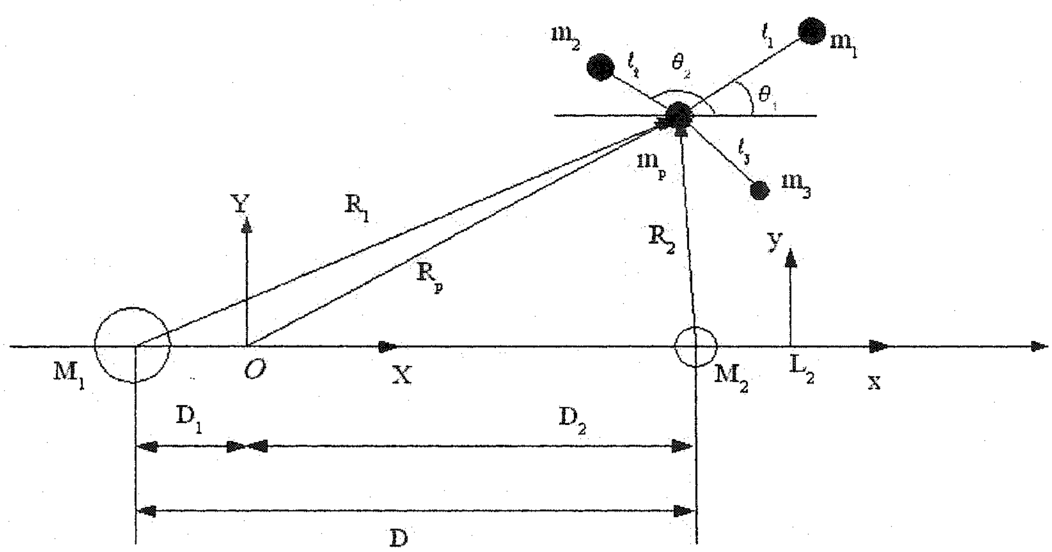

Figure 2.1 Geometry of the System

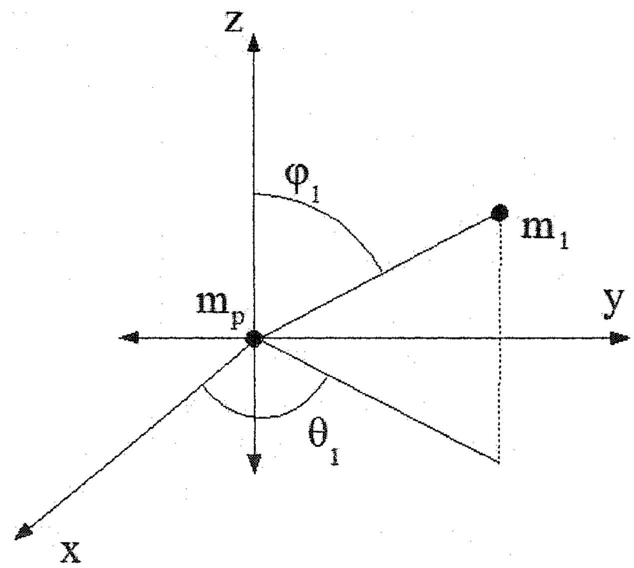

Figure 2.2 Parent Mass Centred Coordinate Frame

2.2 Energy Terms

In order to derive the equations of motion using the method of Lagrange, the kinetic and potential energy terms must first be obtained. The absolute velocities of the parent mass and the end masses are given by

$$\mathbf{V}_{\mathrm{p}} = \dot{\mathbf{R}}_{\mathrm{p}} + n\mathbf{k}\times\mathbf{R}_{\mathrm{p}} \tag{2.9}$$

$$\mathbf{V}_i = \mathbf{V}_p + \dot{\mathbf{r}}_i + n\mathbf{k}\times\mathbf{r}_i \tag{2.10}$$

where n is the angular velocity of the rotating frame attached to the [X Y Z] axes.

The kinetic energy term of the system is given by

$$T = \frac{1}{2} m_p \mathbf{V}_p \bullet \mathbf{V}_p + \frac{1}{2}\sum_{i=1}^{N} m_i \mathbf{V}_i \bullet \mathbf{V}_i \tag{2.11}$$

Using Eqs. (2.3)- (2.5) and (2.8)-(2.10), Eq (2.11) can be written as

$$\begin{aligned}
T = {} & \frac{1}{2}\left(m_p + \sum_{i=1}^{N} m_i\right)\left[\dot{x}_p^2 + \dot{y}_p^2 + \dot{z}_p^2 + 2n\dot{y}_p\left(X_L + x_p\right) - 2n\dot{x}_p\left(Y_L + y_p\right) + n^2\left\{\left(X_L + x_p\right)^2 + \left(Y_L + y_p\right)^2\right\}\right] \\
& + \frac{1}{2}\sum_{i=1}^{N} m_i l_i^2\left[\left(n + \dot{\theta}_i\right)^2 \sin^2\phi_i + \dot{\phi}_i^2\right] + \sum_{i=1}^{N} m_i l_i\Big[\left(n + \dot{\theta}_i\right)\sin\phi_i\left\{\left(nY_L + ny_p - \dot{x}_p\right)\sin\theta_i + \left(nX_L + nx_p + \dot{y}_p\right)\cos\theta_i\right\} \\
& + \dot{\phi}_i\cos\phi_i\left\{\left(\dot{x}_p - nY_L - ny_p\right)\cos\theta_i + \left(\dot{y}_p + nX_L + nx_p\right)\sin\theta_i\right\} - \dot{z}_p\dot{\phi}_i\cos\phi_i\Big]
\end{aligned} \tag{2.12}$$

for constant length tethers.

The potential energy term is given by

$$V = -\frac{GM_1 m_p}{\left|\mathbf{R}_1\right|} - \frac{GM_2 m_p}{\left|\mathbf{R}_2\right|} - \sum_{i=1}^{N}\frac{GM_1 m_i}{\left|\mathbf{R}_1 + \mathbf{r}_i\right|} - \sum_{i=1}^{N}\frac{GM_2 m_i}{\left|\mathbf{R}_2 + \mathbf{r}_i\right|} \tag{2.13}$$

where $\mathbf{R}_1$ and $\mathbf{R}_2$ denote the position vectors of the parent mass relative to the two primary bodies and are given by Eqs.(2.6) and (2.7), respectively. It is assumed that the lengths of the tethers are small compared to the distance between the two primary bodies, which implies that $|\mathbf{r}_i|$ is small compared to $|\mathbf{R}_1|$ and $|\mathbf{R}_2|$. Expanding the denominator of the third term in Eq.(2.13) using the binomial theorem and retaining terms up to the third order, one obtains

$$\frac{1}{|\mathbf{R}_1+\mathbf{r}_i|}\approx\frac{1}{R_1}\left[1-\frac{\mathbf{u}_1\bullet\mathbf{r}_i}{R_1}+\frac{1}{2}\frac{\{3(\mathbf{u}_1\bullet\mathbf{r}_i)^2-r_i^{\,2}\}}{R_1^{\,2}}\right] \tag{2.14}$$

where $R_1 = |\mathbf{R}_1|$ and $\mathbf{u}_1$ is the unit vector along $\mathbf{R}_1$. Similar expansion can be carried out for the last term in Eq.(2.13). Substituting Eqs. (2.5)- (2.8) and (2.14) in Eq.(2.13), setting $Y_L = 0$ and then expanding the result and retaining terms up to the third order, the potential energy term for the system in the vicinity of L_2 becomes

$$\begin{aligned}
V = &-n^2\left(m_p+\sum_{i=1}^{N}m_i\right)\left(-I+Ax_p-B\left(x_p^2-\frac{y_p^2}{2}-\frac{z_p^2}{2}\right)+C\left(x_p^2-\frac{3x_py_p^2}{2}-\frac{3x_pz_p^2}{2}\right)\right)\\
&+\sum_{i=1}^{N}n^2m_i\Bigg[Al_i\cos\theta_i-\frac{Bl_i^2}{2}\left(3\cos^2\theta_i\sin^2\phi_i-1\right)+\\
&x_p\left(\frac{3Cl_i^2}{2}\left(3\cos^2\theta_i\sin^2\phi_i-1\right)-2Bl_i\cos\theta_i\sin\phi_i\right)+\\
&y_p\left(Bl_i\sin\theta_i\sin\phi_i-\frac{3Cl_i^2}{2}\sin2\theta_i\sin^2\phi_i\right)+z_p\left(Bl_i\cos\phi_i-\frac{3Cl_i^2}{2}\cos\theta_i\sin2\phi_i\right)+\\
&3Cl_i\left(\cos\theta_i\sin\phi_i\left(x_p^2-\frac{y_p^2}{2}-\frac{z_p^2}{2}\right)-x_py_p\sin\theta_i\sin\phi_i-x_pz_p\cos\phi_i\right)\Bigg]
\end{aligned} \tag{2.15}$$

where

$$I = D^2\left(\frac{1-\varepsilon}{\delta_1}+\frac{\varepsilon}{\delta_2}\right) \tag{2.16}$$

$$A = D\left(\frac{1-\varepsilon}{\delta_1^2}+\frac{\varepsilon}{\delta_2^{\,2}}\right) \tag{2.17}$$

$$B = \frac{1-\varepsilon}{\delta_1^3} + \frac{\varepsilon}{\delta_2^3} \tag{2.18}$$

$$C = \frac{1}{D}\left(\frac{1-\varepsilon}{\delta_1^4} + \frac{\varepsilon}{\delta_2^4}\right) \tag{2.19}$$

$$\delta_1 = \frac{X_L + D_1}{D} \tag{2.20}$$

$$\delta_2 = \frac{X_L - D_2}{D} \tag{2.21}$$

Using the kinetic and potential energy terms given by Eqs. (2.12) and (2.15), the equations of motion for x_p, y_p, z_p, as well as for θ_i and ϕ_i, can be obtained Because working with nondimensional equations is more convenient, a set of nondimensional quantities are defined. All distance and length measurements are divided through by l_0, the characteristic length of the tethers. This term is chosen as 1 km in this thesis. Mass units are nondimensionalized by dividing them by the total mass of the system m_t giving μ_i and time units are multiplied by n to create nondimensional time units, giving τ. The constants A, B and C are also nondimensionalized.

$$\begin{array}{lll} \hat{x}_p = x_p/l_0, & \hat{y}_p = y_p/l_0, & \hat{z}_p = z_p/l_0 \\ \hat{l}_i = l_i/l_0, & \mu_i = m_i/m_t, & \tau = nt \\ \hat{A} = A/l_0, & \hat{B} = B, & \hat{C} = Cl_0 \end{array} \tag{2.22}$$

2.3 Equations of Motion

With the kinetic and potential energy terms in hand, the equations of motion for the tethered system can be derived using the standard Lagrangian approach. The nondimensional equations of motion for the parent mass in the vicinity of L_2 are

$$\hat{x}_p'' - 2\hat{y}_p' - (2\hat{B}+1)\hat{x}_p + 3\hat{C}\left(\hat{x}_p^{\,2} - \frac{\hat{y}_p^{\,2}}{2} - \frac{\hat{z}_p^{\,2}}{2}\right) + \sum_{i=1}^{N}\mu_i\hat{l}_i\,[\phi_i''\cos\theta_i\cos\phi_i - \theta_i''\sin\theta_i\sin\phi_i$$

$$-\phi_i'^2\cos\theta_i\sin\phi_i - 2\cos\phi_i\left(\theta_i'\cos\theta_i + \phi_i'\sin\theta_i\right) - \left(\theta_i'+1\right)^2\cos\theta_i\sin\phi_i - 2\hat{B}\cos\theta_i\sin\phi_i$$

$$+3\hat{C}\left(2\hat{x}_p\cos\theta_i\sin\phi_i - \hat{y}_p\sin\theta_i\sin\phi_i - \hat{z}_p\cos\phi_i\right) + 3\hat{C}\hat{l}_i\left(3\cos^2\theta_i\cos^2\phi_i - 1\right)\Big] = \frac{Q_{x_p}}{m_t n^2 l_0}$$

(2.23)

$$\hat{y}_p'' + 2\hat{x}_p' + (\hat{B}-1)\hat{y}_p - 3\hat{C}\hat{x}_p\hat{y}_p + \sum_{i=1}^{N}\mu_i\hat{l}_i\,[\theta_i''\cos\theta_i\sin\phi_i + \phi_i''\sin\theta_i\cos\phi_i + 2\theta_i'\phi_i'\cos\theta_i\cos\phi_i -$$

$$\left(\phi_i'^2 + (1+\theta_i')^2 - \hat{B}\right)\sin\theta_i\sin\phi_i - 3\hat{C}\hat{l}_i\sin 2\theta_i\sin^2\phi_i - 3\hat{C}\sin\phi_i\left(\hat{x}_p\sin\theta_i + \hat{y}_p\cos\theta_i\right)\Big] = \frac{Q_{y_p}}{m_t n^2 l_0}$$

(2.24)

$$\hat{z}_p'' + \hat{B}\hat{z}_p - 3\hat{C}\hat{x}_p\hat{z}_p + \sum_{i=1}^{n}\mu_i\hat{l}_i\Big[\ \phi_i''\sin\phi_i + \phi_i'^2\cos\phi_i + \hat{B}\cos\phi_i - 3\hat{C}\hat{l}_i\cos\theta_i\sin 2\phi_i$$

$$-3\hat{C}\left(\hat{x}_p\sin\phi_i + \hat{z}_p\cos\theta_i\sin\phi_i\right)\Big] = \frac{Q_{z_p}}{m_t n^2 l_0}$$

(2.25)

The equations governing the in-plane and out-of-plane rotation of the i^{th} tether connecting the parent mass to the i^{th} mass are

$$\theta_i''\sin^2\phi_i + \phi_i'(\theta_i'+1)\sin 2\phi_i + \frac{3}{2}\left(\left(\hat{B}+3\hat{C}\hat{x}_p\right)\sin 2\theta_i\sin^2\phi_i - 2\hat{C}\hat{y}_p\cos 2\theta_i\sin^2\phi_i + \hat{C}\hat{z}_p\sin\theta_i\sin 2\phi_i\right)$$

$$+\frac{\sin\phi_i}{\hat{l}_i}\Bigg[\left(\hat{y}_p''\cos\theta_i - \hat{x}_p''\sin\theta_i\right) + \left(2\hat{x}_p' + \left(\hat{B}-1\right)\hat{y}_p\right)\cos\theta_i + \left(2\hat{y}_p' + \left(2\hat{B}+1\right)\hat{x}_p\right)\sin\theta_i$$

$$-3\hat{C}\left(\left(\hat{x}_p^2 - \frac{\hat{y}_p^2}{2} - \frac{\hat{z}_p^2}{2}\right)\sin\theta_i + \hat{x}_p\hat{y}_p\cos\theta_i\right)\Bigg] = \frac{Q_{\theta_i}}{m_t n^2 l_i^2}$$

(2.26)

$$\phi_i'' - (1+\theta_i')^2\cos\phi_i\sin\phi_i - \frac{3\sin 2\phi_i}{2}\left(\left(\hat{B}-3\hat{C}\hat{x}_p\right)\cos^2\theta_i + \hat{C}\hat{y}_p\sin 2\theta_i\right) +$$

$$\frac{\cos\phi_i}{\hat{l}_i}\Bigg[\hat{x}_p''\cos\theta_i + \hat{y}_p''\sin\theta_i + \left(2\hat{x}_p' + \left(\hat{B}-1\right)\hat{y}_p\right)\sin\theta_i - \left(2\hat{y}_p' + \left(2\hat{B}+1\right)\hat{x}_p\right)\cos\theta_i +$$

$$3\hat{C}\left(\hat{x}_p\hat{y}_p\sin\theta_i - \cos\theta_i\left(\hat{x}_p^2 - \frac{\hat{y}_p^2}{2} - \frac{\hat{z}_p^2}{2}\right)\right)\Bigg] - 3\hat{C}\hat{z}_p\cos\theta_i\cos 2\phi_i - \frac{\hat{z}_p\sin\phi_i}{l_i}\left(\hat{B}-3\hat{C}\hat{x}_p\right) = \frac{Q_{\phi_i}}{m_t n^2 l_i^2}$$

(2.27)

The generalized forces $Q_{x_p}, Q_{y_p}, Q_{z_p}, Q_{\theta_i}, Q_{\phi_i}$ can either be control forces applied by the satellite control system and/or other applied forces acting on the parent mass or the end masses. Setting all the time derivative terms to zero, the equilibrium position of the system can be found and from these results the equations of motion can be linearized. Some insight can be obtained from an approximate analysis of the linearized equations, while numerical studies of the full nonlinear system would illustrate the behavior of the system under some specified conditions.

2.4 Generalized Forces/Control Forces

In the Lagrangian formulation of the problem, applied forces are formulated into the equations of motion as generalized forces. The term Q_k is called the generalized force in the direction of the k^{th} generalized coordinate and is defined to be

$$Q_k = \mathbf{f} \bullet \frac{\partial \boldsymbol{\rho}_i}{\partial q_k} \tag{2.28}$$

where $\mathbf{f}$ is the resultant force vector acting on the k^{th} mass from the thrusters and/or perturbations. In this thesis, only control forces are considered. For the parent mass, $\boldsymbol{\rho}_i = \mathbf{R}_p$ and $\boldsymbol{\rho}_i = \mathbf{R}_p + \mathbf{r}_k$, $k = 1 \ldots N$ for end masses. For the parent mass, $\mathbf{f}$ has components f_{xp}, f_{yp} and f_{zp} in the $\mathbf{i}$, $\mathbf{j}$ and $\mathbf{k}$ directions. At each end mass $\mathbf{f}$ has components 0, $\mathbf{f}_{\theta_k}$ and $\mathbf{f}_{\phi_k}$, acting in the θ and ϕ directions, respectively, in the same spherical coordinate as used to define the location of the end masses. These forces are applied perpendicular to the tether. The control forces acting on the end masses will provide the required torques for tether libration control. When calculating the generalized force terms Q_{x_p}, Q_{y_p} and Q_{z_p} in the parent mass equations, $\frac{\partial \mathbf{p}_i}{\partial q_k} = 1$. The generalized force expressions for the parent mass equations are

$$Q_{x_p} = \mathrm{f_{xp}} \tag{2.29}$$

$$Q_{y_p} = \mathrm{f_{yp}} \tag{2.30}$$

$$Q_{z_p} = \mathrm{f_{zp}} \tag{2.31}$$

Q_{θ_k} and Q_{ϕ_k} are a bit harder to derive as the thrusts are not acting on the centre of the coordinate frame but at the k^{th} end mass. The generalized force terms for the libration equations of k^{th} tether can be written as

$$Q_{\theta_k} = \mathrm{f}_{\theta_k} l_k \sin\phi_k \tag{2.32}$$

$$Q_{\phi_k} = \mathrm{f}_{\phi_k} l_k \tag{2.33}$$

2.5 Equilibrium Positions

The first step to finding the equilibrium configuration of the system is to obtain the equilibrium equations. Setting all time derivatives to zero, the equilibrium equations are

$$\begin{aligned} &-(2\hat{B}+1)\hat{x}_p + 3\hat{C}\left(\hat{x}_p^{\,2} - \frac{\hat{y}_p^{\,2}}{2} - \frac{\hat{z}_p^{\,2}}{2}\right) + \sum_{i=1}^{N} \mu_i \hat{l}_i \Big[\left(2\hat{B}-1\right)\cos\theta_i \sin\phi_i \\ &+ 3\hat{C}\left(2\hat{x}_p \cos\theta_i \sin\phi_i - \hat{y}_p \sin\theta_i \sin\phi_i - \hat{z}_p \cos\phi_i\right) + 3\hat{C}\hat{l}_i\left(3\cos^2\theta_i \cos^2\phi_i - 1\right)\Big] = 0 \end{aligned} \tag{2.34}$$

$$\begin{aligned} &(\hat{B}-1)\hat{y}_p - 3\hat{C}\hat{x}_p\hat{y}_p + \sum_{i=1}^{N} \mu_i \hat{l}_i \Big[\left(\hat{B}-1\right)\sin\theta_i \sin\phi_i - 3\hat{C}\hat{l}_i \sin 2\theta_i \sin^2\phi_i - \\ &3\hat{C}\sin\phi_i\left(\hat{x}_p \sin\theta_i + \hat{y}_p \cos\theta_i\right)\Big] = 0 \end{aligned} \tag{2.35}$$

$$\hat{B}\hat{z}_p - 3\hat{C}\hat{x}_p\hat{z}_p + \sum_{i=1}^{n}\mu_i\hat{l}_i\left[B\cos\phi_i - 3\hat{C}\hat{l}_i\cos\theta_i\sin 2\phi_i - 3\hat{C}\left(\hat{x}_p\sin\phi_i + \hat{z}_p\cos\theta_i\sin\phi_i\right)\right] = 0 \tag{2.36}$$

$$\begin{aligned}&\frac{3}{2}\left(\left(\hat{B}+3\hat{C}\hat{x}_p\right)\sin 2\theta_i\sin^2\phi_i - 2\hat{C}\hat{y}_p\cos 2\theta_i\sin^2\phi_i + \hat{C}\hat{z}_p\sin\theta_i\sin 2\phi_i\right)\\ &+\frac{\sin\phi_i}{\hat{l}_i}\left[\left(\hat{B}-1\right)\hat{y}_p\cos\theta_i + \left(2\hat{B}+1\right)\hat{x}_p\sin\theta_i \ -3\hat{C}\left(\left(\hat{x}_p^2-\frac{\hat{y}_p^2}{2}-\frac{\hat{z}_p^2}{2}\right)\sin\theta_i + \hat{x}_p\hat{y}_p\cos\theta_i\right)\right]=0\end{aligned} \tag{2.37}$$

$$\begin{aligned}&-\cos\phi_i\sin\phi_i - \frac{3\sin 2\phi_i}{2}\left(\left(\hat{B}-3\hat{C}\hat{x}_p\right)\cos^2\theta_i + \hat{C}\hat{y}_p\sin 2\theta_i\right)+\\ &\frac{\cos\phi_i}{\hat{l}_i}\left[\left(\hat{B}-1\right)\hat{y}_p\sin\theta_i - \left(2\hat{B}+1\right)\hat{x}_p\cos\theta_i + 3\hat{C}\left(\hat{x}_p\hat{y}_p\sin\theta_i - \cos\theta_i\left(\hat{x}_p^2-\frac{\hat{y}_p^2}{2}-\frac{\hat{z}_p^2}{2}\right)\right)\right]\\ &-3\hat{C}\hat{z}_p\cos\theta_i\cos 2\phi_i - \frac{\hat{z}_p\sin\phi_i}{\hat{l}_i}\left(B-3\hat{C}\hat{x}_p\right)=0\end{aligned} \tag{2.38}$$

The above equations are nonlinear and have multiple solutions. The solution that is of practical importance is

$$\theta_{ieq} = (i-1)\pi \tag{2.39}$$

$$\phi_{ieq} = \frac{\pi}{2} \tag{2.40}$$

$$\hat{x}_{eq} = \frac{\sum_{i=1}^{N}\mu_i\left[\frac{3C}{D}\hat{l}_i^2 - (2B+1)\hat{l}_i(-1)^{i-1}\right]}{2B-1-\frac{6C}{D}\sum_{i=1}^{N}\mu_i\hat{l}_i(-1)^{i-1}} \tag{2.41}$$

$$\hat{y}_{eq} = 0 \tag{2.42}$$

$$\hat{z}_{eq} = 0 \tag{2.43}$$

where θ_{ieq}, ϕ_{ieq} are the angles at equilibrium of the tether connecting the i^{th} end mass to the parent mass. For the system under consideration here, the above values describe a particular equilibrium configuration on the x-axis. The equilibrium position of the parent mass is slightly displaced from L_2 in the x direction with no displacement in the y and z directions. The tethers are extended towards and away from the primary bodies. The equilibrium distance between the parent mass and L_2 depend on factors such as the mass ratios, the length of the tethers and the number of end masses. In this configuration the end masses are bunched up at two locations. For a three-body system this situation is not a concern, but for $N>3$ this is dangerous, especially if the end masses contain sensitive astronomical instruments.

Looking at the equilibrium equations for the libration angles, one can see that there are other equilibrium possibilities. These additional configurations depend on the equilibrium position of the parent mass, while the equilibrium position of the parent mass in general depends on the tether angles in a recursive manner. Both equilibrium positions and tether angles depend on the lengths of the tethers. Therefore to find these other positions an iteration scheme is needed.

2.6 Analysis of the Motion of the Parent Mass and Tether Rotation

After obtaining the equilibrium values, a linear analysis can be carried out for the parent mass motion and tether librations. Linearizing the equations at the system's equilibrium position given by Eqs. (2.39)-(2.43) yields

$$\hat{x}_p'' - 2\hat{y}_p' - \left(2\hat{B}+1\right)\hat{x}_p + \sum_{i=1}^{N} \mu_i \hat{l}_i \left[\left(3\hat{C}\hat{l}_i^2 - 2\hat{B} - 1\right)(-1)^{i-1} - 2\theta'\hat{l}_i(-1)^{i-1}\right] = 0 \tag{2.44}$$

$$\hat{y}_p'' + 2\hat{x}_p' + \left(\hat{B}-1\right)\hat{y}_p - \sum_{i=1}^{N} \mu_i \hat{l}_i \left[\left(\theta_i'' + \left(\hat{B}-1\right)\theta_i - 3\hat{C}\hat{y}_p\right)\hat{l}_i(-1)^{i-1} - 3\hat{C}\theta_i\hat{l}_i^2\right] = 0 \tag{2.45}$$

$$\hat{z}_p'' + \hat{B}\hat{z}_p - \sum_{i=1}^{N} \mu_i \hat{l}_i \left[\phi'' - 3\hat{C}\hat{z}_p(-1)^{i-1} + \left(3\hat{C}\hat{l}_i^2(-1)^{i-1} - \hat{B}\hat{l}_i\right)\phi_i\right] = 0 \tag{2.46}$$

$$\theta_i'' + 3\hat{B}\theta_i + 3\hat{C}\hat{y}_p + \frac{(-1)^{i-1}}{\hat{l}_i}\left[\hat{y}_p'' + 2\hat{x}_p' + (\hat{B}-1)\hat{y}_p\right] = 0 \tag{2.47}$$

$$\phi_i'' + (3\hat{B}+1)\phi_i - 3\hat{C}\hat{z}_p + \frac{1}{\hat{l}_i}\left[\hat{z}_p'' + \hat{B}\hat{z}_p\right] = 0 \tag{2.48}$$

From the above equations, it can be shown that the tethered system is not stable in the plane of rotation of the primary bodies. The out-of-plane motion of the parent mass is decoupled from its in-plane motion and is oscillatory in nature. The nondimensional libration frequencies of the tethers are roughly $\sqrt{3B}$ for in-plane motion and $\sqrt{3B+1}$ for out-of-plane motion. The oscillation frequencies of the parent mass depends on the number of end masses, the mass ratios and the lengths of the tethers. For the Sun-Earth system, B is roughly 3.94. Therefore the in-plane and out-of-plane frequencies are roughly 3.43 and 3.58 times the angular velocity of the Sun-Earth system, respectively. Since the above frequencies are obtained assuming small parent mass motions, if the motions are not small the libration frequencies could be different due the coupling between the tether librations and the parent mass motions. Once the motion of the parent mass is sufficiently large, the nonlinear effects become significant and the frequencies change.

If the system is placed in a halo orbit, the full equations of motion must be used to describe the system as Eqs (2.44)-(2.48) are linearized about the equilibrium point and are not quite valid if the halo orbit is large. In such a case it is easier to get a sense of the dynamics of the system by numerical simulations of the full equations of motion than by analytical methods. In chapter 3 the results of such numerical experiments will be presented.

Chapter 3

FREE DYNAMICS OF MULTI-TETHERED SYSTEMS AT SUN-EARTH L_2

The equations of motion derived in chapter 2 are now implemented in a numerical simulation software. The goals of the simulations are to (1) investigate the motions of the parent mass when it is slightly displaced from the Lagrangian point, (2) investigate the librations of the tethers when the parent mass is freely moving and (3) when it is held in a halo or Lissajous orbit of different dimensions.

3.1 Simulation Setup

The equations of motion are solved numerically using MATLAB for several cases. The integrator used is ODE45 with the default tolerance. The parameters are for L_2 of the Sun-Earth system and all of the results obtained are nondimensional. They are later re-dimensionalized for plotting purposes. All masses are assumed equal and all tethers are 1 km long. The in-plane angular displacements θ_i and out-of-plane angular displacements ϕ_i, along with the respective angular velocities, are measured with respect to the [X Y Z] axes. The displacements of the end masses can be calculated from

$$x_i = x_p + l_i \cos\theta_i \sin\phi_i, \quad y_i = y_p + l_i \sin\theta_i \sin\phi_i, \quad z_i = z_p + l_i \cos\phi_i \tag{3.1}$$

The numerical studies focused mostly on the 3-body case, and the free dynamics of a 4-body case was also briefly examined. As can be seen in Eqs. (2.26)-(2.27), there are more than one 2nd derivative terms in the libration angle equations. If the motion of the parent mass is prescribed, $\hat{x}_p''$, $\hat{y}_p''$ and $\hat{z}_p''$ are known and can be moved to the right hand side of the equations. The resulting equations of motion can be solved with the usual methods. However, if the motion of the parent mass is unknown, a little bit of linear algebra is required to isolate the desired 2nd derivative term. Moving all the second derivative terms to the left hand size, the equations of motion can be written in a matrix form:

$$\mathbf{A}\ddot{\mathbf{q}} = \mathbf{f}(\mathbf{q}) \tag{3.2}$$

where $\mathbf{A}$ is a matrix containing the coefficients of the second derivative terms, $\ddot{\mathbf{q}}$ is the vector of the second derivatives and $\mathbf{f}$ is the vector composed of the rest of the equations. The system of equations that needs to be solved then becomes

$$\ddot{\mathbf{q}} = \mathbf{A}^{-1}\mathbf{f}(\mathbf{q}) \tag{3.3}$$

3.2 Unconstrained Parent Mass Motions

Figure 3.1 compares the in-plane and out-of-plane motions of the three-body system when the masses are untethered with those when they are connected together. The displacements are measured from the second Lagrangian point, and the three masses are initially displaced from L_2 by 1.5 km, 11.5 km and 21.5 km respectively in the x direction, and 11.5 km in the y and z directions respectively. The initial angles of the tethers when the three bodies are connected are set as $\theta_1(0) = 0$, $\theta_2(0) = \pi$, $\phi_1(0) = \phi_2(0) = \pi/2$. For the untethered case, it can be seen that the three free masses go their separate ways quickly, while the tethered masses in the tethered system maintain their positions relative to each other. On the other hand, the tethered system as a whole drifts away from L_2 more quickly than the free mass case when they are given the same initial displacements. In practical terms, the cost of keeping the masses together is lower for a connected system, but more control effort is needed to keep it near L_2 as opposed to a single free mass.

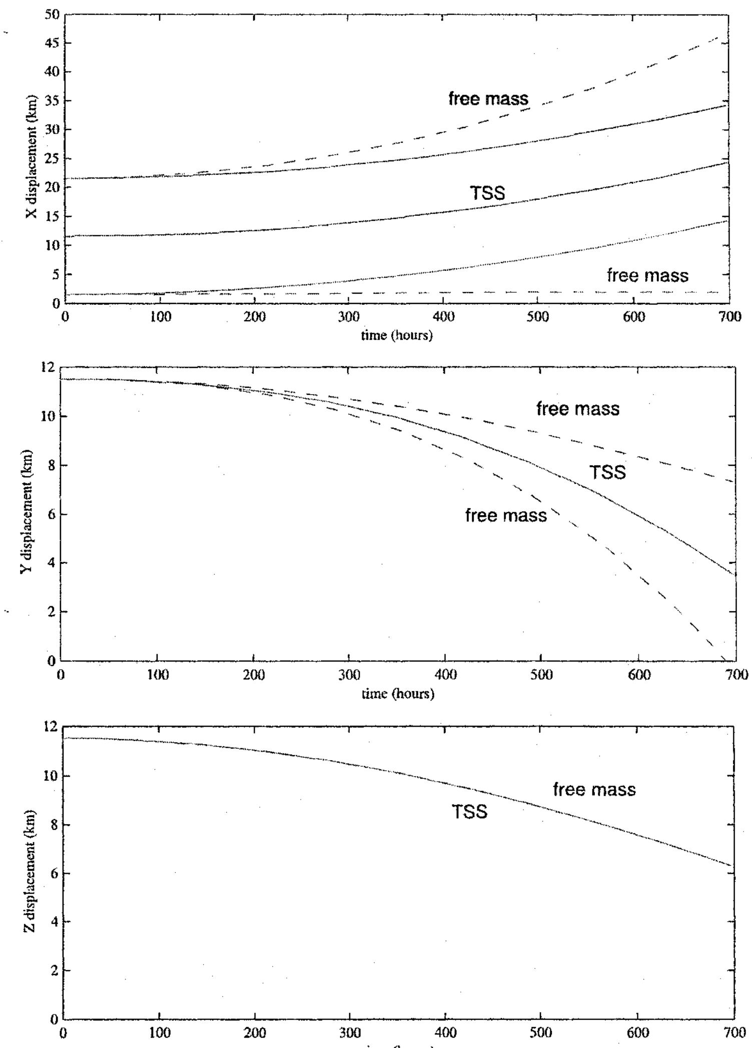

Figure 3.1 Comparison of displacements for a 3-body tethered system and a single mass

Figures 3.2, 3.3 and 3.4 show the parent mass motions and the in-plane and out-of-plane rotations of the 3-body tethered system for the case where the parent mass has initial displacements $x_p(0)=y_p(0)=z_p(0)=$ 11.5 km, with $\theta_1(0)=5\deg$,

$\theta_2(0)=185\,\mathrm{deg}$, $\phi_1(0)=85\,\mathrm{deg}$ and $\phi_2(0)=95\,\mathrm{deg}$ describing the initial orientation of the tethers. These initial conditions represent a small perturbation from the equilibrium configuration of a 3-body system. Exponential drift of the parent mass from L_2 in the x and y directions, as well as the sinusoidal motion in the z direction can be clearly noticed. Similar to the in-plane motions of the parent mass, the in-plane tether librations are also unstable. The out-of-plane librations are roughly periodic, mirroring the motion of the parent mass. As the tethered system moves very quickly away L_2, the linearized model developed in chapter 2 does not apply.

From the numerical results, it can be seen that the in-plane equilibrium is unstable as there are no restoring forces. Out-of-plane motions for both the parent mass and the tethers are periodic as the out-of-plane components of the gravitational and the centripetal forces act as restoring forces, pushing the masses back and forth across the ecliptic plane. Similar behaviour can also be seen for a single body in the vicinity of L_2.

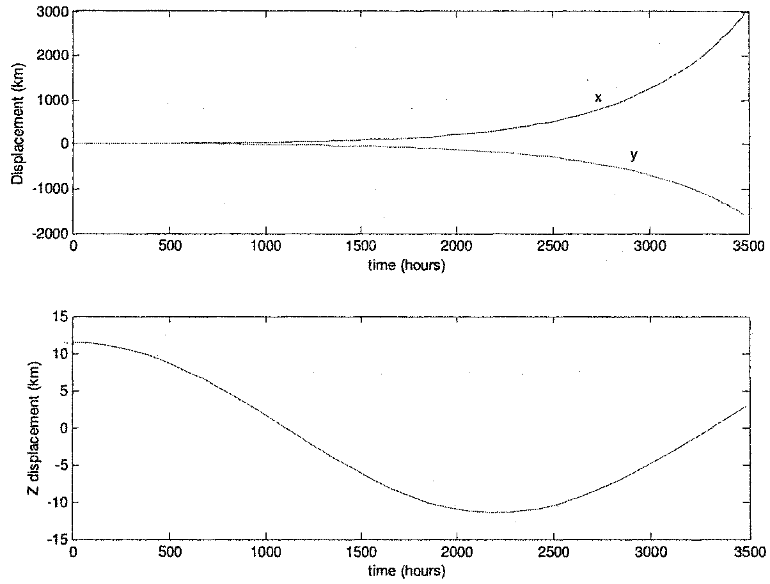

Figure 3.2 Parent Mass Displacements for a System Given Small Initial Displacements, xp(0)=yp(0)=zp(0)=11.5 km, $\theta_1(0)=5°$, $\theta_2(0)=185°$, $\phi_1(0)=85°$, $\phi_2(0)=95°$

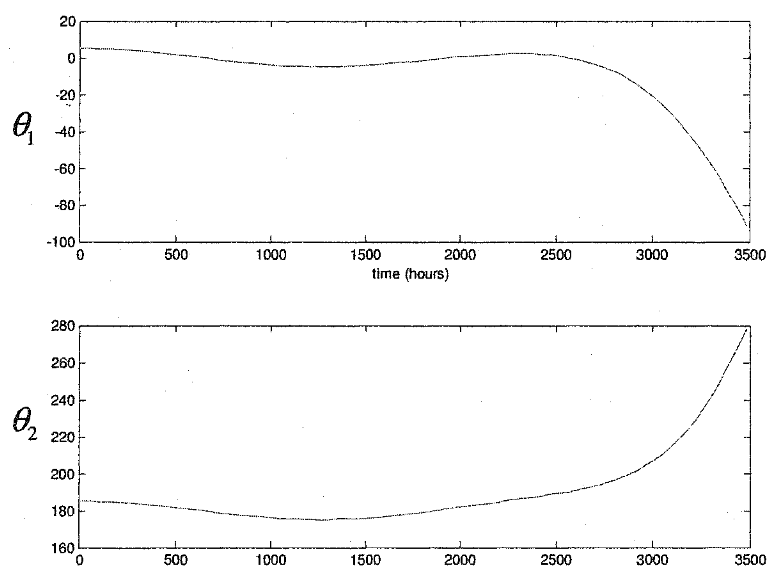

Figure 3.3 In-Plane Tether Librations, $x_p(0)=y_p(0)=z_p(0)=11.5$**km,** $\theta_1(0)=5°$, $\theta_2(0)=185°$, $\phi_1(0)=85°$, $\phi_2(0)=95°$

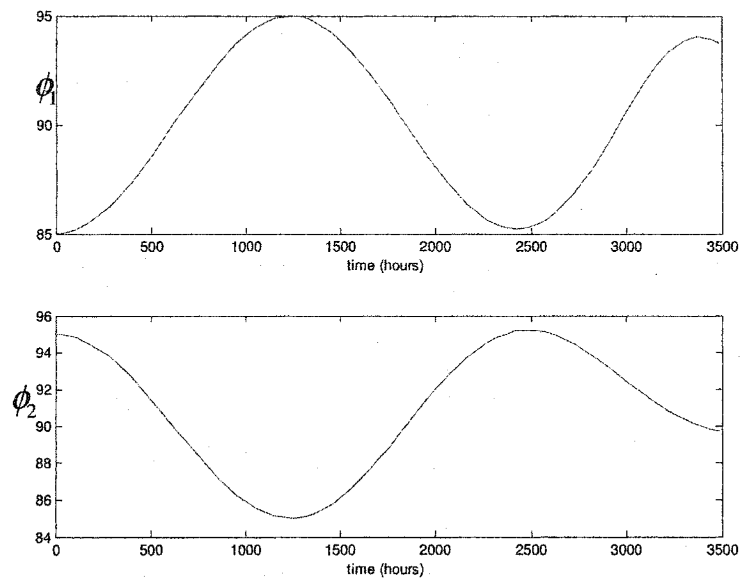

Figure 3.4 Out-Of-Plane Tether Librations, $x_p(0)=y_p(0)=z_p(0)=11.5$ km,
$\theta_1(0)=5°$, $\theta_2(0)=185°$, $\phi_1(0)=85°$, $\phi_2(0)=95°$

The number of end masses does not appear to have a significant effect on the motions of the parent mass. Since the tether equations of motion are independent from each other, the action of one tether only affects the others through its effect on the parent mass and are apparent only for high mass ratios. Figures 3.5-3.7 show the parent mass motions and tether rotations of a 4-body system. Comparing figure 3.5 to 3.1, one can see that the two graphs look almost exactly alike. The unstable nature of the parent mass is not affected by the additional tether. Figures 3.6 and 3.7 show the librations of the three tethers and again they are unstable in-plane and periodic out of the ecliptic plane. In practice, the initial angular separations of the tethers should be greater than what is simulated here, but since the in-plane motions are not stable anyways it does not play a significant role in the dynamics of the system.

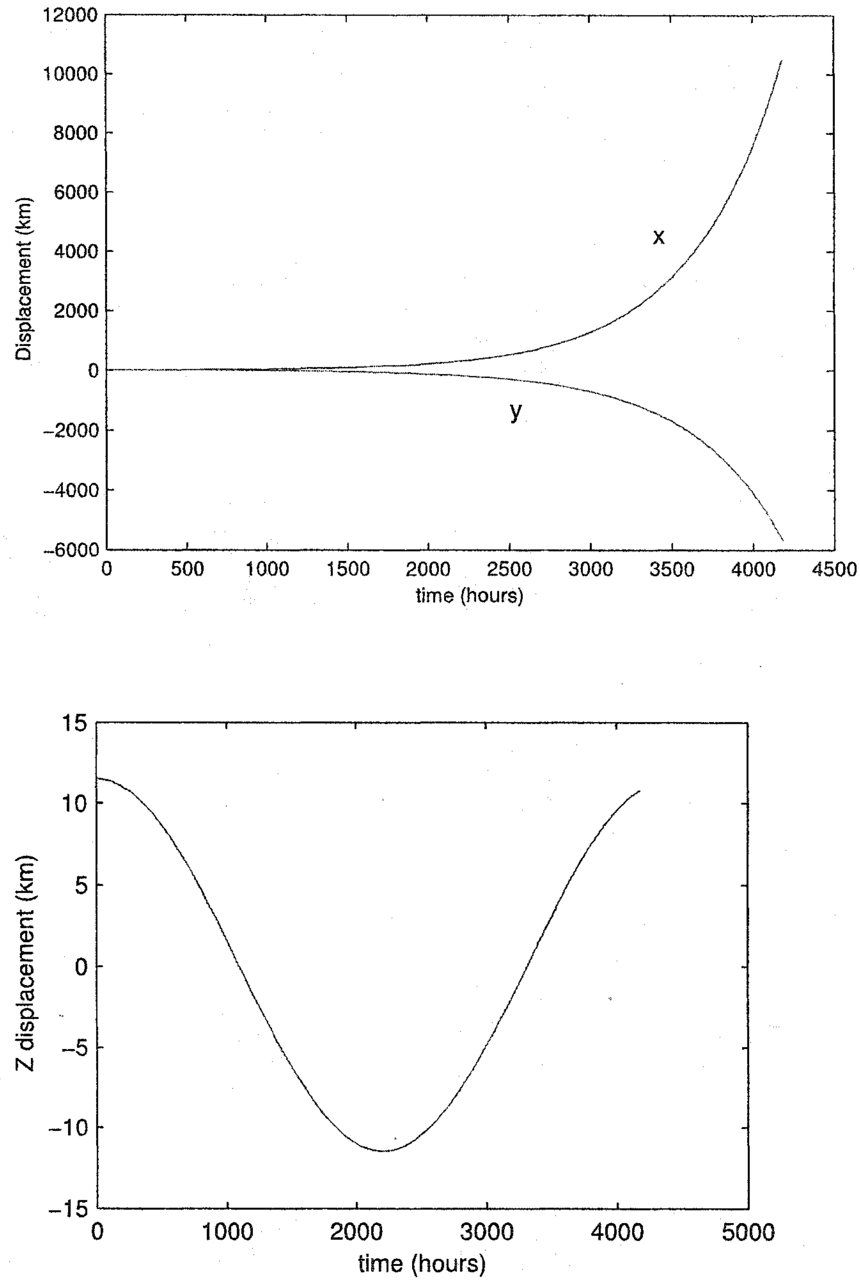

Figure 3.5 Parent Mass Motion for the 3-tether System, $x_p(0)=y_p(0)=z_p(0)=11.5$km,
$\theta_1(0)=30°$, $\theta_2(0)=150°$, $\theta_3(0)=330°$, $\phi_1(0)=85°$, $\phi_2(0)=95°$, $\phi_3(0)=90°$

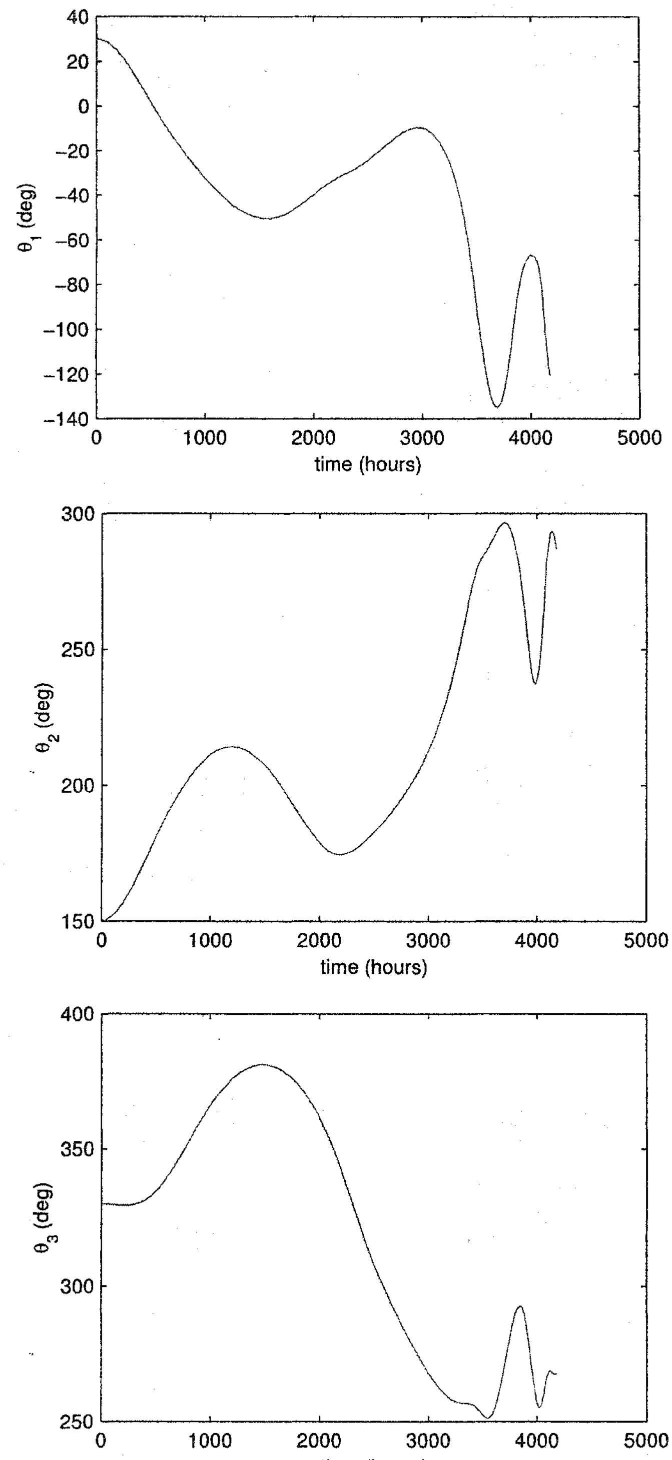

Figure 3.6 In-Plane Tether Libration Angles, $x_p(0)=y_p(0)=z_p(0)=11.5$km,
$\theta_1(0)=30°$, $\theta_2(0)=150°$, $\theta_3(0)=330°$, $\phi_1(0)=85°$, $\phi_2(0)=95°$, $\phi_3(0)=90°$

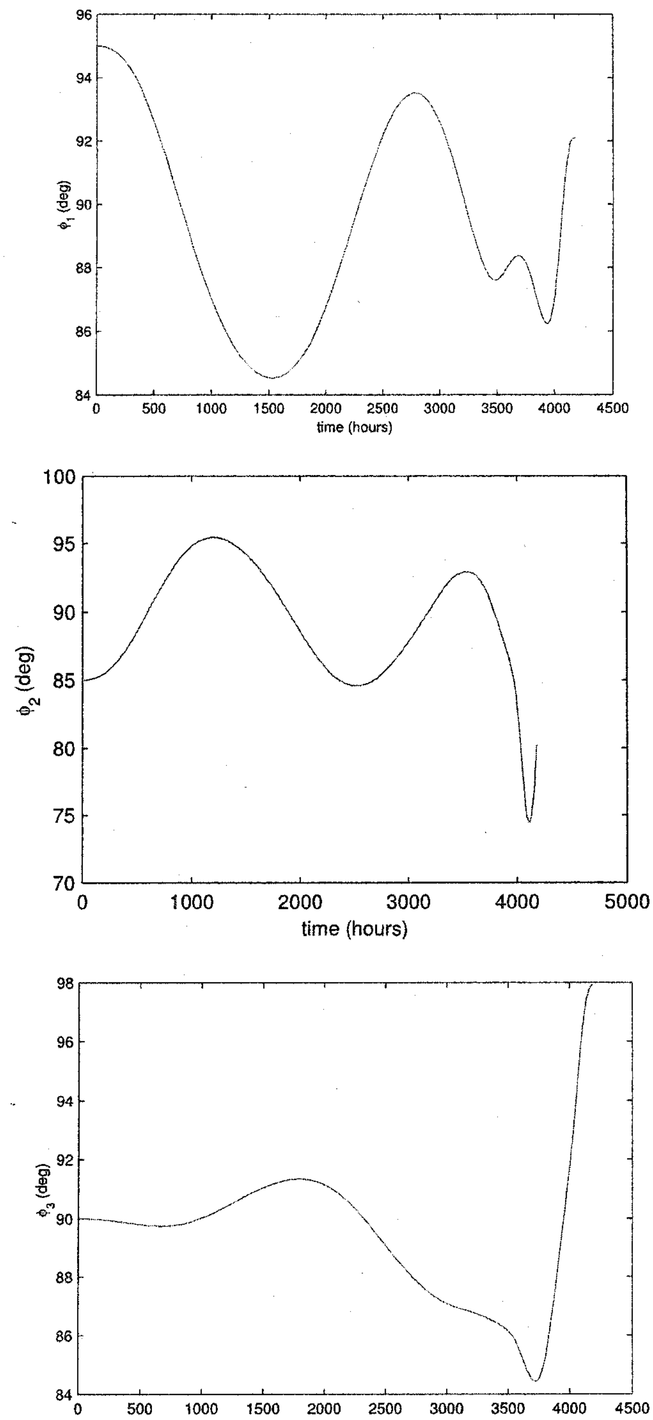

Figure 3.7 Out-Of-Plane Tether Libration Angles, $x_p(0)=y_p(0)=z_p(0)=11.5$km,
$\theta_1(0)=30°$, $\theta_2(0)=150°$, $\theta_3(0)=330°$, $\phi_1(0)=85°$, $\phi_2(0)=95°$, $\phi_3(0)=90°$

3.3 Parent Mass in Halo Orbits

One way to stabilize the motions of the parent mass over the long term is to place it in a halo orbit. Since the interferometer proposed by the SPECS project is spin stabilized, it is important to know how the tethers would behave in a spinning system with the parent mass occupying a halo orbit. Specifically of interest are how the out-of-plane librations and the angular velocities of the tethers are affected by different initial conditions. Angular velocities are measured as multiples of n, where n is the rate of rotation of the Sun-Earth system in radians/sec. Whenever θ and ϕ are used without subscripts, those values refer to both tethers.

If the parent mass is placed in a small halo orbit with initial conditions $A_x = 10$ km, $\dot{\theta}(0) = 10n$, and the out-of-plane angles are displaced ± 5 degrees from their equilibrium, the free librations of the tethers appear as in Figures 3.8 and 3.9. The behaviour of the system in this configuration would serve as the baseline case. The average in-plane angular velocities are a bit more than $10n$, oscillating about $13n$. The reason for this increase is unknown at this moment and more research is needed. The out-of-plane motions of the tethers can be described as "flapping", as both of them are librating in the same direction and by the same amount despite their different initial displacements. As the parent mass travels up in the positive z direction, the tethers begin to angle down and start to a small amplitude libration about the $\phi = 120$ degrees value. The shape of ϕ vs time is almost like that of a crown with a small magnitude, with higher frequency components embedded in the larger amplitude, lower frequency overall shape. As the parent mass goes below the ecliptic plane the same thing happens in reverse, this time the tethers are librating about $\phi = 60°$.

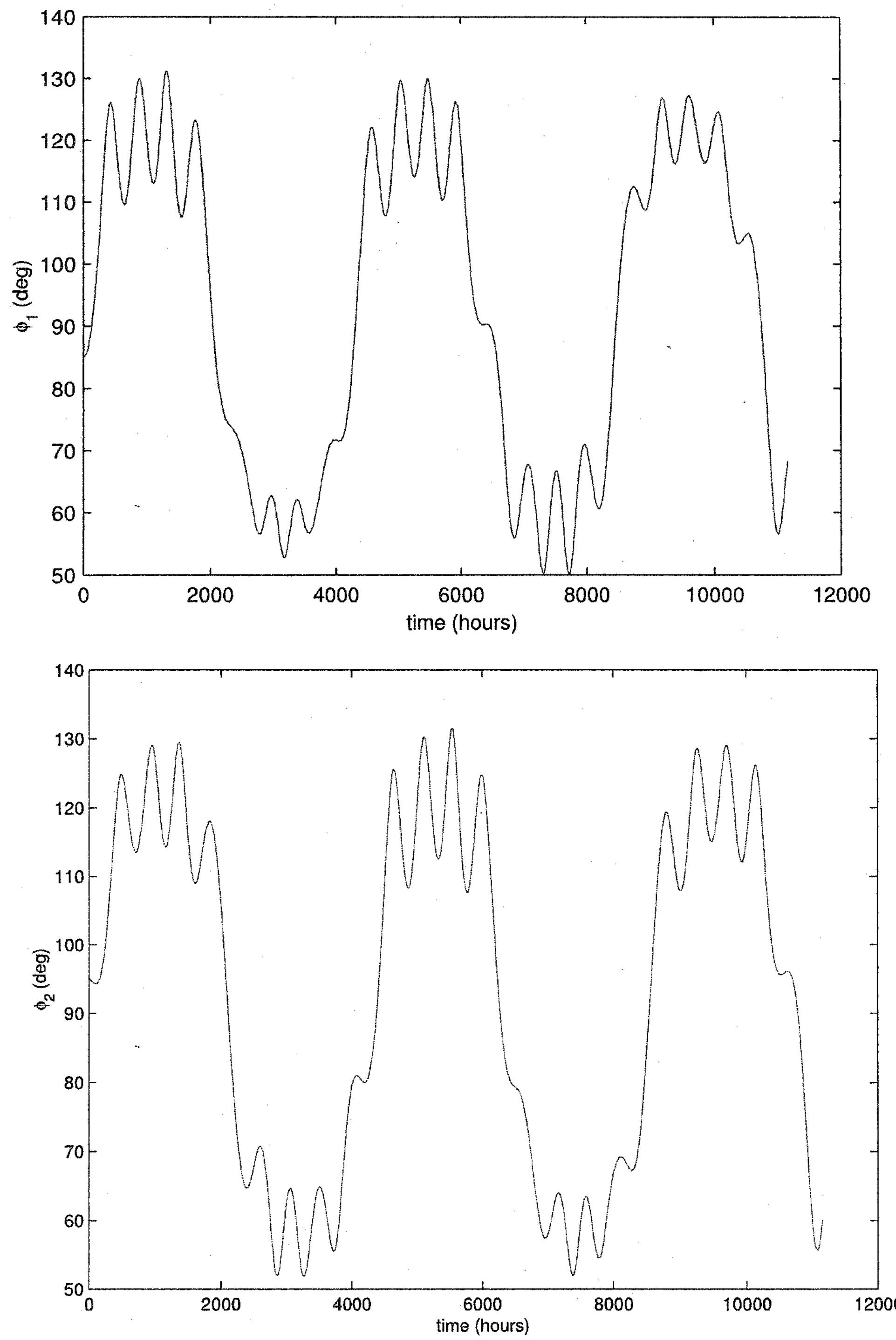

Figure 3.8 Baseline Out-Of-Plane Tether Librations Results, A_x=10 km, $\dot{\theta}=10n$, $\phi_1(0)=85$ deg, $\phi_2(0)=95$ deg

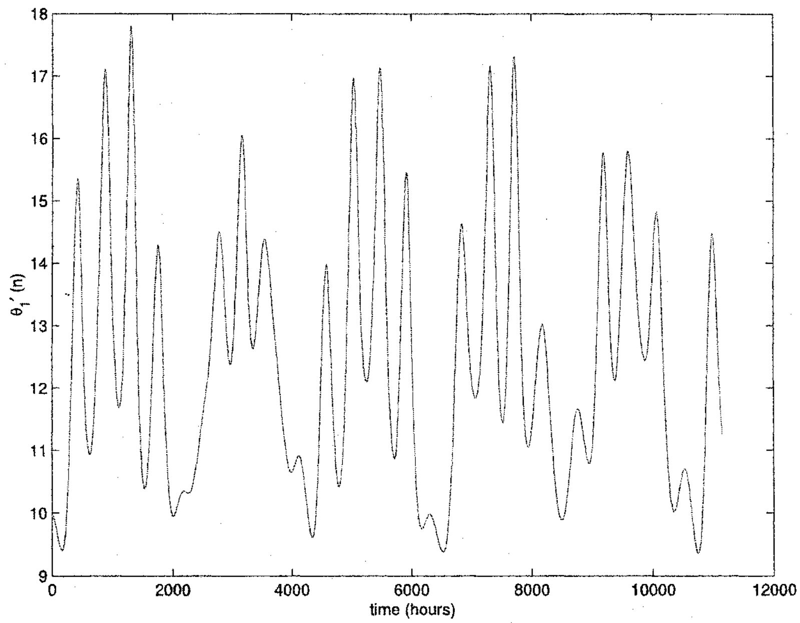

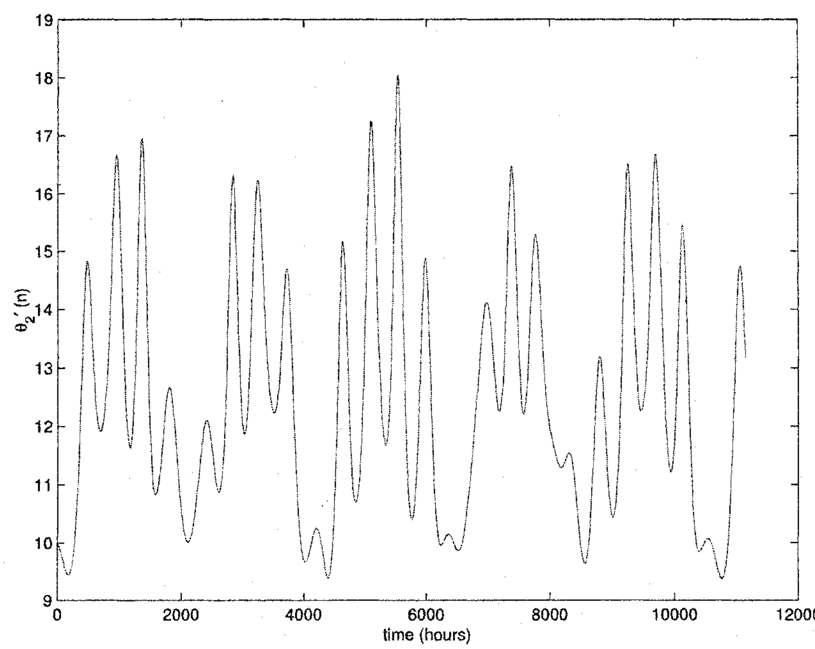

Figure 3.9 Baseline Tether Angular Velocity Results, A_x=10 km, $\dot{\theta}=10n$, $\phi_1(0)=85$ deg, $\phi_2(0)=95$ deg

Larger halo orbits lead to larger out-of-plane libration amplitudes as well as even higher frequencies for the high frequency component of the librations. Figures 3.10 and 3.11 illustrate the differences in the out-of-plane librations and in-plane angular velocities for different sized halo orbits. In these figures $\dot{\theta}(0)=30n$ and A_x goes from 10 km to 1000 km. The amplitudes of $\phi(t)$, both the high frequency and the low frequency components, increase as A_x grows. The variations of $\dot{\theta}$ also grow as a function of A_x. This pattern can be seen for other $\dot{\theta}(0)$ as well. Figures 3.12 and 3.13 show what happens when $\dot{\theta}(0)=70n$

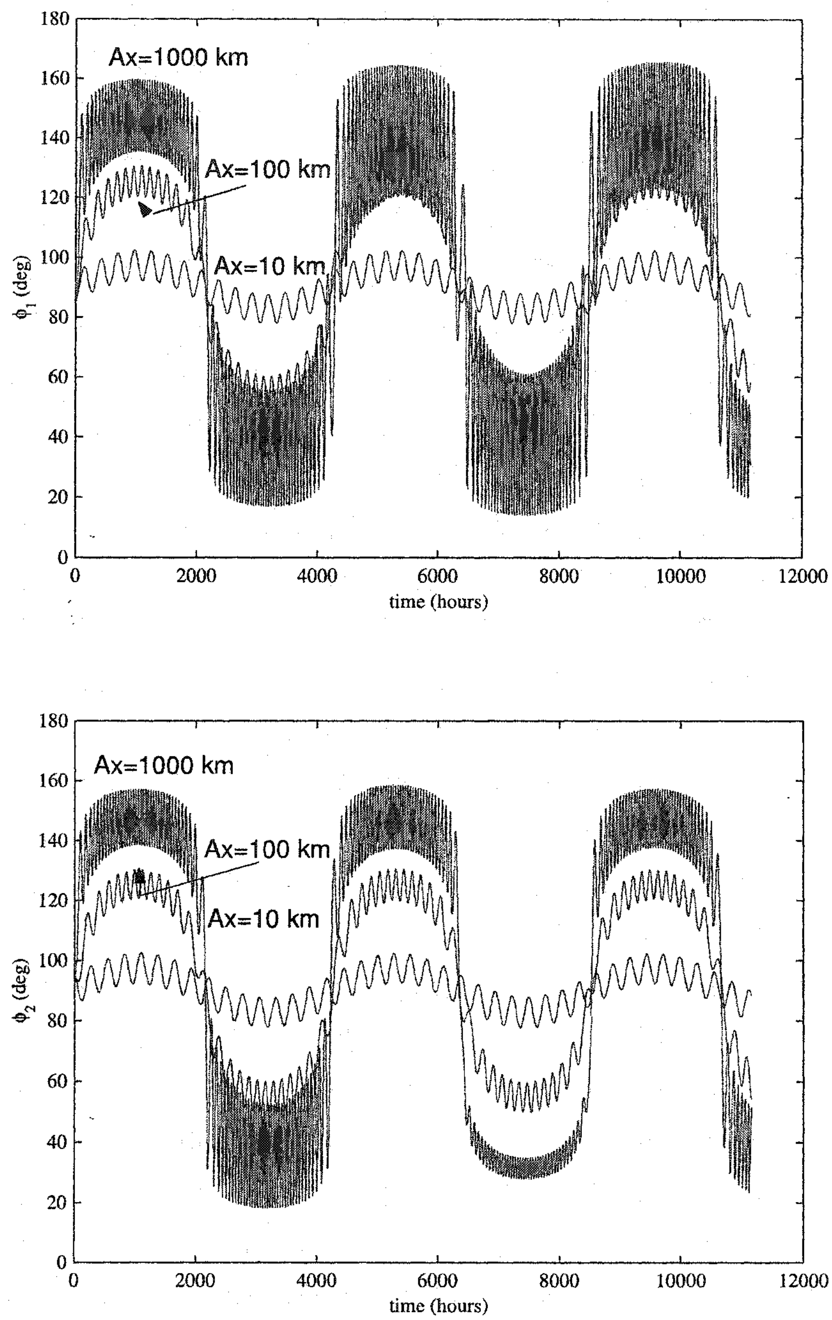

Figure 3.10 Out-of-Plane Tether Librations, $\dot{\theta}(0)=30n$

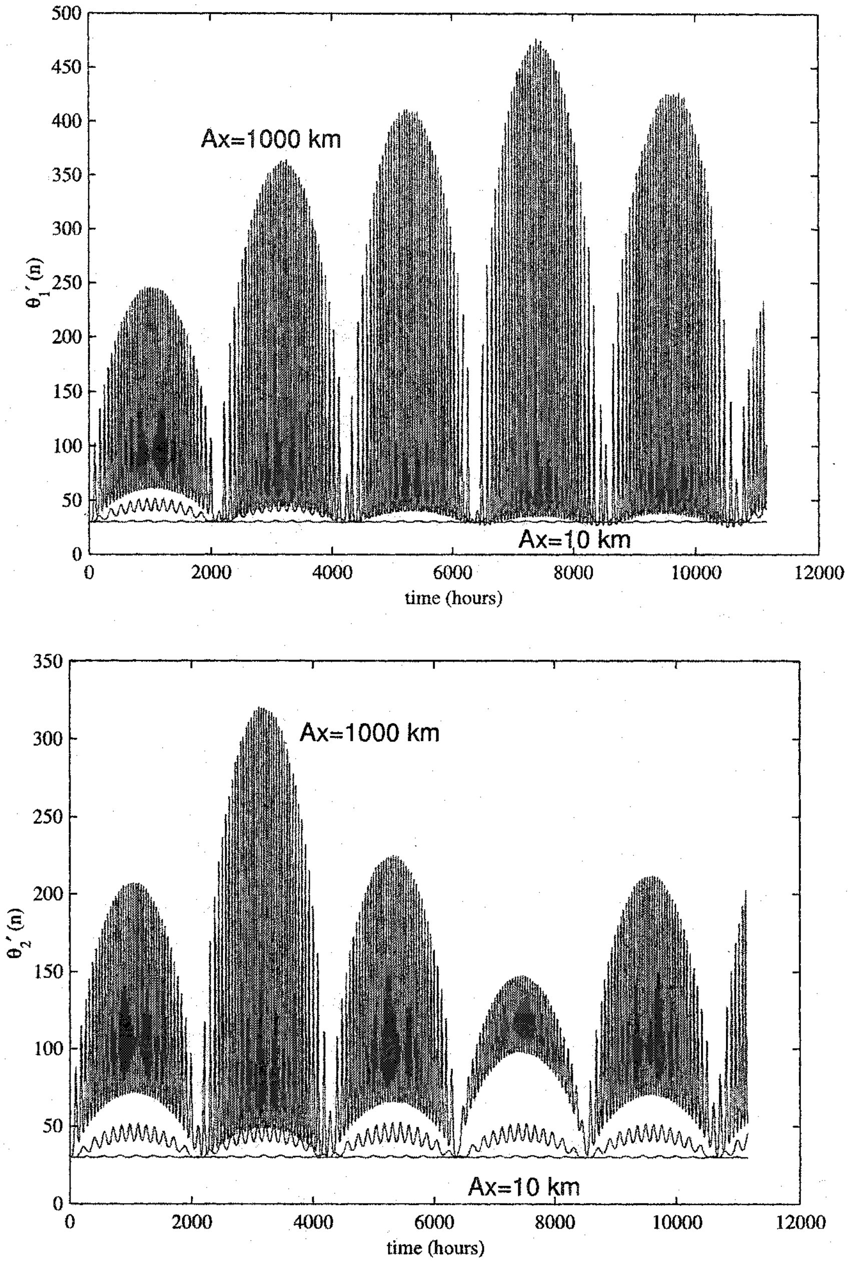

Figure 3.11 In-Plane Tether Angular Velocities, $\dot{\theta}(0)=30n$

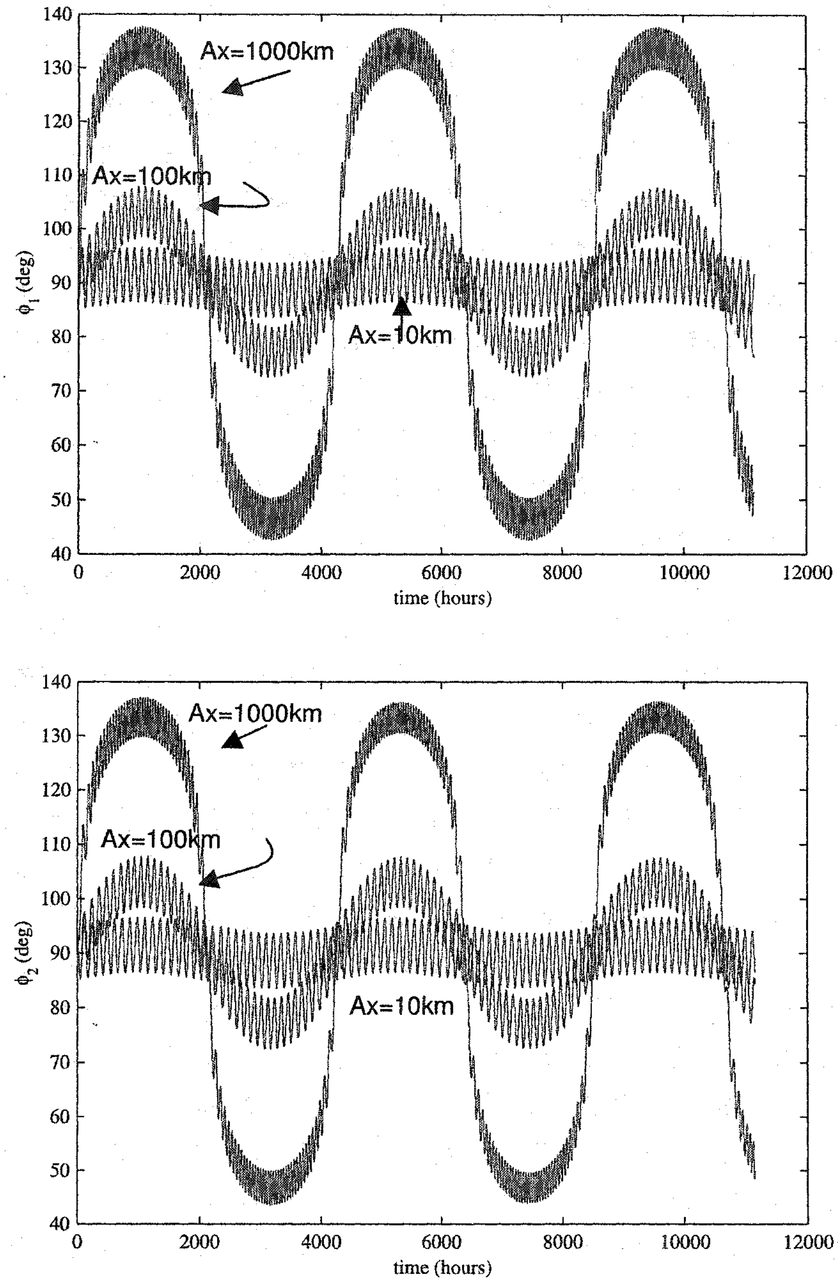

Figure 3.12 Out-Of-Plane Tether Librations, $\dot{\theta}(0)=70n$

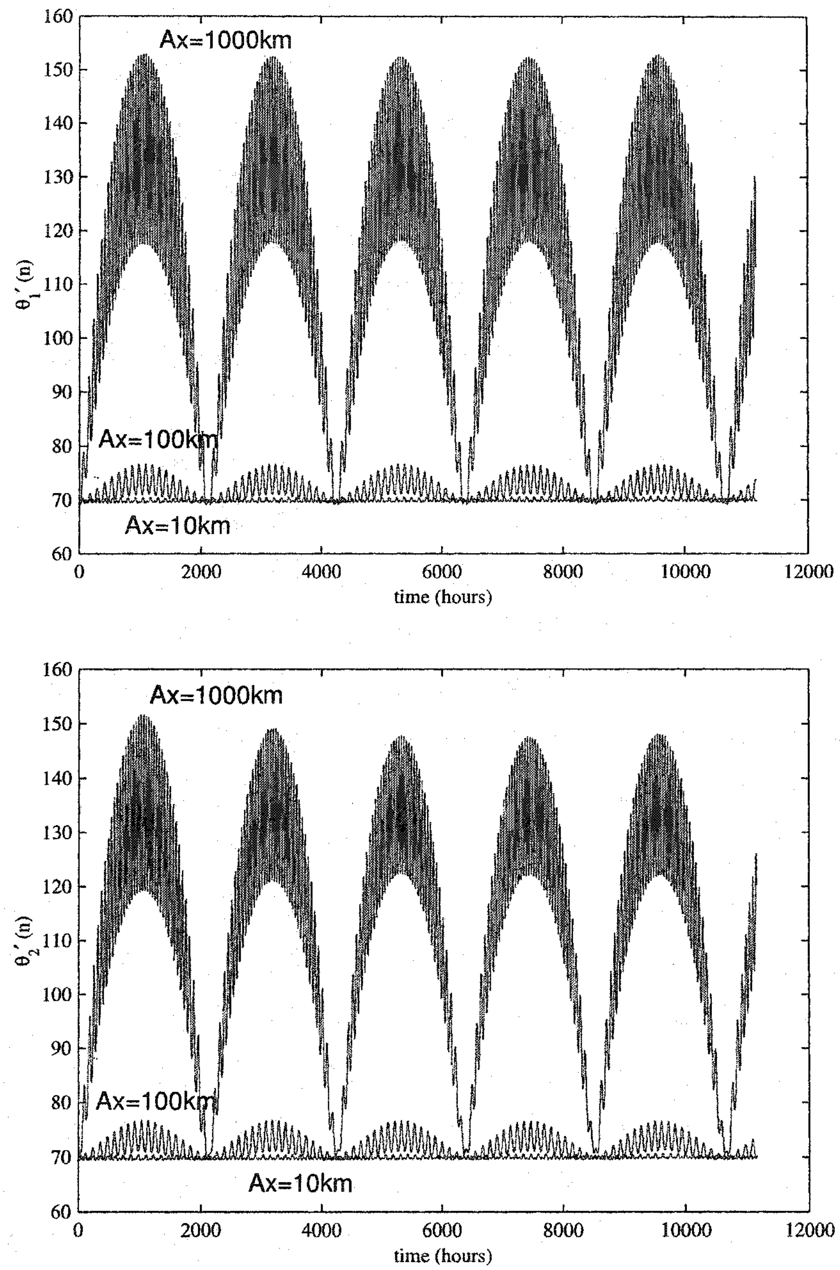

Figure 3.13 In-Plane Tether Angular Velocities, $\dot{\theta}(0)=70n$

Figures 3.9 to 3.13 indirectly hint that the amplitudes of the out-of-plane tether librations can be reduced by increasing $\dot{\theta}(0)$. The amplitudes of the high and low frequency librations tend to diminish as the tether's angular velocity increases for all sized orbits, with the high frequency librations becoming less distinct and more integrated with the overall librations. The variations of the in-plane angular velocities are also diminished. The flip side to this increased stability is that the frequency of the high frequency librations would become even higher. To illustrate this pattern, system dynamics with different initial in-plane angular velocities were simulated for A_x=10 km. Figures 3.14 and 3.15 show how the amplitudes of the out-of-plane librations and the variations of tether angular velocities decrease for increasing initial angular velocity. The initial in-plane angular velocities are 10n, 20n and 50n and the initial out-of-plane displacements are 5 degrees from the equilibrium positions. Maximum ϕ excursions from $\pi/2$ is a bit more than 40 degrees when $\dot{\theta}(0)$ is 10n, but slightly less than 10 degrees when $\dot{\theta}(0)$=50n. The same pattern can be seen when the parent mass is in a larger halo orbit. In the A_x = 50 km case, tether librations and angular velocities are shown in Figures 3.16 and 3.17. The initial in-plane-angular velocities are 10n, 30n and 90n and the initial out-of-plane displacements are again ± 5 degrees from equilibrium. Maximum ϕ deviation from the equilibrium value is a bit less than 70 degrees when $\dot{\theta}(0)=10n$, but around 8 degrees when $\dot{\theta}(0)=90n$. The same pattern is seen again for the A_x=1000 km halo orbit case, as can be seen in Figures 3.18 and 3.19. The initial in-plane angular velocities this time are 50n and 150n.

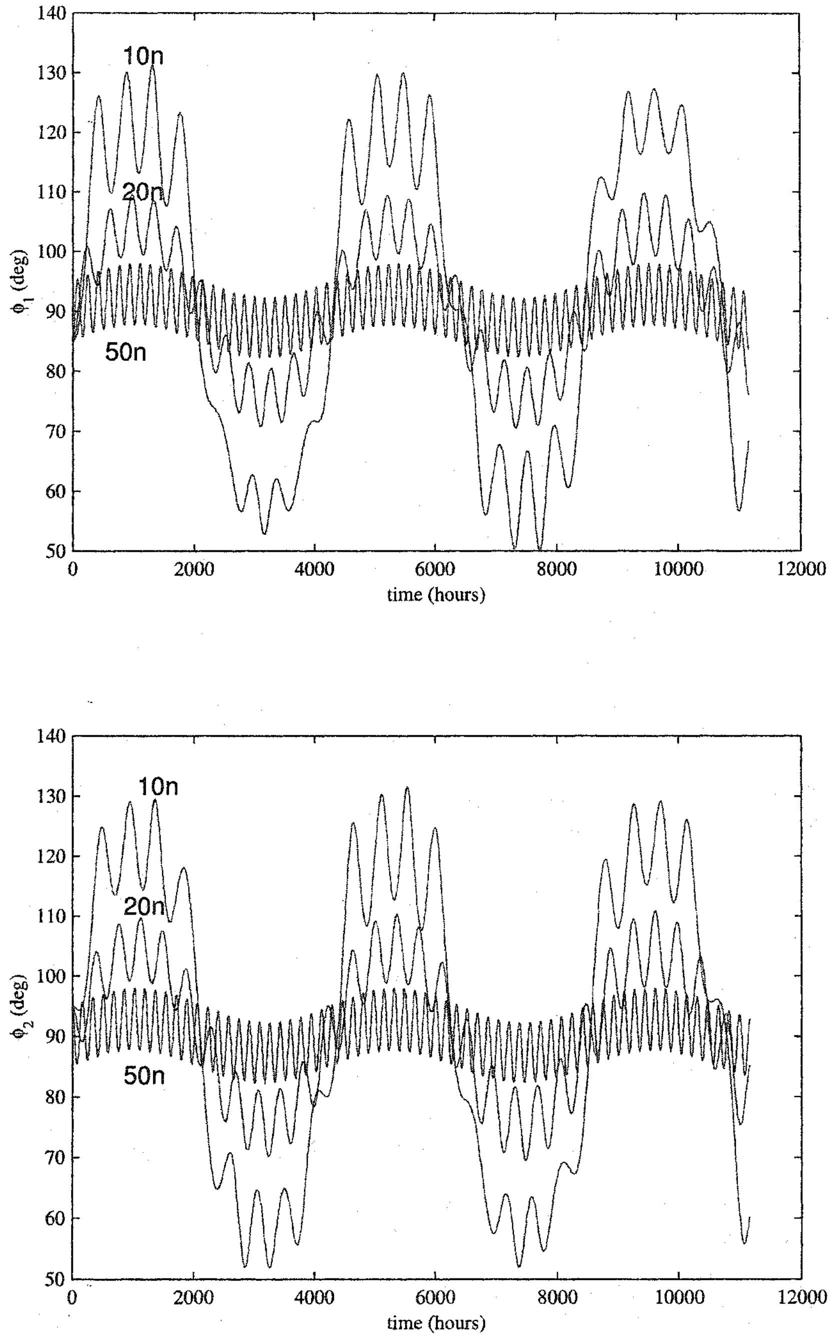

Figure 3.14 Out-of-Plane Tether Librations, A_x=10 km Halo orbit

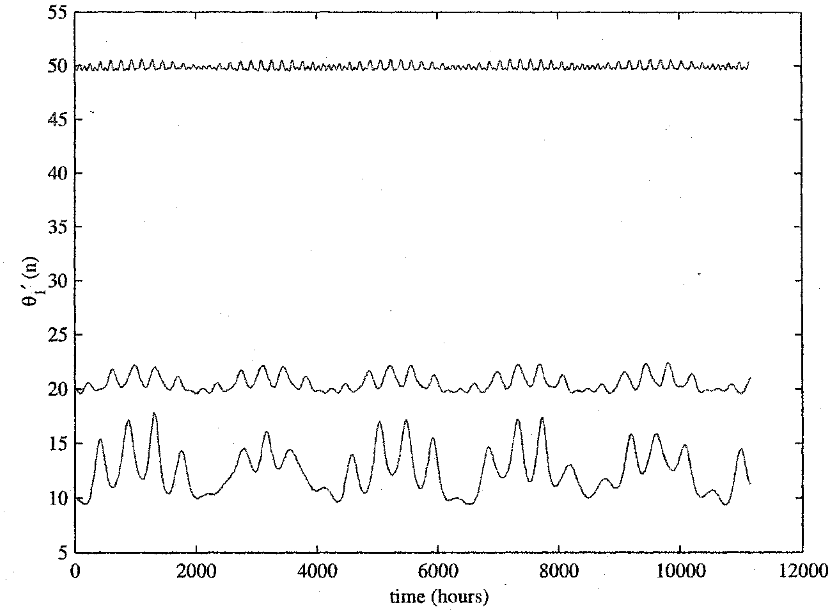

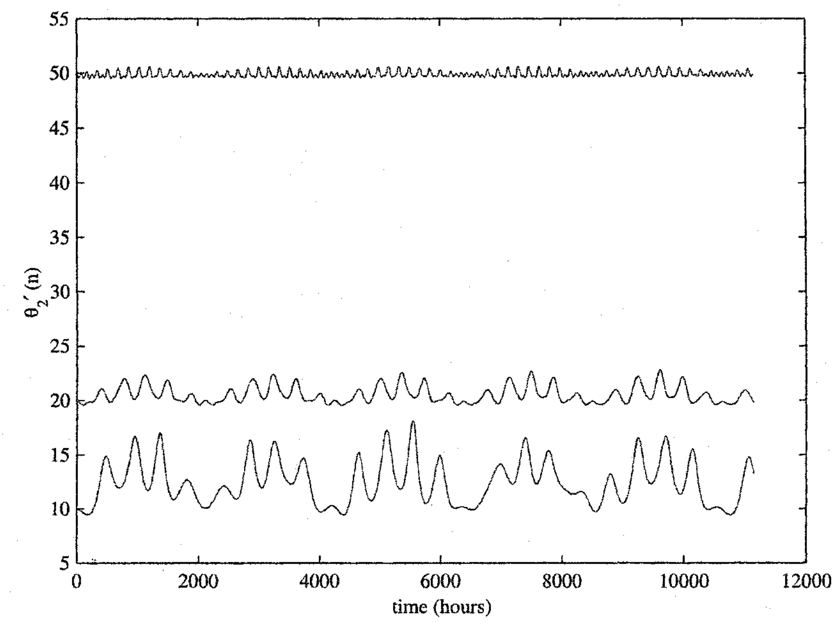

Figure 3.15 Tether Angular Velocities, A_x=10 Halo

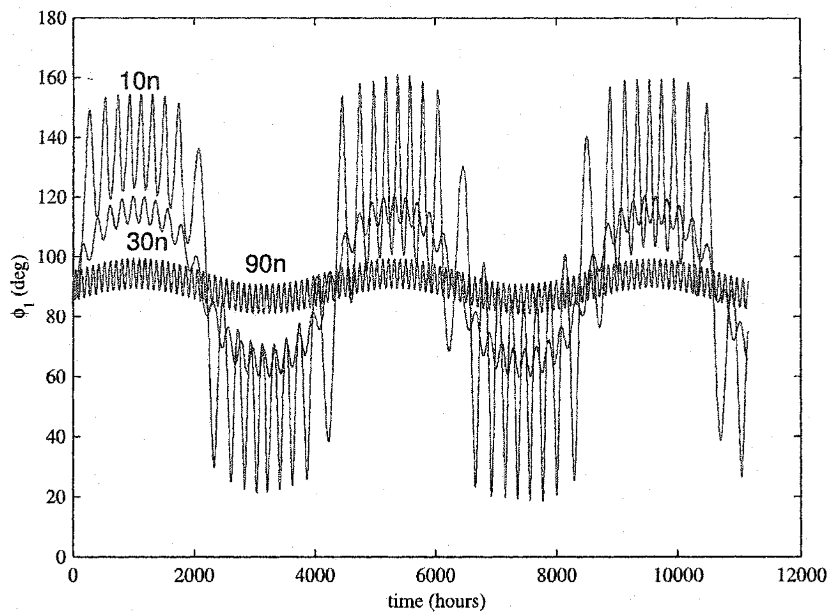

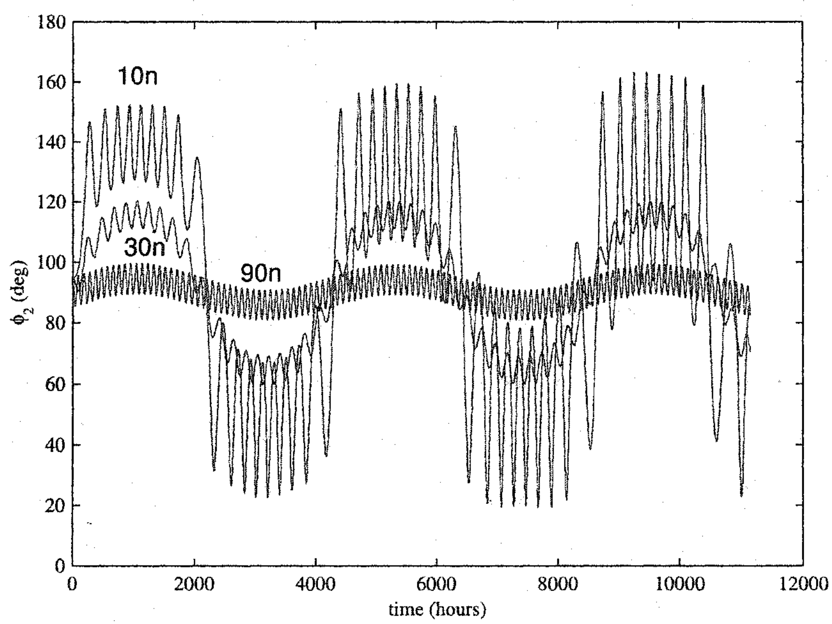

Figure 3.16 Out-of-Plane Tether Librations, A_x=50 km Halo

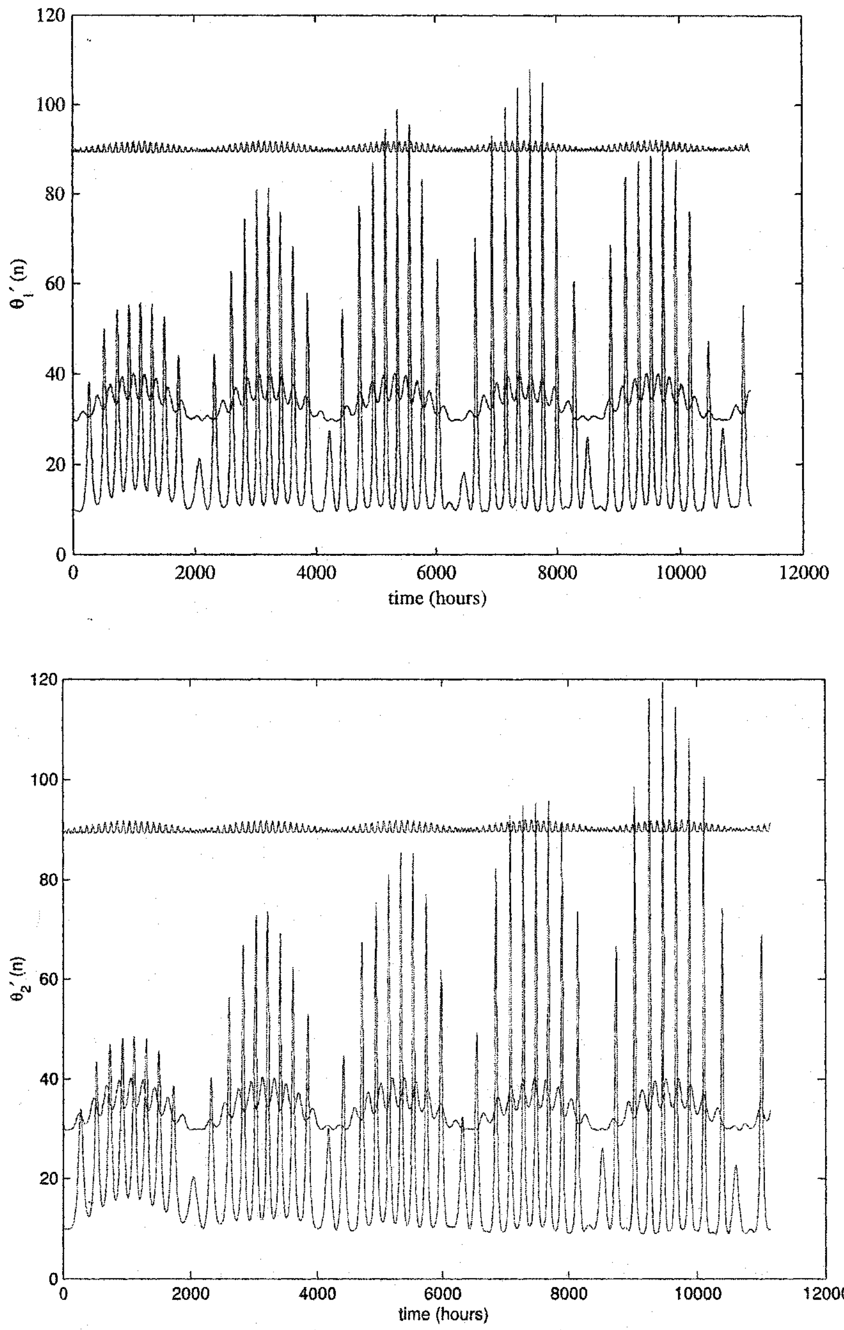

Figure 3.17 Tether Angular Velocities, A_x=50 km halo

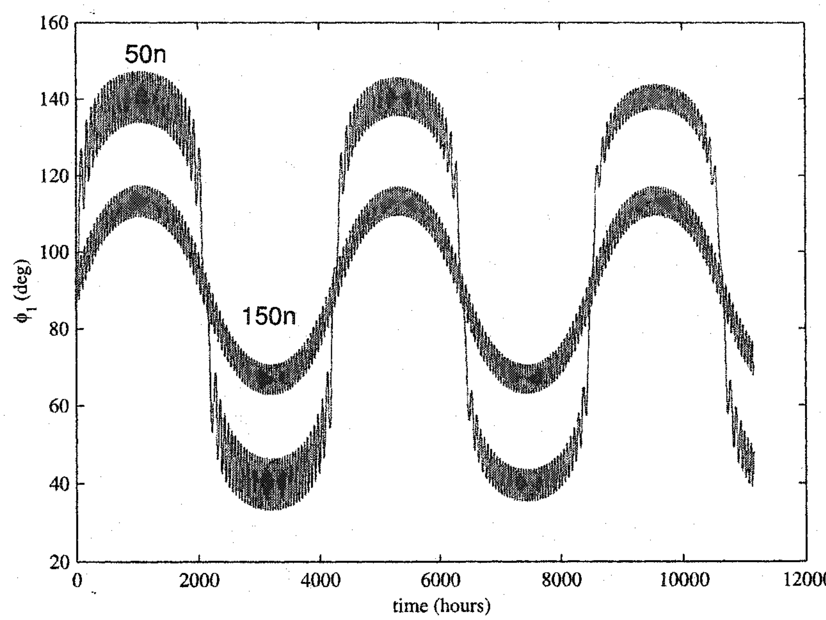

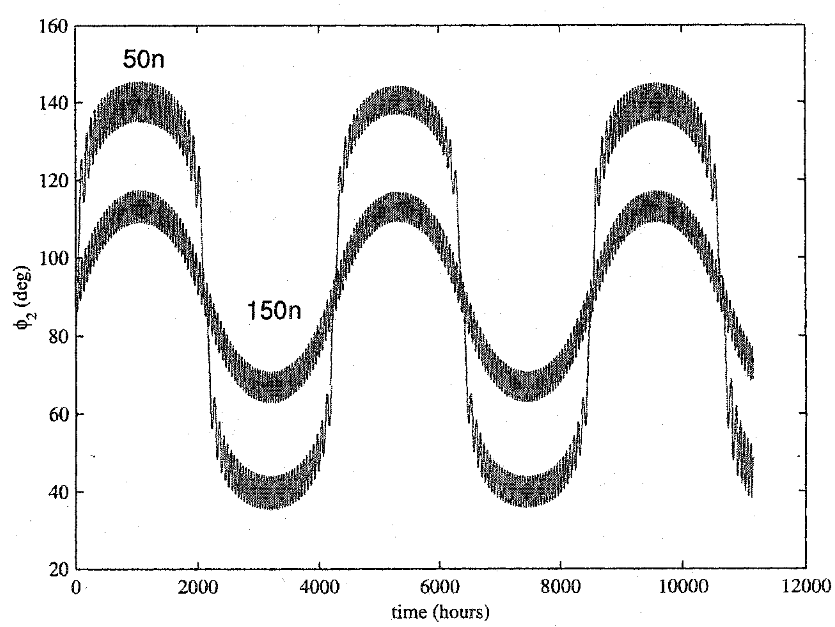

Figure 3.18 Out-Of-Plane Tether Librations, A_x=1000 km

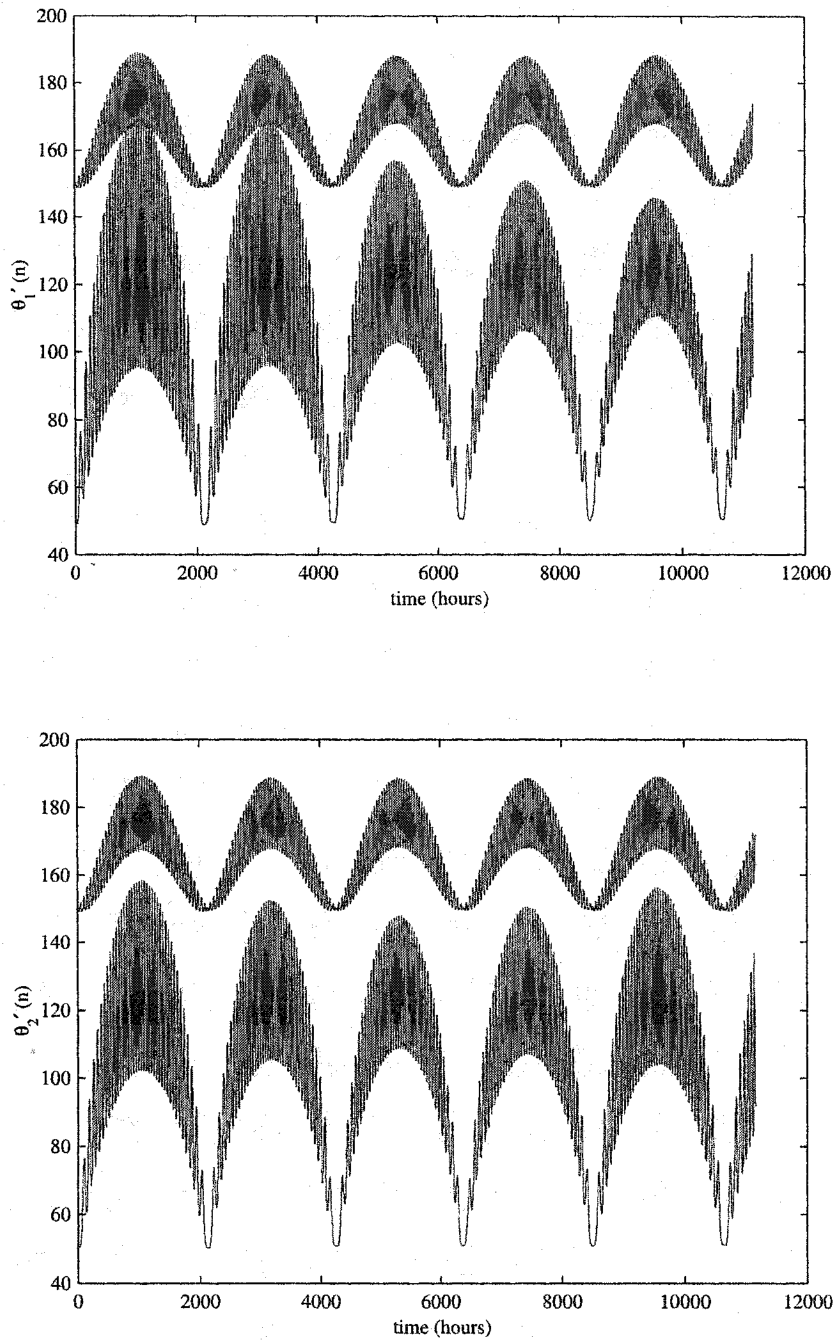

Figure 3.19 In-Plane Angular Velocities, A_x=1000 km Halo

In theory, the tether librations can be flattened out with a sufficiently high spin rate. In practice, however, the maximum spin rate is limited by several factors such as the material strength of the tethers, the observational requirements of the interferometer and the fuel requirements.

The results of the numerical simulations in this chapter show that an uncontrolled tethered system is unsuitable for use as an orbiting interferometer Control strategies are needed for both parent mass motions and tether librations and chapter 4 would go into those topics in more detail.

Chapter 4

CONTROL OF MULTI-TETHERED SYSTEMS AT SUN-EARTH L_2

4.1 Control System Design

As was seen in the previous chapter, the tethered system, like a single satellite, is unstable when placed at a collinear Lagrangian point and some form of control must be applied if it is to perform some useful function. Given the way the numerical simulation was set up, it is easier to integrate a time domain state feedback controller into the simulator than a classical frequency based design. An LQR controller was chosen to calculate the gains.

4.2 State Feedback Controller:

Dynamical systems theory allows one to reduce the behaviour of a system near a fixed point to a linear time invariant problem in the form of

$$\dot{\mathbf{x}} = \mathbf{A}\mathbf{x} + \mathbf{B}\mathbf{u} \tag{4.1}$$

where $\mathbf{x}$ is the state vector, $\mathbf{u}$ is the input vector, $\mathbf{A}$ is the state transition matrix and $\mathbf{B}$ is the input selection matrix. If the matrix $\mathbf{A}$ has eigenvalues on the right hand side of the complex plane, i.e. positive real parts, the system is unstable as the states would grow exponentially. The goals of a controller are to first stabilize the system and then impart some desired response characteristics by moving the eigenvalues to some desired location on the closed left half side of the complex plane. In a state feedback control system, the state vector **x** is multiplied by a gain matrix **K** and fed back into the control input,

$$\mathbf{u} = -\mathbf{K}\mathbf{x} \tag{4.2}$$

The closed loop system then becomes

$$\dot{\mathbf{x}} = (\mathbf{A} - \mathbf{K}\mathbf{B})\mathbf{x} \tag{4.3}$$

If the system is controllable, then selecting an appropriate **K** matrix could modify the closed loop eigenvalues and therefore change the dynamics of the controlled system.

There are two main types of state feedback controllers: Pole Placement and Linear Quadratic Regulator (LQR). Pole Placement controllers attempt only to influence the closed loop poles of the linear system, without regards to the amount of effort required. The Linear Quadratic Regulator can be optimized both in terms of performance and control effort required. In this thesis the LQR controller is chosen to stabilize the motions of the tethered system.

4.3 Linear Quadratic Controller:

The LQR controller calculates **K** in a way such that the linear quadratic performance index

$$J = \frac{1}{2}\int_0^\infty \left(\mathbf{x}^T\mathbf{Q}\mathbf{x} + \mathbf{u}^T\mathbf{R}\mathbf{u}\right)dt \tag{4.4}$$

is minimized. **Q** is the state weighting matrix and **R** is the control input weighting matrix. **K** can be calculated using

$$\mathbf{K} = \mathbf{R}^{-1}\mathbf{B}^T\mathbf{P} \tag{4.5}$$

where **P** is obtained by solving the algebraic Riccati equation

$$0 = \mathbf{A}^T\mathbf{P} + \mathbf{P}\mathbf{A} - \mathbf{P}\mathbf{B}\mathbf{R}^{-1}\mathbf{B}^T\mathbf{P} + \mathbf{Q} \tag{4.6}$$

Several conditions must be satisfied for a unique positive-definite solution to the Riccati equation. **Q** must be symmetric and positive semi-definite, **R** must be symmetric positive definite, and the system must be controllable and observable. Increasing the weights in **R** produces a **K** matrix with more emphasis on reducing the control effort required, while cranking up the **Q** matrix minimizes the error signal. While it is certainly desirable to both minimize the error signal and the required control effort, this is far from what is possible in a normal situation. It is up to the designer to choose a balance that would satisfy those two somewhat conflicting goals.

4.4 Goals of the Control System in TSS:

The proposed control system of the tethered system must accomplish two goals: stabilize the motion of the parent mass in the vicinity of L_2, and control the observation axis of the interferometer, $\boldsymbol{\eta}$, which is perpendicular to the plane of tether rotation. Since the motions of the parent mass and of the tethers are coupled, the two goals are not as distinct as it first appears.

A fuel-efficient way of stabilizing the motions of the parent mass is to put it in a halo or Lissajous trajectory as described in chapter 1. As shown in chapter 3 the dynamics of the parent mass in a tethered system are not very different from those of a single body, and well known methods can be used to control the parent mass either on its own or as part of the overall system. Since the tether librations depend on the motions of the parent mass, the latter is included as a part of the overall control system developed here. The reference parent mass trajectories, as described in section 1.9, are

$$x = -A_x \sin\left(\omega_{xy} t\right) \tag{4.7}$$

$$y = -A_y \cos\left(\omega_{xy} t\right) \tag{4.8}$$

$$z = A_z \sin\left(\omega_z t\right) \tag{4.9}$$

In order to use the tethered system as an astronomical interferometer, the system must have an ability to orientate its observation axis. This is done by changing the plane of tether rotation relative to the [*X Y Z*] axes. A normal telescope is pointed by specifying a desired set of azimuth and elevation angles relative to the inertial axes. These angles are defined as α for elevation and γ for azimuth in this thesis. Similarly, the desired observation axis of the space interferometer, $\boldsymbol{\eta}_d$, can also be specified in terms of its azimuth and elevation angles relative to the Sun-Earth line and the ecliptic plane (Figure 4.1). In the [*X Y Z*] axes, the desired observation axis can be written as

$$\boldsymbol{\eta}_d = \cos\gamma\cos\alpha\mathbf{i} + \sin\gamma\cos\alpha\mathbf{j} + \sin\alpha\mathbf{k} \tag{4.10}$$

Since the system has two independent tethers, there are actually two planes of rotations and two normal vectors. The task of the control system is to vary θ_i and ϕ_i in a way such that both tethers are spinning in the same plane and the normal vector of that plane matches up to the desired $\boldsymbol{\eta}$. The normal axis to the i^{th} tether's plane of rotation can be written in terms of the tether rotation angles:

$$\boldsymbol{\eta}_i = -\cos\theta_i\cos\phi_i\mathbf{i} - \sin\theta_i\cos\phi_i\mathbf{j} + \sin\phi_i\mathbf{k} \tag{4.11}$$

When the two end masses are rotating in the same plane, the normal vector of that plane is labelled $\boldsymbol{\eta}$. The free librations of the tethers while the parent mass is occupying a halo orbit is described in chapter 3 and are determined to be unsuitable for astronomical applications. Without control, the overall tether librations do not trace out a defined plane of rotation, but rather cones. In order to ensure that the tethers are spinning in the desired plane and the normal vector of that plane is parallel to $\boldsymbol{\eta}_d$, a set of time dependent control goals must be developed.

The two tethers are assumed to be spinning at a constant desired rate $\dot{\theta}_d$. Controlling the elevation of the plane of rotation is fairly simple. One tether must be at ϕ_{max} while the other is at ϕ_{min}, and half a revolution later the libration angles are reversed. ϕ_{max} and ϕ_{min} are calculated from the desired elevation angle of the $\boldsymbol{\eta}_d$ vector. Controlling the azimuth angle of the plane of rotation in terms of tether libration angles is more complex. One tether, say tether 1, must be at ϕ_{max} when $\theta_1 = \gamma$, and at the other end tether 2 must be at ϕ_{min} when $\theta_2 = \gamma + \pi$. Half a revolution later, tether 2 will be at ϕ_{min} while tether 1 will be at ϕ_{max}. Figure 4.2 shows the location of the tethers when the system is frozen at $\theta_1 = \gamma$. The up and down motions of the tethers are harmonic in nature, so a cosine function was the reference function for the out-of-plane libration angles. The control goals for a 3-body system are:

$$\theta_1(t) = \dot{\theta}_d t \tag{4.12}$$

$$\theta_2(t) = \dot{\theta}_d t \tag{4.13}$$

$$\phi_1(t) = \frac{\pi}{2} + \left(\frac{\pi}{2} - \alpha\right)\cos\left(\gamma - \theta_1(t)\right) \tag{4.14}$$

$$\phi_2(t) = \frac{\pi}{2} + \left(\frac{\pi}{2} - \alpha\right)\cos\left(\gamma - \theta_2(t)\right) \tag{4.15}$$

where $\dot{\theta}_d$ is the desired in-plane angular velocity relative to the [*X Y Z*] axes. The above conditions ensure that when $\theta_1 = \gamma$ and $\theta_2 = \gamma + \pi$, $\phi_1 = \max(\phi_1) = \pi - \alpha$ and $\phi_2 = \min(\phi_2) = \alpha$. Recall that ϕ_i is relative to the Z-axis.

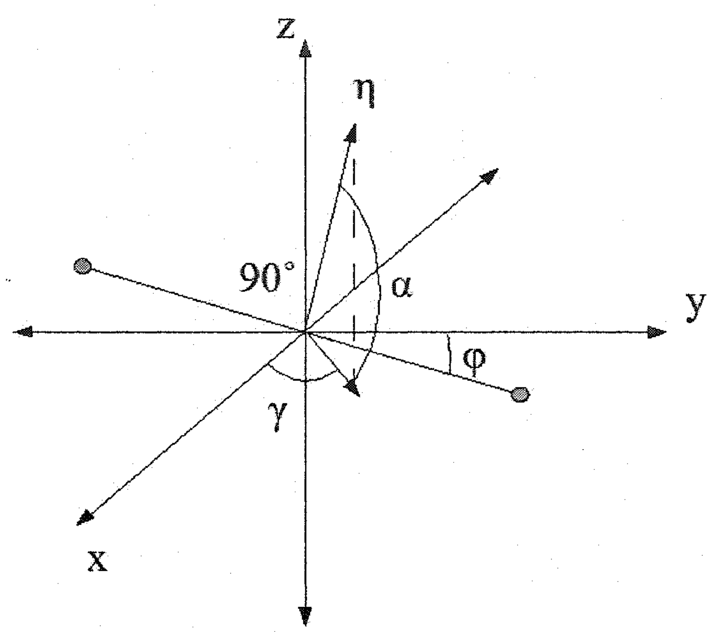

Figure 4.1 Geometry of the Observation Axis

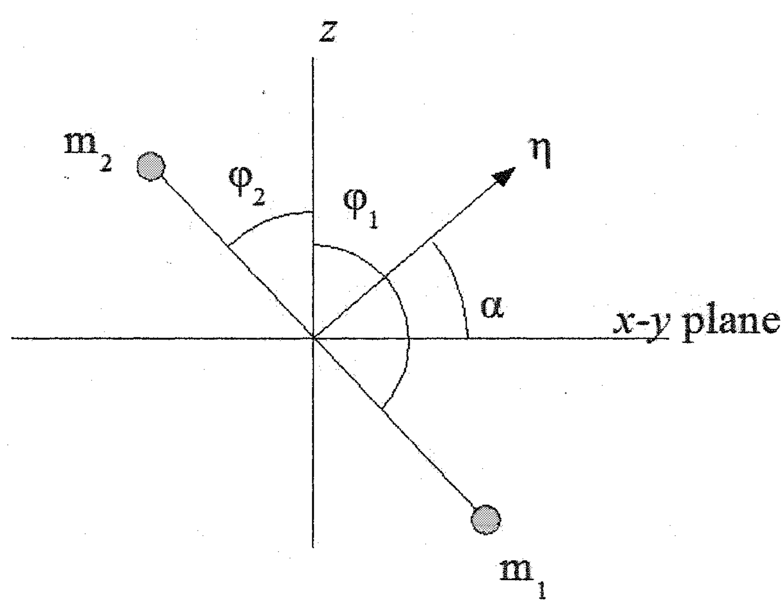

Figure 4.2 Control Goal Geometry when θ = γ

It is assumed that thrusters attached to the parent mass are aligned along the **i**, **j** and **k** directions and those mounted on two end masses are along the y and z axis in the body frame. Since the masses are assumed to be point masses, effect of these control thrusts on the attitude of the three bodies is not an issue in this thesis.

While it is desirable for $\boldsymbol{\eta}$ to point exactly as intended, this is not practicable in reality. Given the nonlinear dynamics of the system as well as other perturbations (which are not modeled), a more reasonable goal for the satellite control system is to get $\boldsymbol{\eta}$ within a certain level of tolerance and let the finer mirror control mechanisms do the rest.

4.5 Implementation of Proposed Control System

The design is of a simple feedback type. The desired trajectories of the parent mass and end masses are generated based on the control goals stated in the above section. These are subtracted by the outputs of the plant and the gain matrix K generated by the LQR controller multiplies the resulting error signal. The control signals are then fed into the plant. It is assumed that the full state is available.

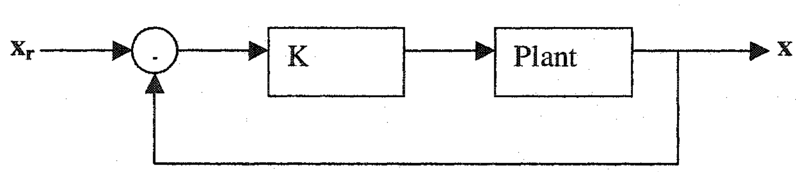

Figure 4.3 Block Diagram of the Proposed Control System

There is one small twist. Good results depend on having an accurate linear system representation of the nonlinear equations and linear system theory states that this representation is only accurate within the neighbourhood of the state where the equations are linearized about. Since both the parent mass and the tethers are commanded to follow certain trajectories, any single linear system considered at a particular time would be outdated very quickly. While it is mathematically possible to constantly update the linear system and the associated **K** at every moment this involves a lot of extra work and is usually not desirable. A compromise solution is to use Gain Scheduling, which is a fancy way of saying let **K** be recalculated periodically using an updated linear system. The designer can choose the time interval between **K** updates. Appendix A has a better description of how to calculate the linear system for any arbitrary time.

4.6 Results

After the Gain Scheduling LQR controller was integrated into the numerical model of the 3-body tethered system, a series of simulations were performed with varying dimensions of the halo/Lissajous trajectory and tether spin rate. The goals of the simulation are to determine 1) whether it is possible to control the tethered system, 2) the performance of the control system for different size orbits and tether angular velocities, and 3) the amount of ΔV required both to maintain the desired trajectory and tether librations. The equations of motion solved were nondimensional, and the results were later re-dimensionalized for presentation. The integrator used is again ODE45, with the default tolerances. In all cases, tether lengths were fixed at 1 km and all three tethered bodies have the same mass. The parameters are set to simulate system dynamics around L_2 of the Sun-Earth Lagrangian point and with ω_{xp}

and ω_z calculated using a method given by Bong Wie[24], which works out to be ω_{xp} =2.0571n and ω_z =1.9851n. The dimensions of the periodic reference orbit are measured in kilometers. A new gain matrix **K** is calculated every 0.2/n based on the most recent state. The values of α and γ are 85 and 10 degrees, respectively.

The simulations were performed for A_x equal to 10 km, 100 km or 1000 km for halo and Lissajous trajectories and $\dot{\theta}_d = 10n$ or 30n, where n is the rate of rotation of the Sun-Earth system. A typical set of parent mass commands for the halo orbit can be seen in Figures 4.4 and 4.5. A plot of a model Lissajous trajectory is presented in Figure 4.6. Note that the Lissajous trajectory does not close. A set of tether libration commands corresponding to the parent mass commands is shown in Figure 4.7 and the resulting end mass trajectories are on Figure 4.8. To start off, the system was commanded to follow a model halo orbit with A_x = 10 km, $A_y = A_z = kA_x = 31.8732$ km with the tether angular velocity $\dot{\theta}_d = 10n$. The behaviour of the system with this setup would serve as a basis of comparison for the performance of the control system under various conditions. The ΔV cost associated with control will be discussed in the next section. When everything is working properly, the parent mass is in its assigned trajectory and the plane of tether rotation remains fixed at its desired orientation. The normal vectors of the tethers, $\boldsymbol{\eta}_i$, point in the direction of the observation axis without wobbling. As the tether librations deviate from their command values, the planes of rotation of the two tethers wobble and their normal vectors no longer point straight and traces out a trajectory. The larger the departure, the more pronounced the wobble. For the baseline case, the error signal can be seen in Figures 4.9 and 4.10. The resulting plane of rotation can be seen in Figure 4.11. For this value of A_x, increasing the spin rate did not affect the system dynamics much except for an increase in the ΔV required as a result of gyroscopic stiffening. As A_x increases from 10 km to 100 km to 1000 km for the same commanded tether angular velocities, the displacements of the parent mass remain stable and close to the desired vales but the tether librations became increasingly harder to control and the wobble becomes more pronounced. This can be seen in Figure 4.12 to Figure 4.17. An interesting thing to note is that for $A_x = 1000$ km, the tether libration controls are no longer consistent as the error signals for tether 1 are much greater than those for tether 2. The reason for this difference is unknown at the moment, but a good place to begin the investigation is the starting positions of the tethers. One tether begins closer to the gravitational sources than the other does and the initial difference in the potential energy of the end masses could affect the final result. Increasing $\dot{\theta}_d$ with A_x again does not improve the controller's performance as the increased gyroscopic stiffness of the system makes it even harder to control. Figures 4.18 to 4.20 illustrate this for the case of $A_x = 1000$ km halo orbit, with the tether angular velocity equal to $30n$.

If the system is allowed to follow a Lissajous trajectory, however, much better results can be obtained at a lower cost as can be seen on Figures 4.21 to 4.29. The parent mass again remains in a controlled trajectory and the tether libration error signals are very small even when A_x increases from 10 km to 1000 km for $\dot{\theta}_d = 10n$. As a result, the tether planes of rotation remains stable and the its normal vectors pointed in the correct direction. Increasing the tether spin rate does not increase nor degrade the performance of the controller except that the ΔV cost is increased. An example of this can be seen on Figures 4.30-4.32 for the case of the A_x=1000 km with $\dot{\theta}_d = 30n$. The Lissajous trajectory results are comparable to the baseline case and are much better than those when the parent mass is placed in a halo orbit. It is important to note that tether libration controls are also not consistent for large size Lissajous trajectories, although not nearly to the same degree as in the halo orbit case.

In the halo orbit cases the tethered system is forced to act against its natural dynamics and this is the primary reason why the control system performs better when the parent mass is following a Lissajous trajectory. Recall from chapter 1 that the natural in-plane frequency of a body in the vicinity of L_2 is different from its out-of-plane frequency, and this applies to the end masses as well as the to the parent mass. Choosing a halo orbit means forcing those two values to match and closing the orbit using control. For small periodic orbits the difference between ω_{xp} and ω_z is not big enough to cause a major difference in the motion of the masses and the control system does not need to put forth a lot of effort to force ω_z match ω_{xp}. For large halo orbits, however, the difference between the natural motions of the system and the trajectories the control system wishes it to follow is great enough, so that substantial effort is required to maintain the halo orbit. While the parent mass can be controlled directly, the end masses are affected through the tether libration angles and the control laws do not take into account the natural dynamics of the end mass. Therefore in large halo orbits, control of the tethers is weaker than desired.

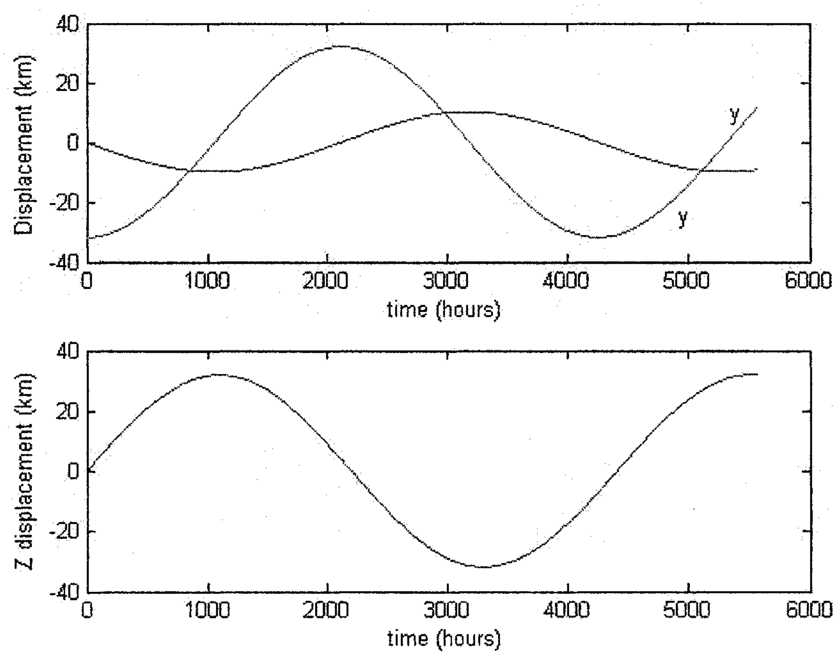

Displacement (km)
40
20
0
-20
-40
0
1000
2000
3000
4000
5000
6000
time (hours)
y
y
Z displacement (km)
40
20
0
-20
-40
0
1000
2000
3000
4000
5000
6000
time (hours)

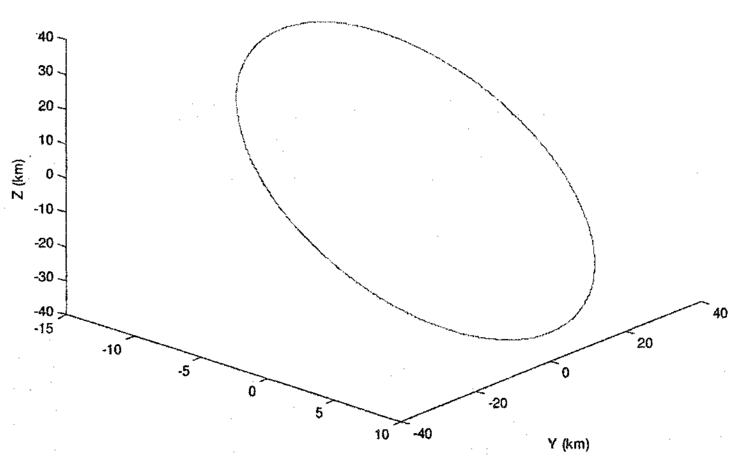

Z (km)
40
30
20
10
0
-10
-20
-30
-40
-15
-10
-5
0
5
10
X (km)
-40
-20
0
20
40
Y (km)

Figure 4.5 Model Parent Mass Trajectory, A_x = 10 km Halo orbit

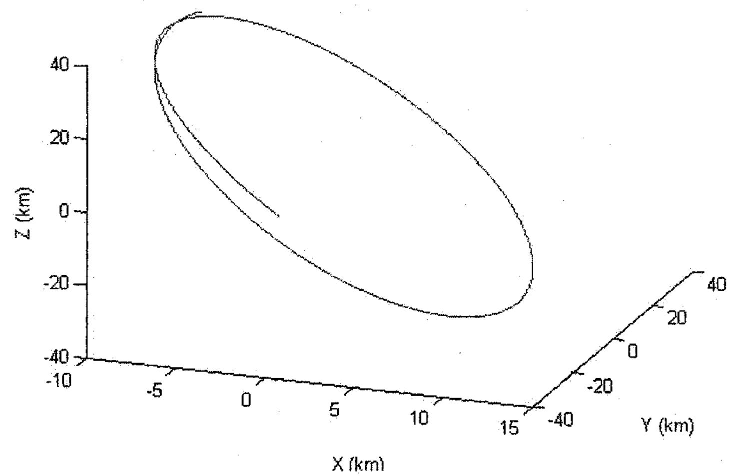

Figure 4.6 Model Parent Mass Trajectory, A_x=10 km Lissajous Trajectory

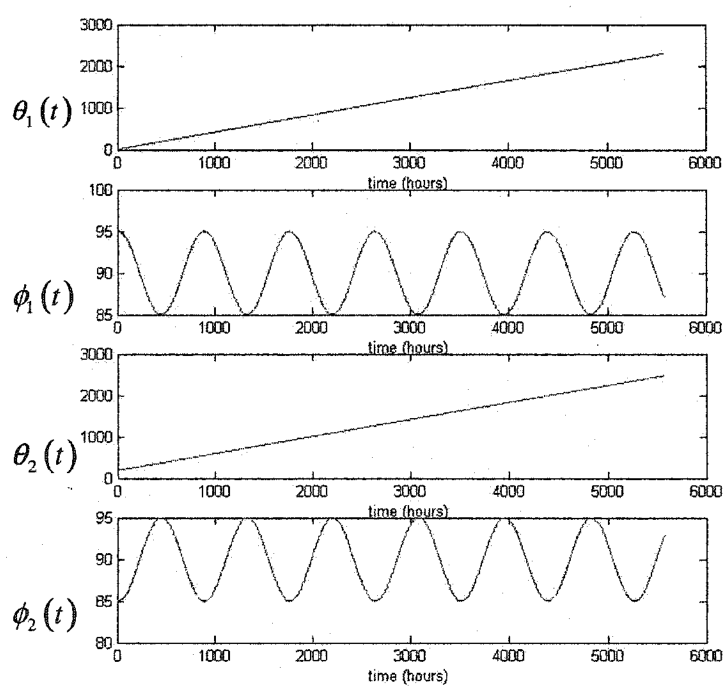

Figure 4.7 Model Tether Librations, A_x = 10 km, Halo orbit

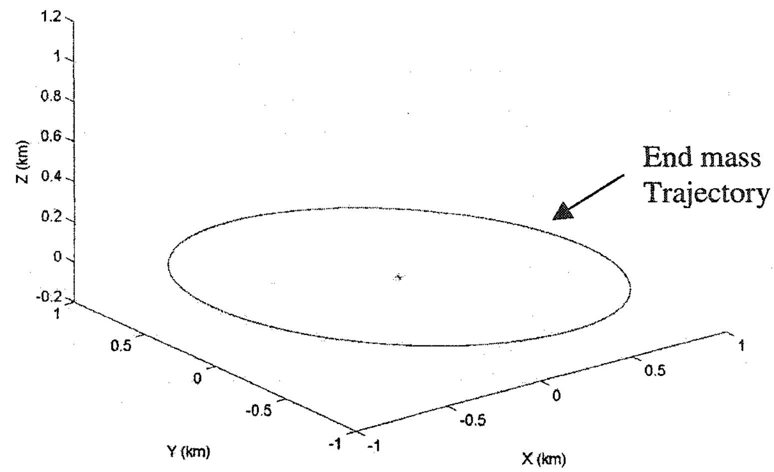

Figure 4.8 Model Tether Plane of Rotation, A_x = 10 km Halo orbit, $\dot{\theta}_d = 10n$

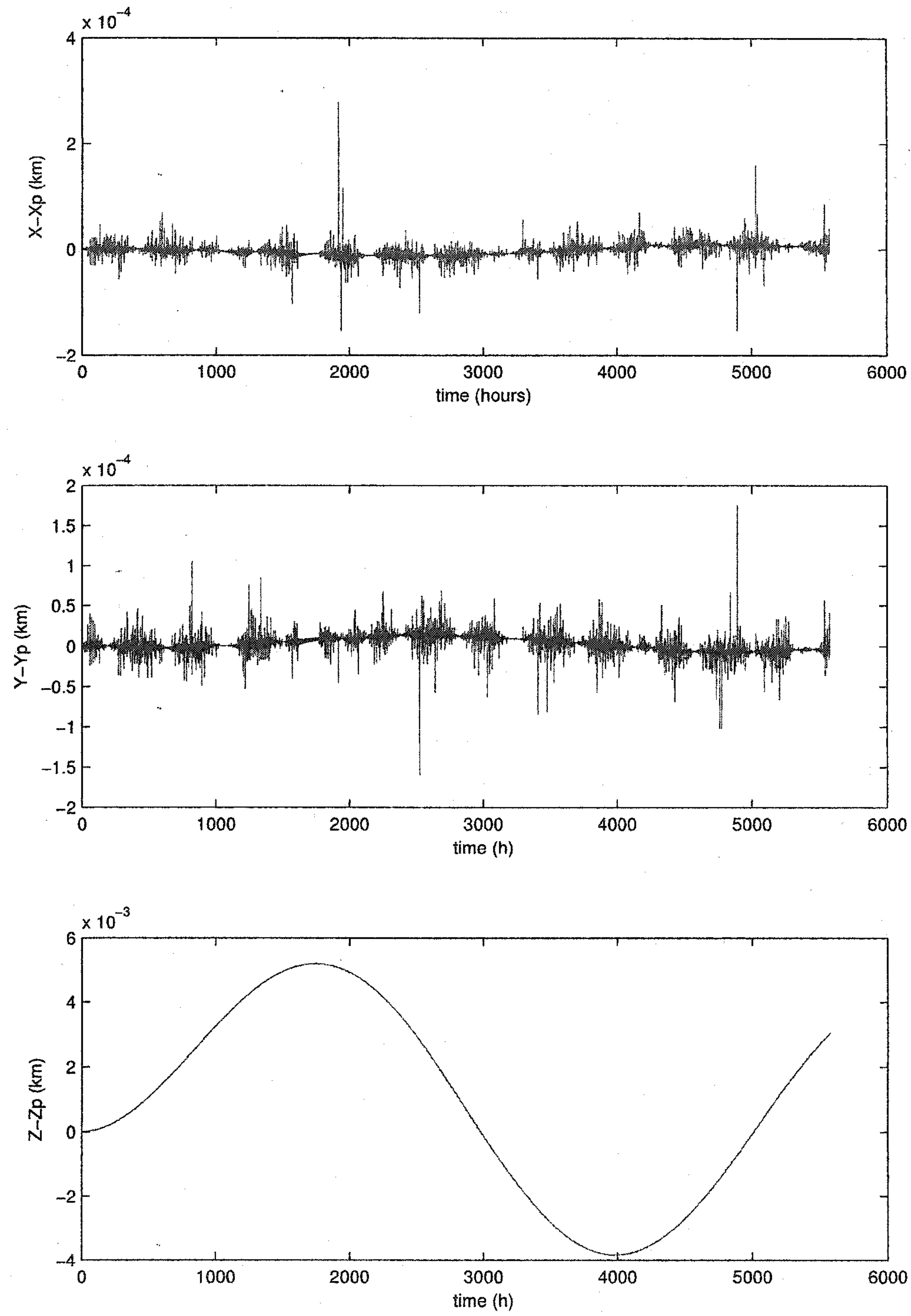

Figure 4.9 Parent Mass Displacement Error Signals, Baseline Case

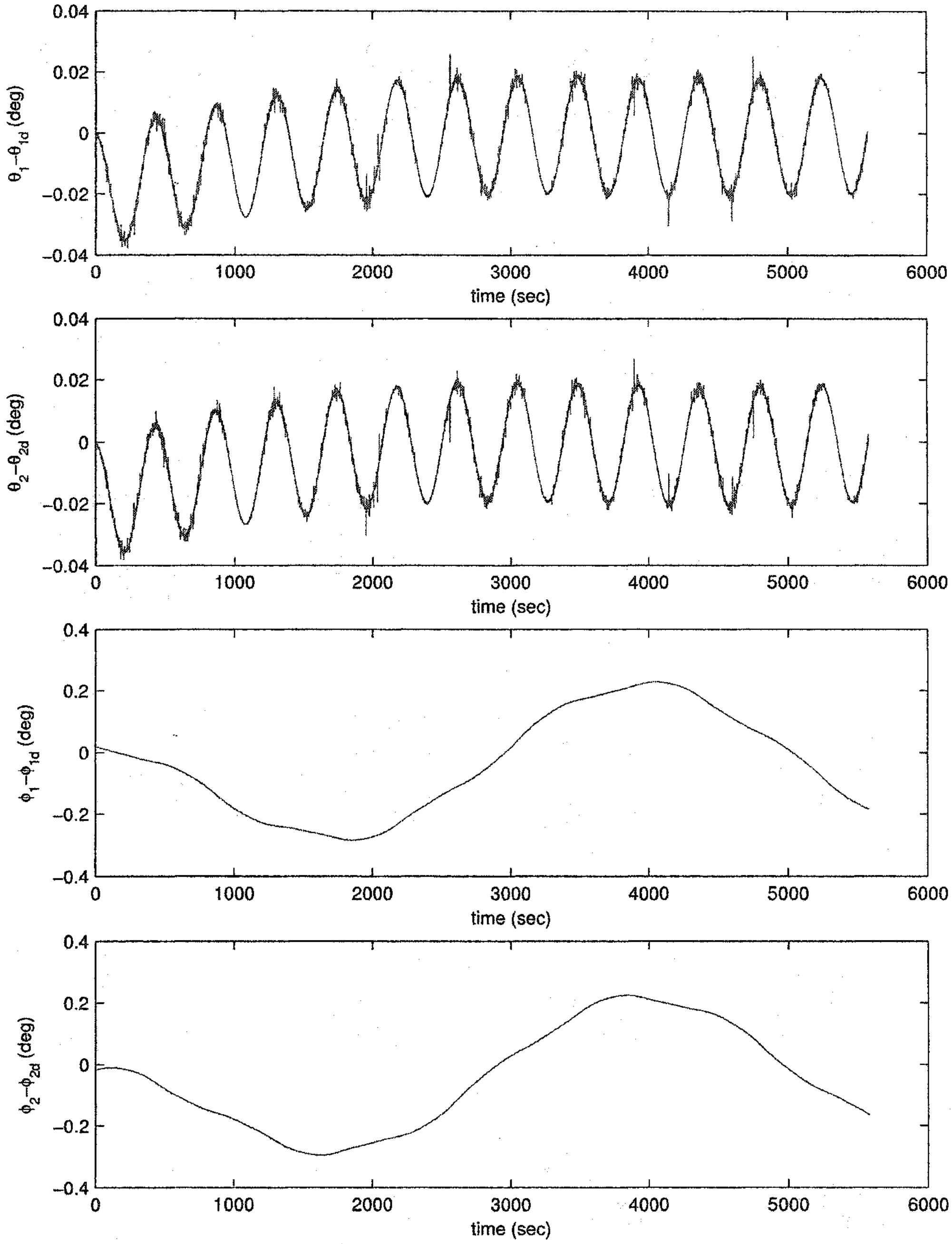

Figure 4.10 Tether Libration Error Signals, Baseline Case

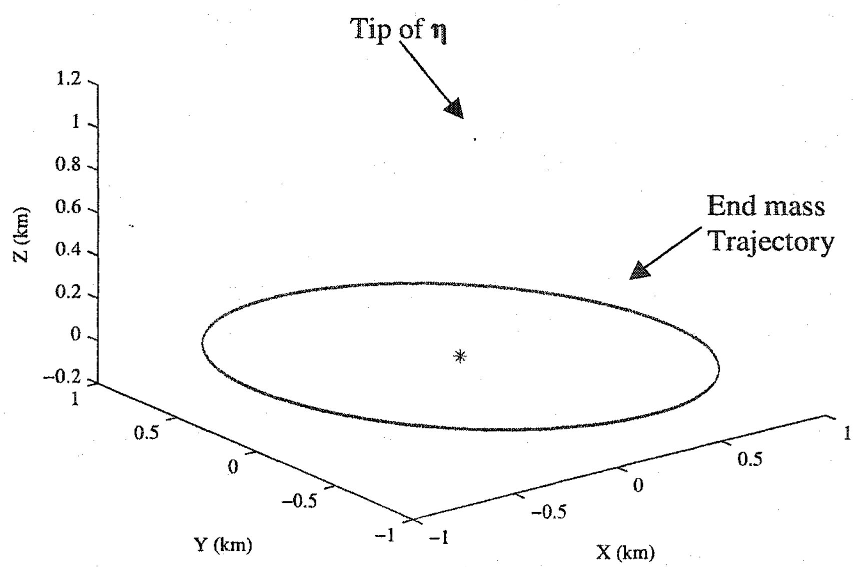

Figure 4.11 Tether Plane of Rotation, Baseline Case

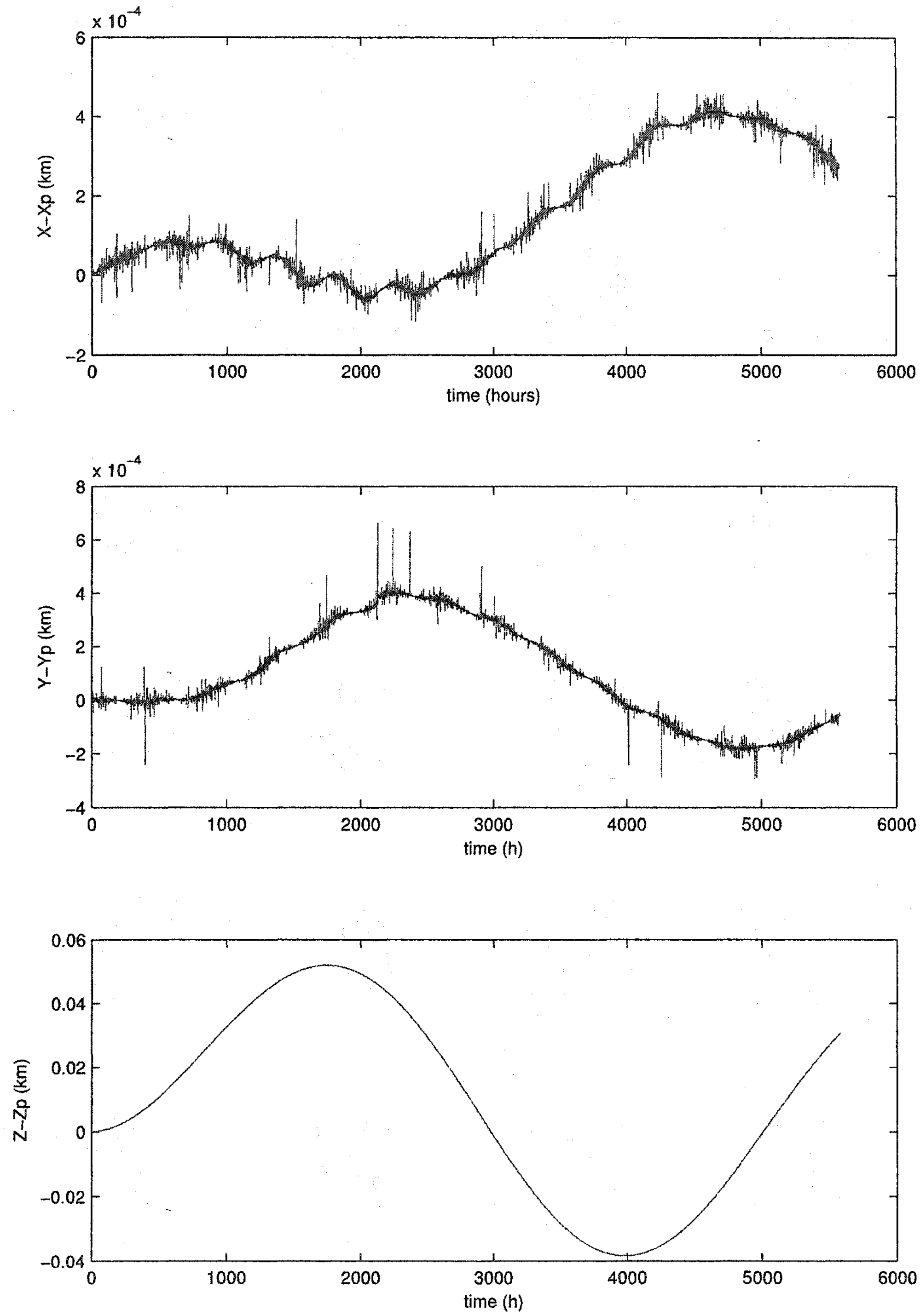

Figure 4.12 Parent Mass Error Signals, A_x=100 km Halo Orbit, $\dot{\theta}_d$ =10n

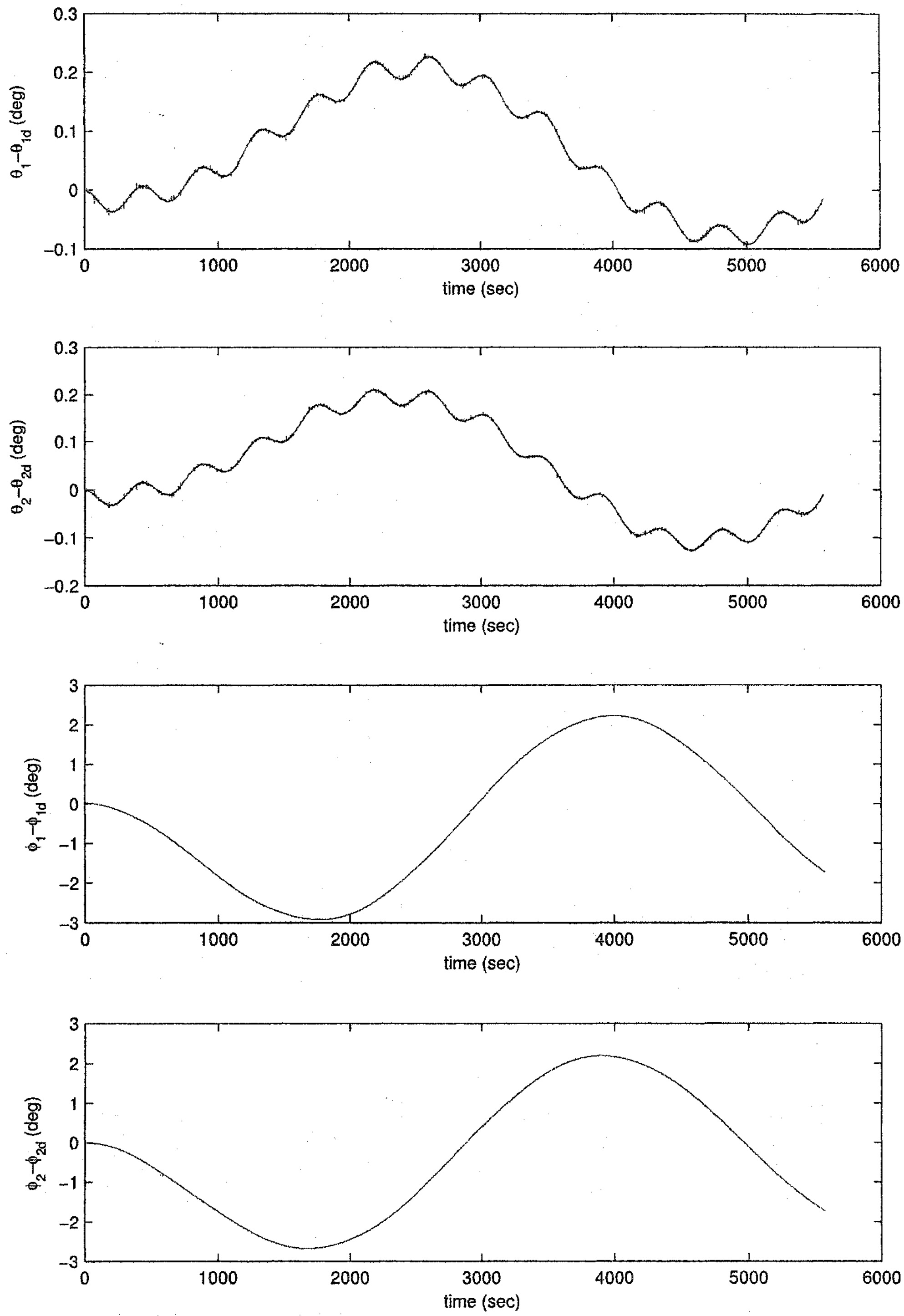

Figure 4.13 Tether Libration Error Signals, A_x=100 km Halo Orbit, $\dot{\theta}_d$ =10n

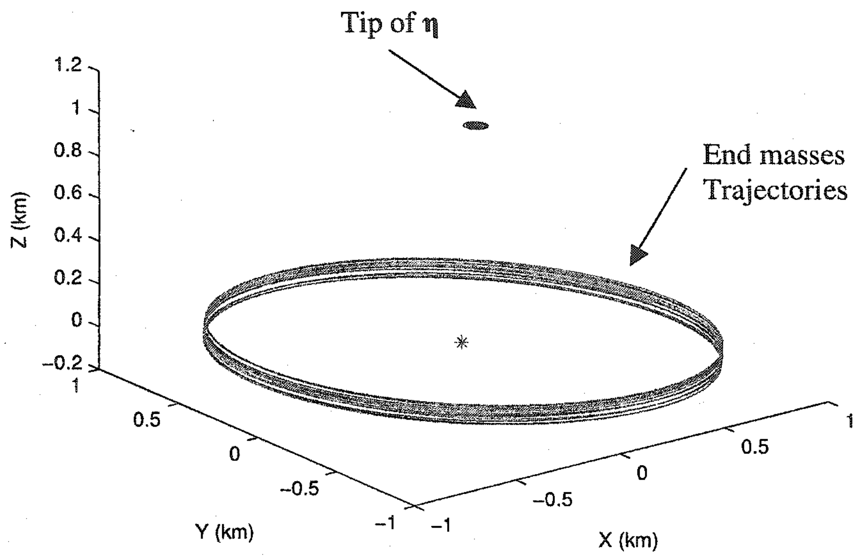

Figure 4.14 Tether Plane of Rotation, A_x=100 km Halo Orbit, $\dot{\theta}_d$ =10n

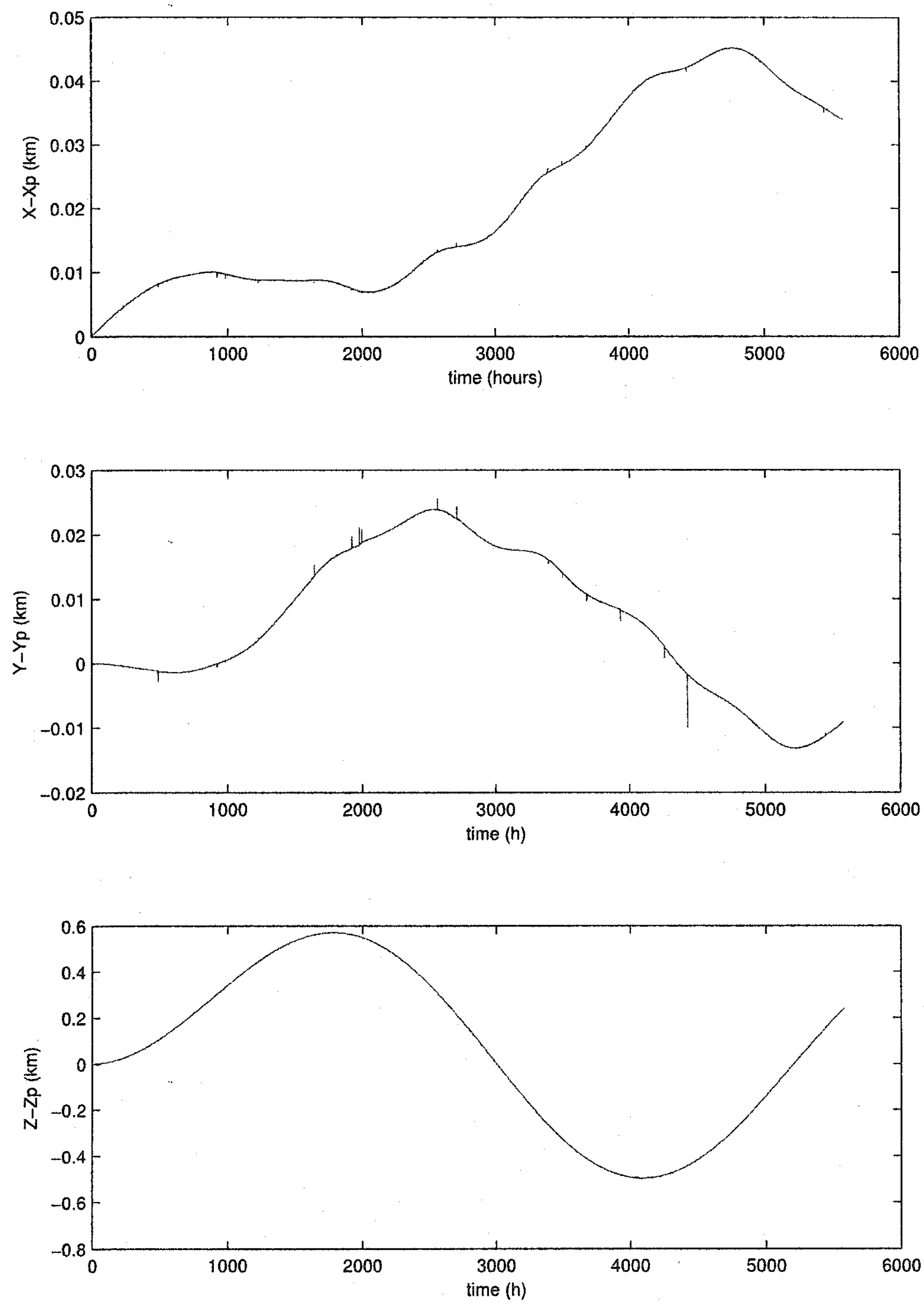

Figure 4.15 Parent Mass Error Signal, A_x = 1000 km Halo orbit, $\dot{\theta}_d$ =10n

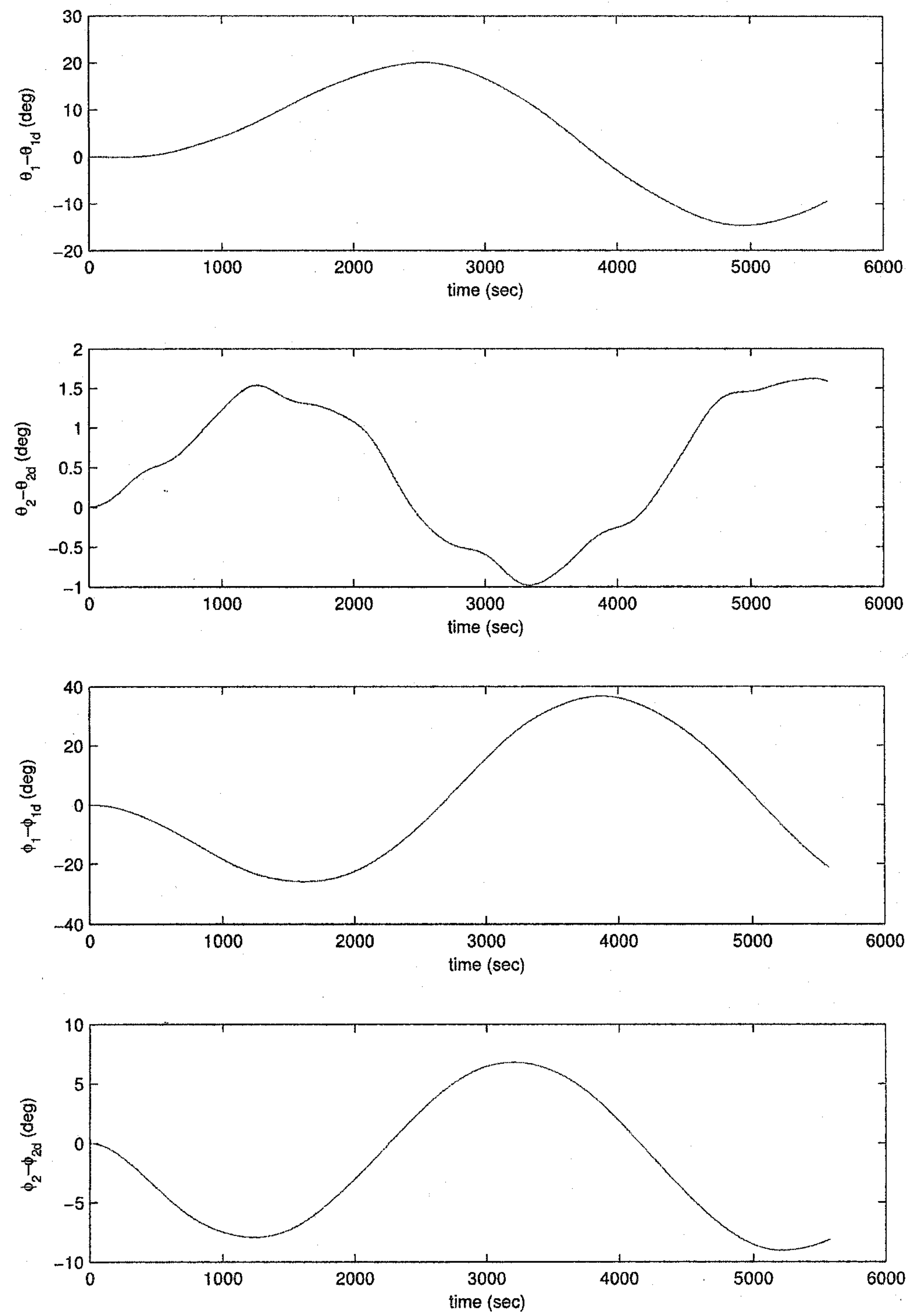

Figure 4.16 Tether Librations Error Signal, A_x = 1000 km Halo orbit, $\dot{\theta}_d$ =10n

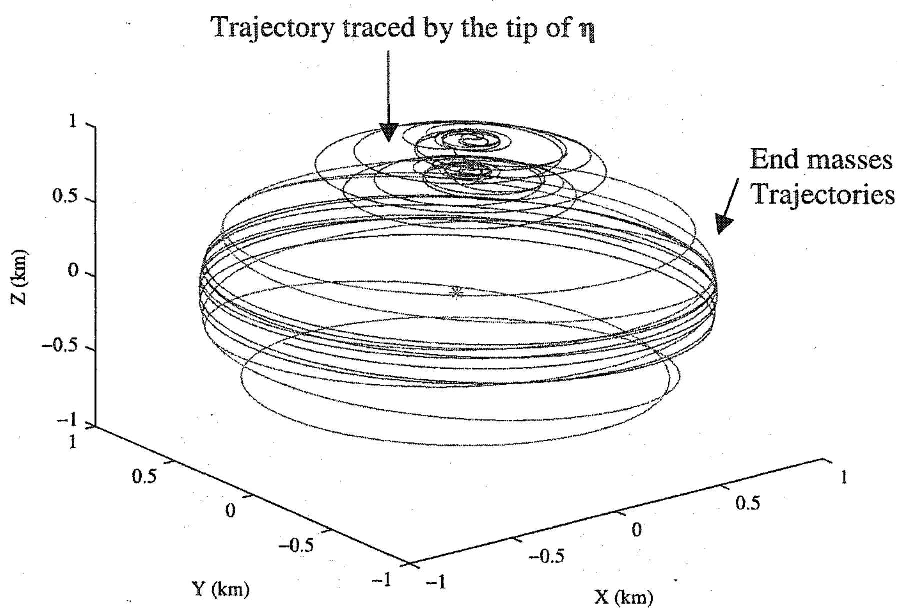

Figure 4.17 Tether Plane of Rotation, A_x = 1000 km Halo orbit, $\dot{\theta}_d$ =10n

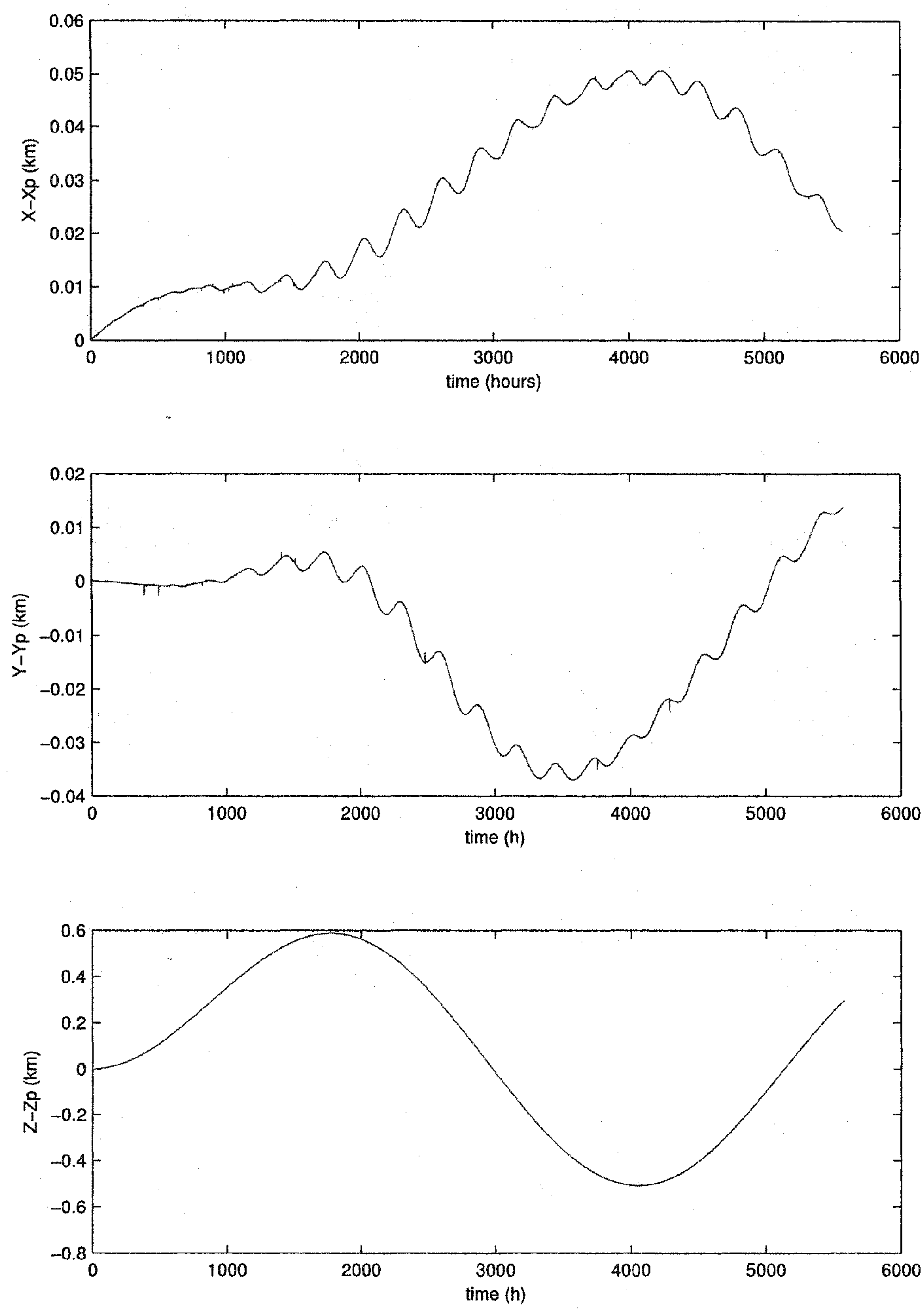

Figure 4.18 Parent Mass Error Signal, A_x = 1000 km Halo orbit, $\dot{\theta}_d$ =30n

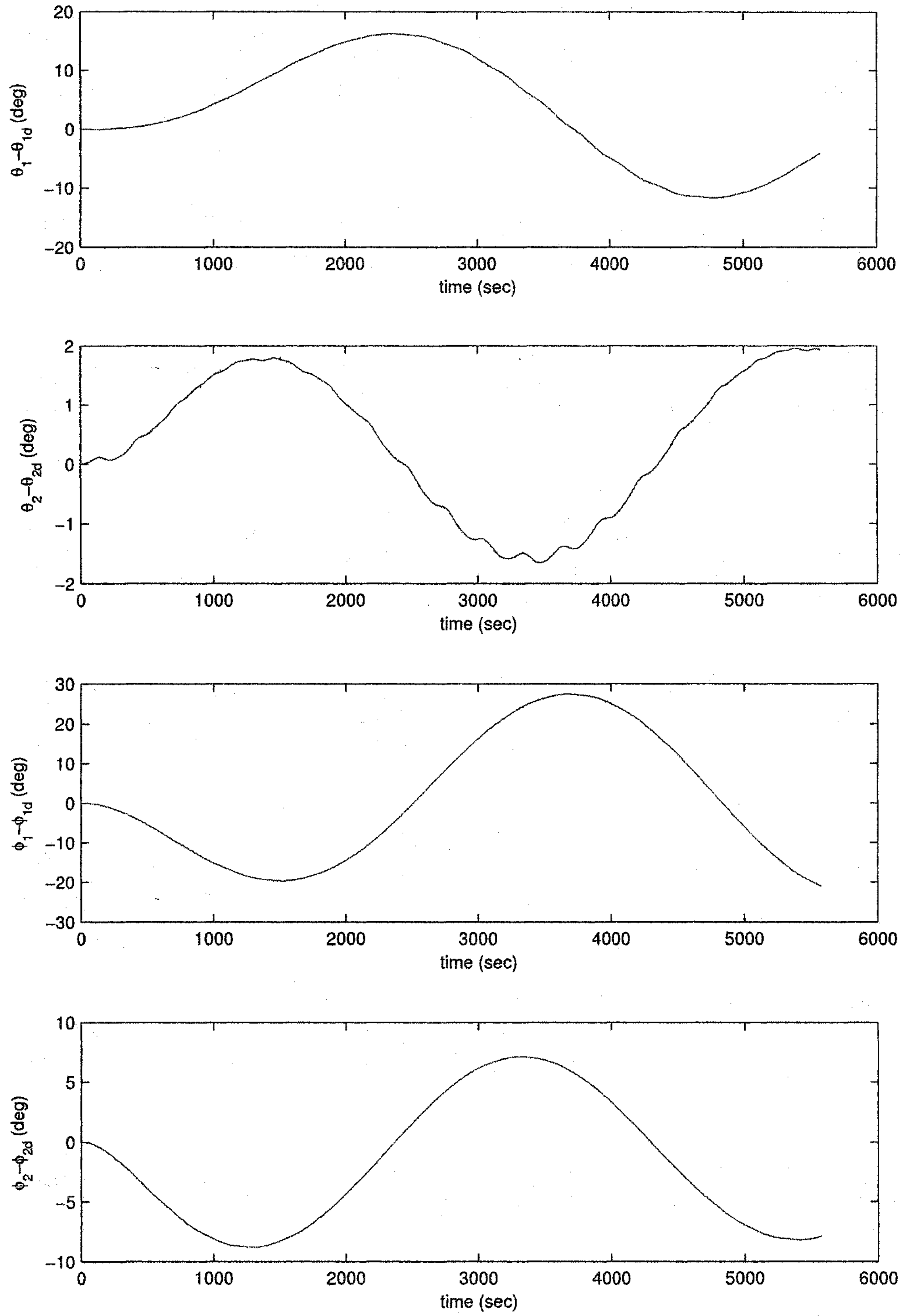

Figure 4.19 Tether Librations Error Signal, A_x = 1000 km Halo orbit, $\dot{\theta}_d$ =30n

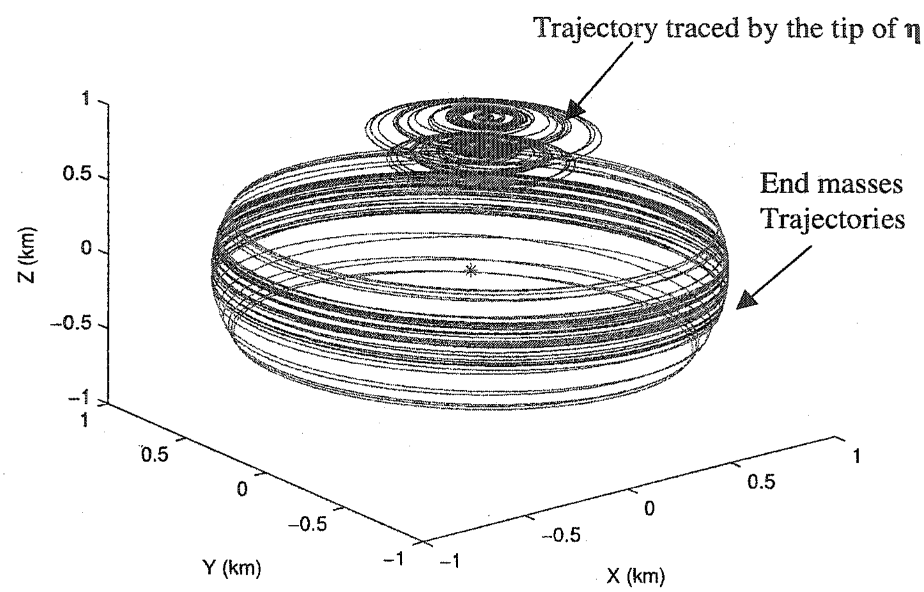

Figure 4.20 Tether Plane of Rotation, A_x=1000 km halo, $\dot{\theta}_d$ =30n

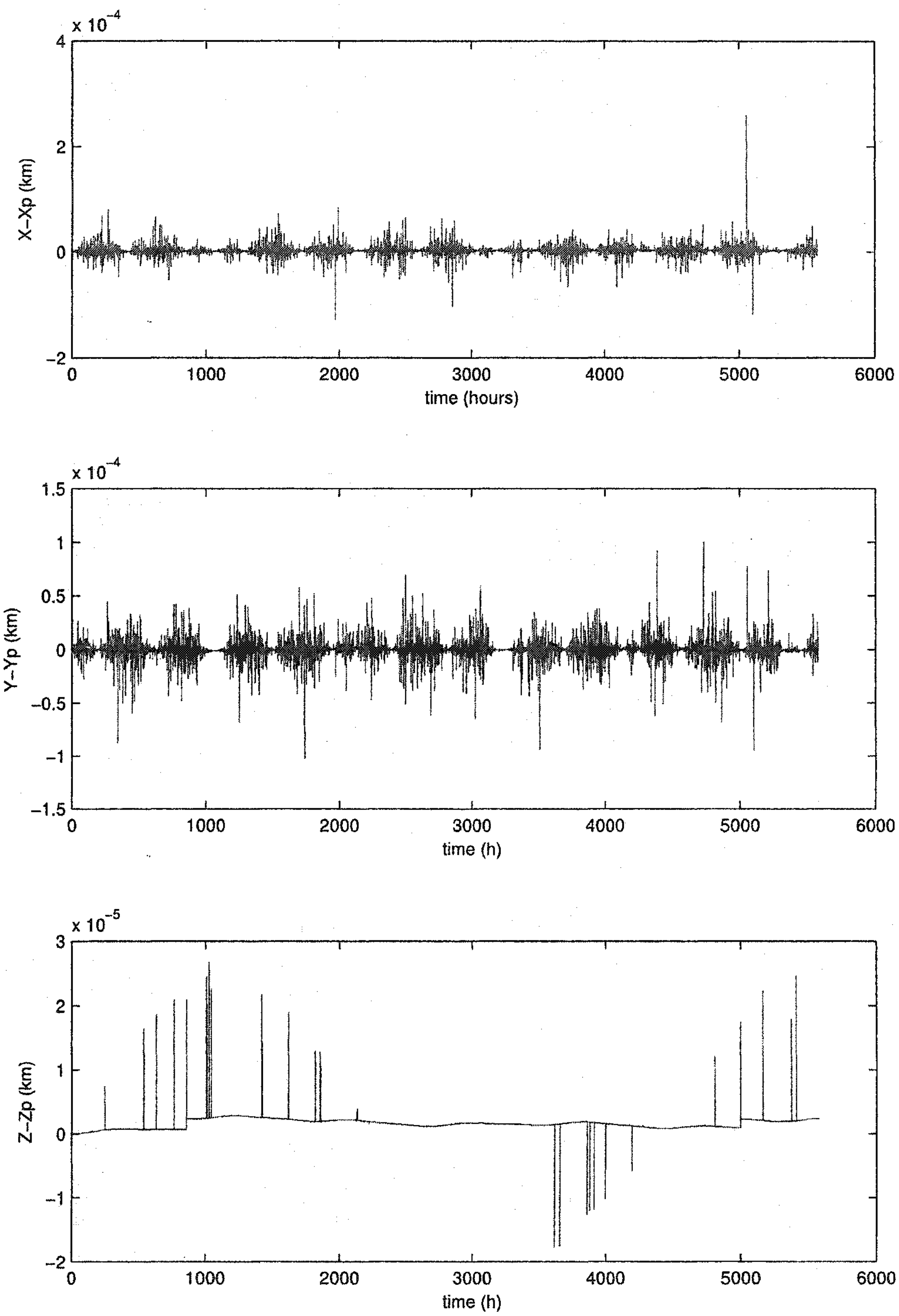

Figure 4.21 Parent Mass Error Signal, A_x=10 km Lissajous Trajectory, $\dot{\theta}_d$ =10n

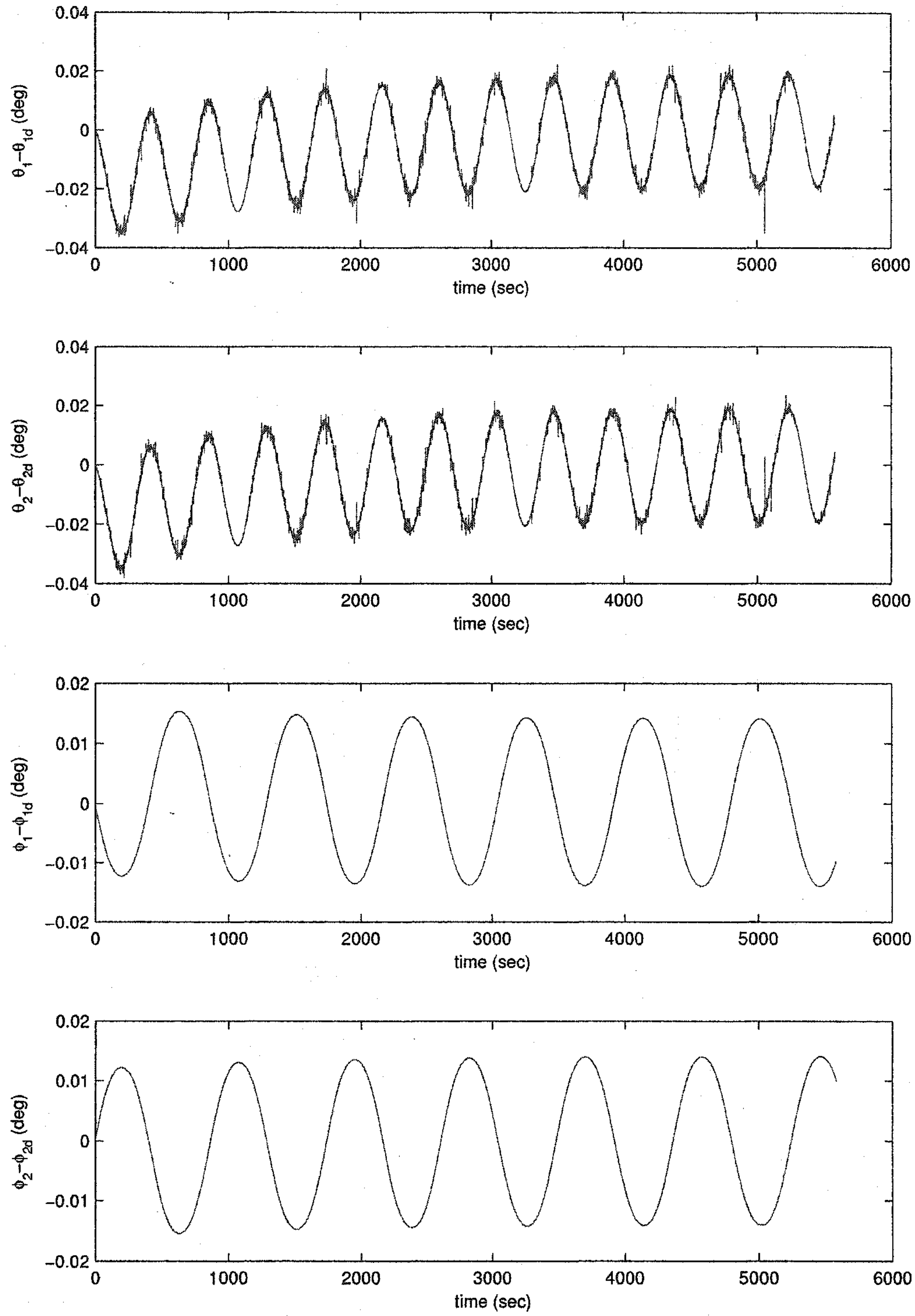

Figure 4.22 Tether Librations Error Signal, A_x=10 km Lissajous Trajectory, $\dot{\theta}_d$ =10n

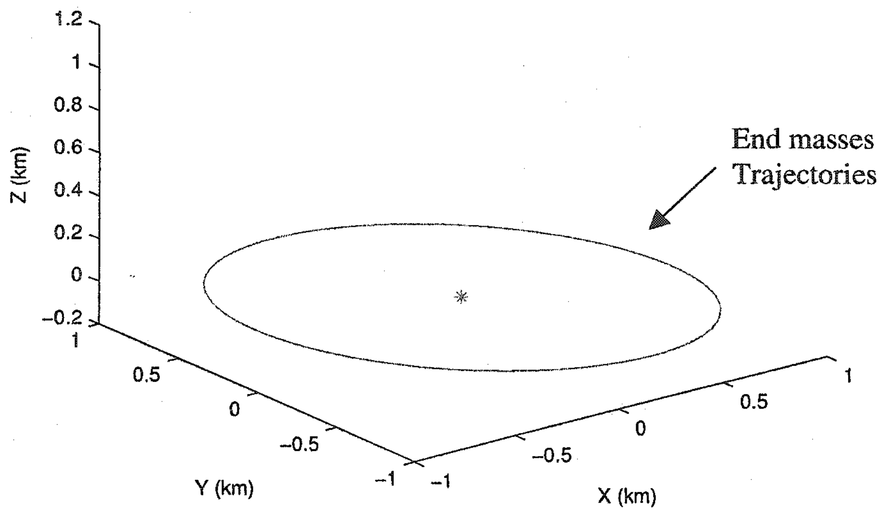

Figure 4.23 Tether Plane of Rotation, A_x=10 km Lissajous Trajectory, $\dot{\theta}_d$ =10n

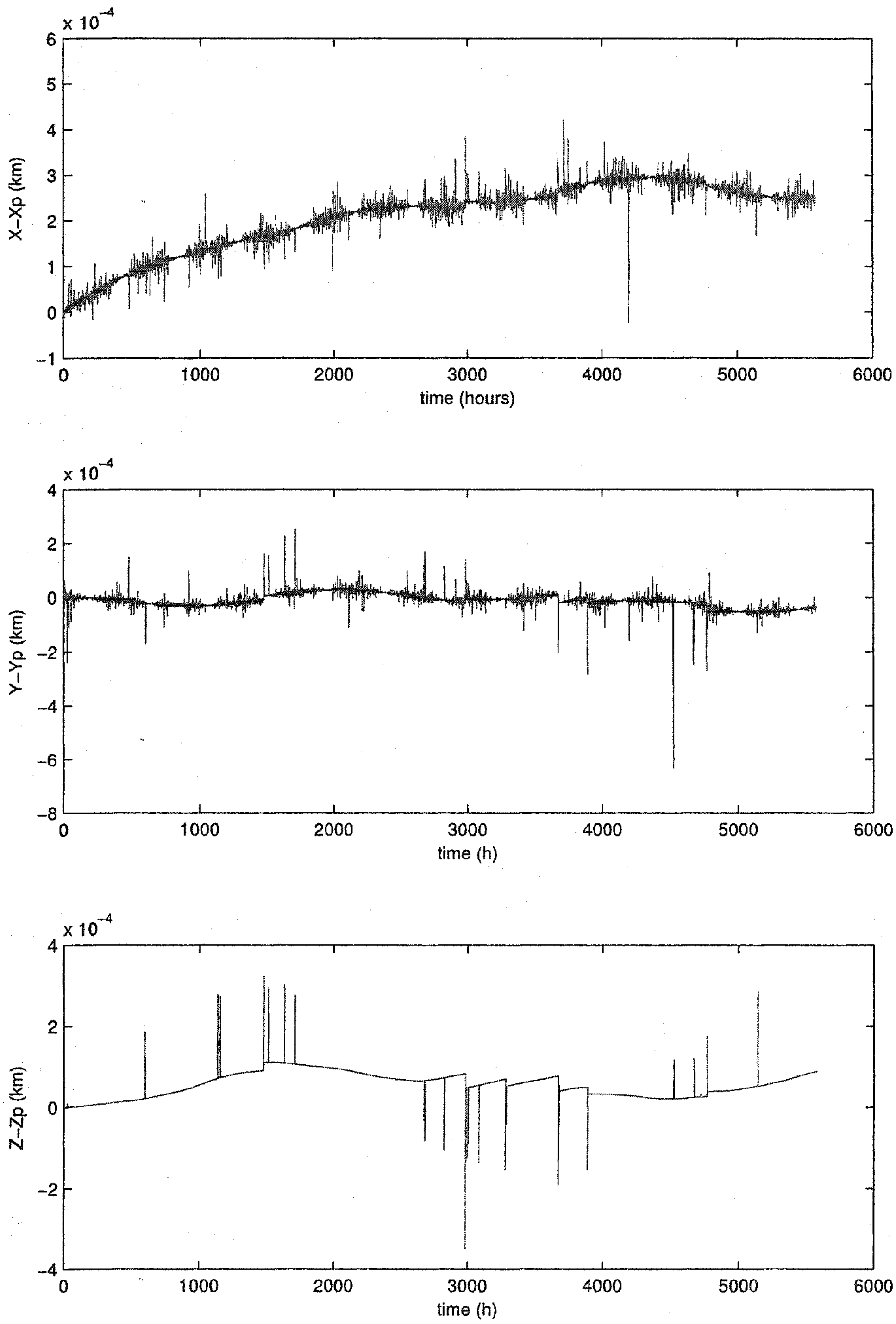

Figure 4.24 Parent Mass Error Signal, A_x=100 km Lissajous Trajectory, $\dot{\theta}_d$ =10n

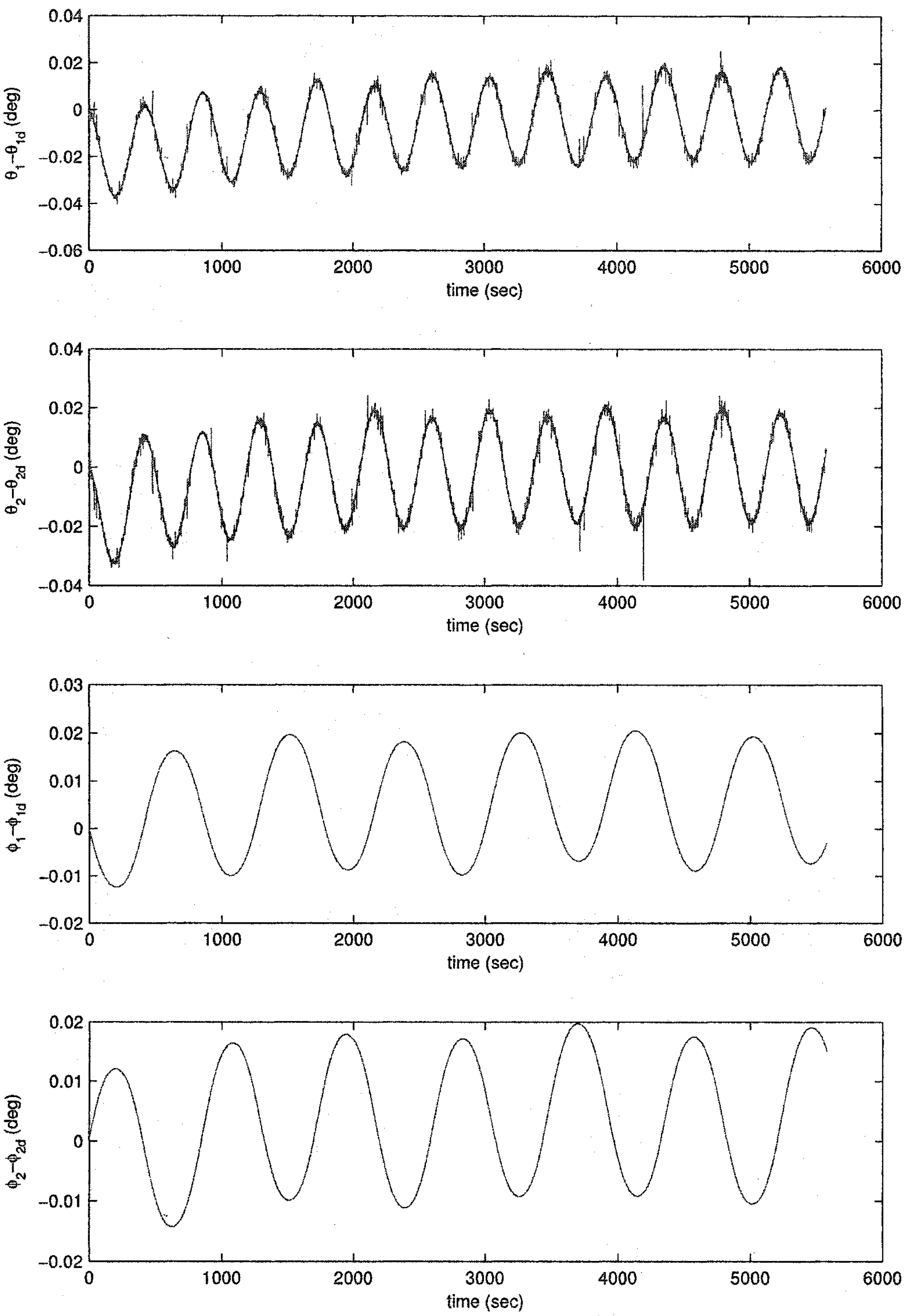

Figure 4.25 Tether Libration Error Signals, A_x=100 km Lissajous Trajectory, $\dot{\theta}_d$ =10n

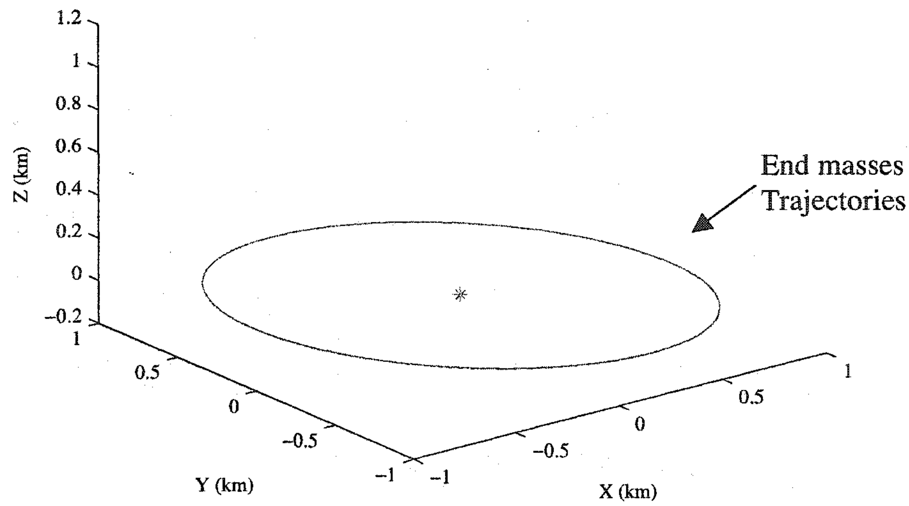

Figure 4.26 Tether Plane of Rotation, A_x=100 km Lissajous Trajectory, $\dot{\theta}_d$ =10n

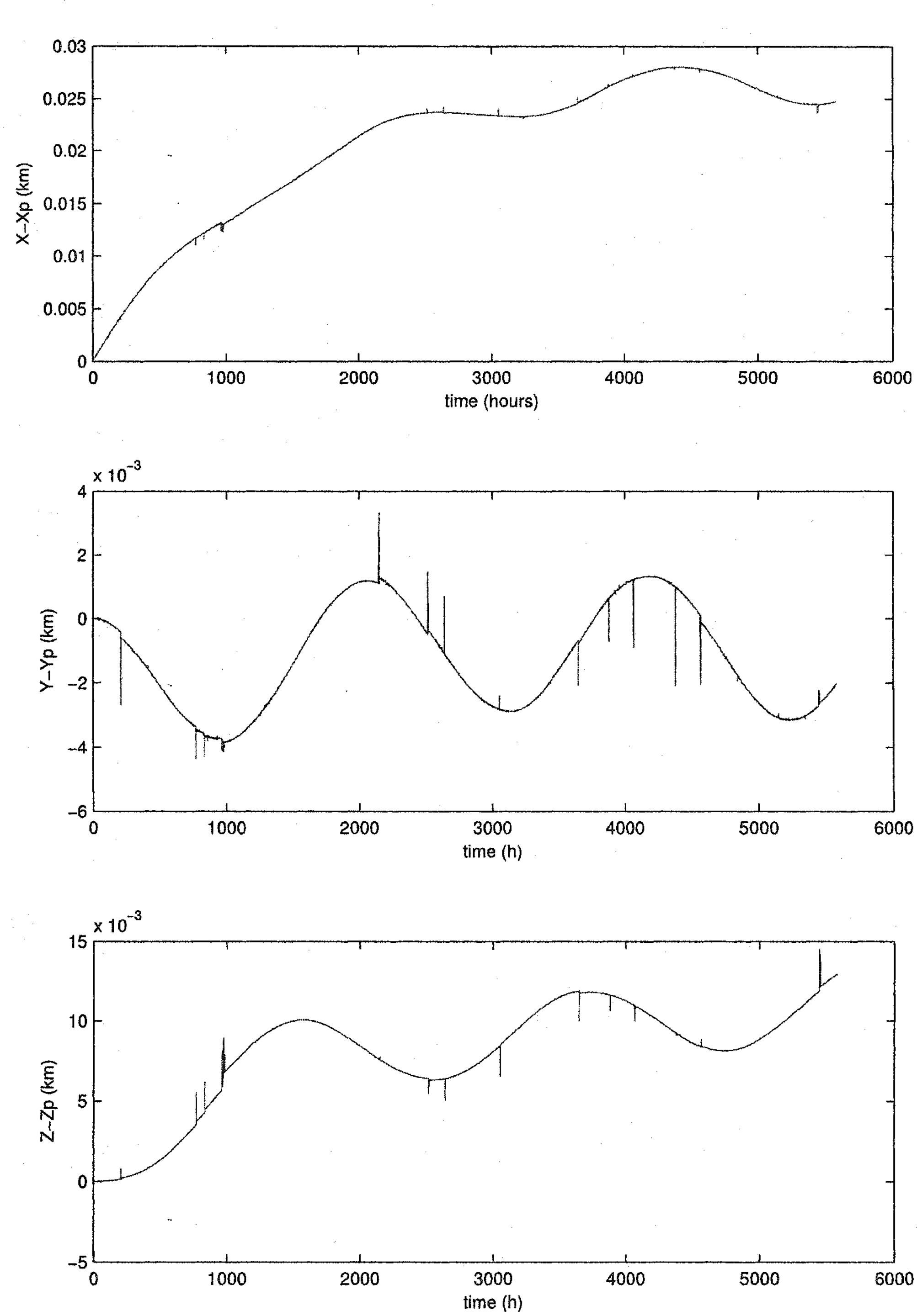

Figure 4.27 Parent Mass Error Signal, A_x=1000 km Lissajous Trajectory, $\dot{\theta}_d$ =10n

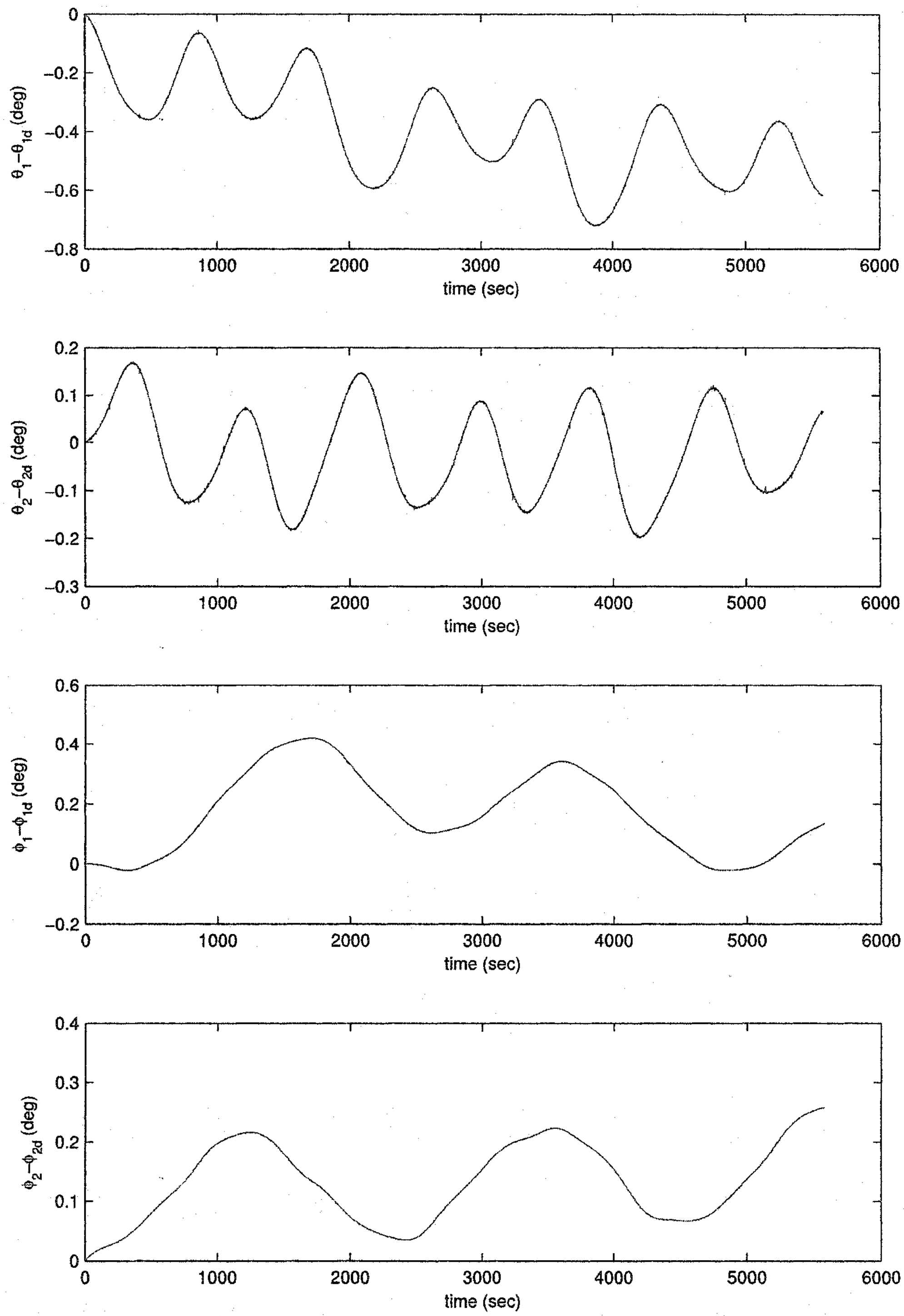

Figure 4.28 Tether Libration Error Signals, A_x=1000 km Lissajous Trajectory, $\dot{\theta}_d$ =10*n*

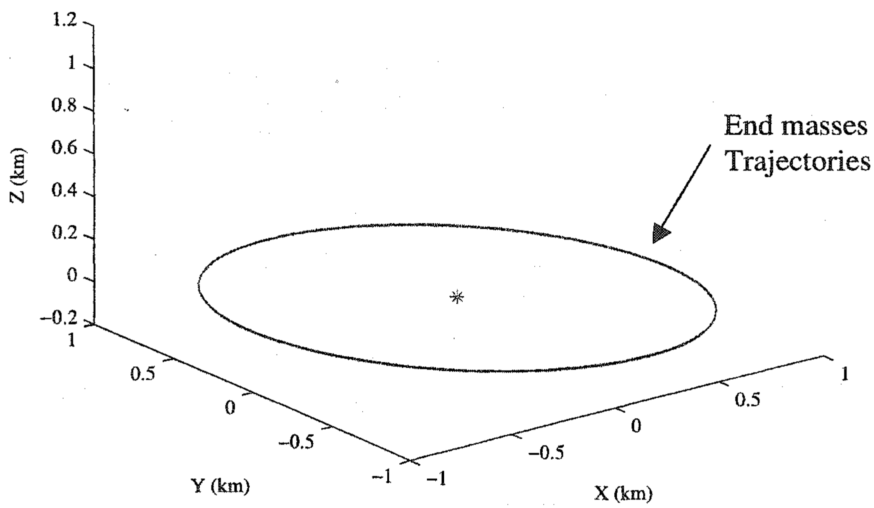

Figure 4.29 Tether Plane of Rotation, A_x=1000 km Lissajous Trajectory, $\dot{\theta}_d$ =10n

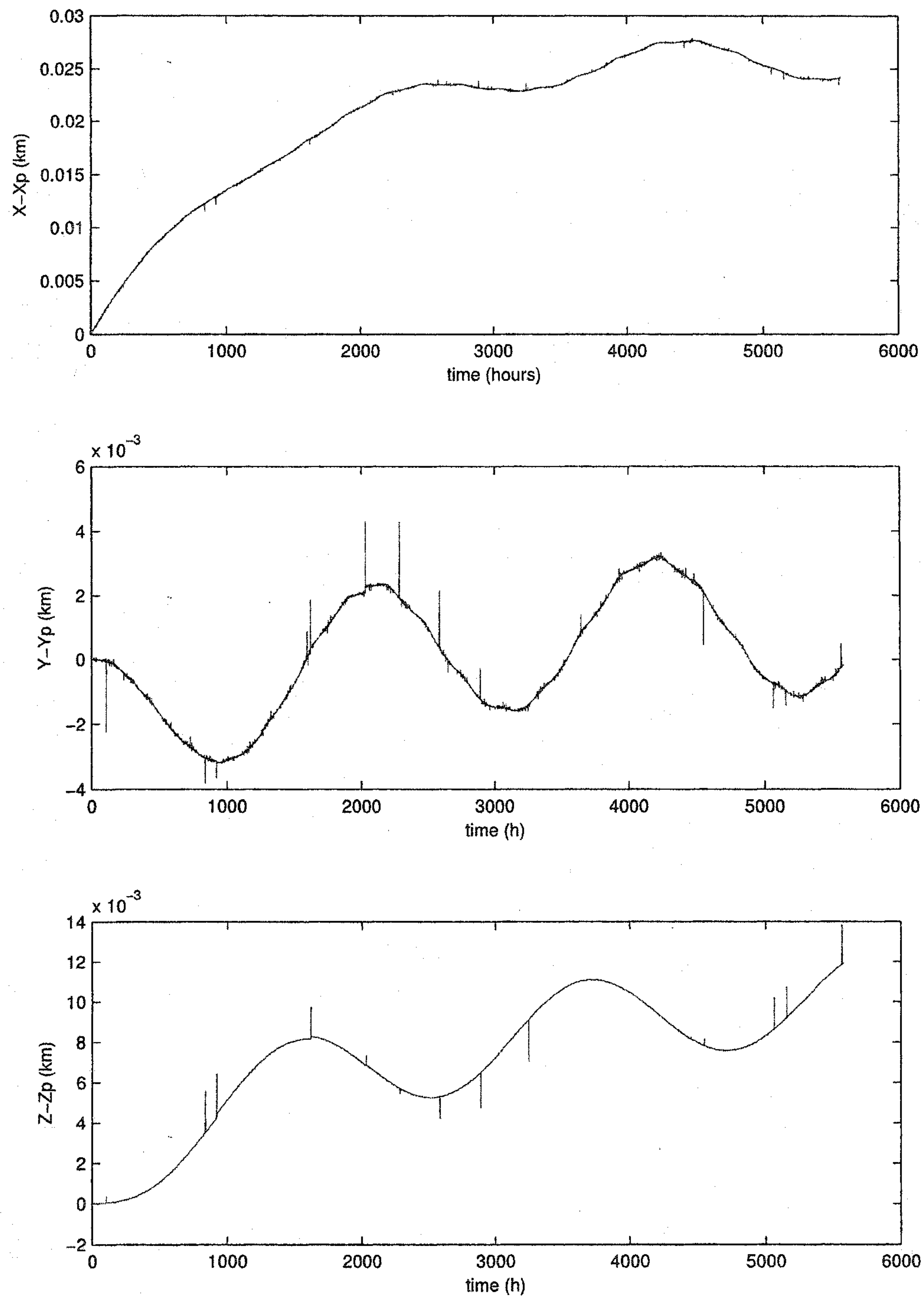

Figure 4.30 Parent Mass Error Signal, A_x=1000 km Lissajous Trajectory, $\dot{\theta}_d$ =30n

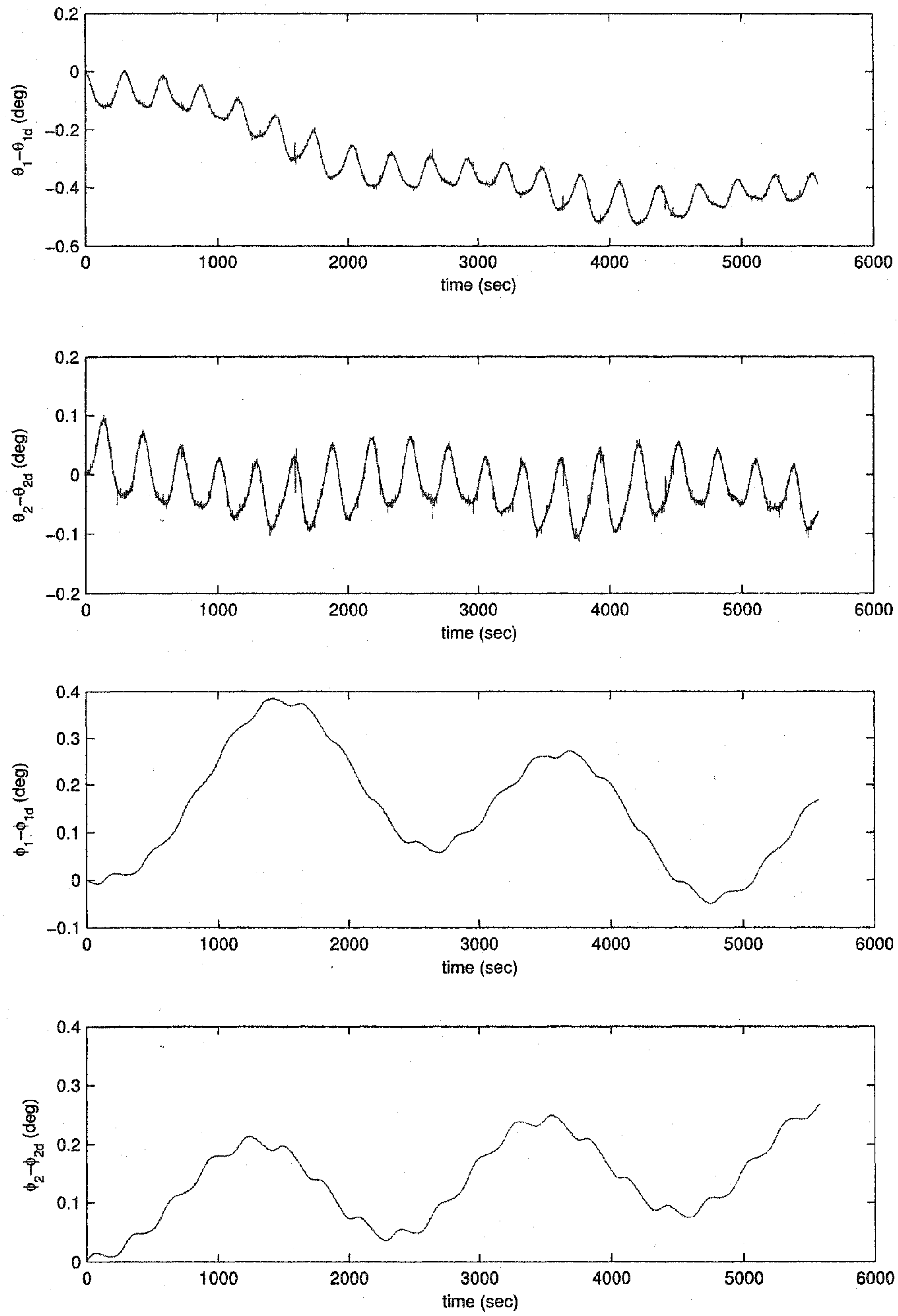

Figure 4.31 Tether Libration Error Signals, A_x=1000 km Lissajous Trajectory, $\dot{\theta}_d$ =30n

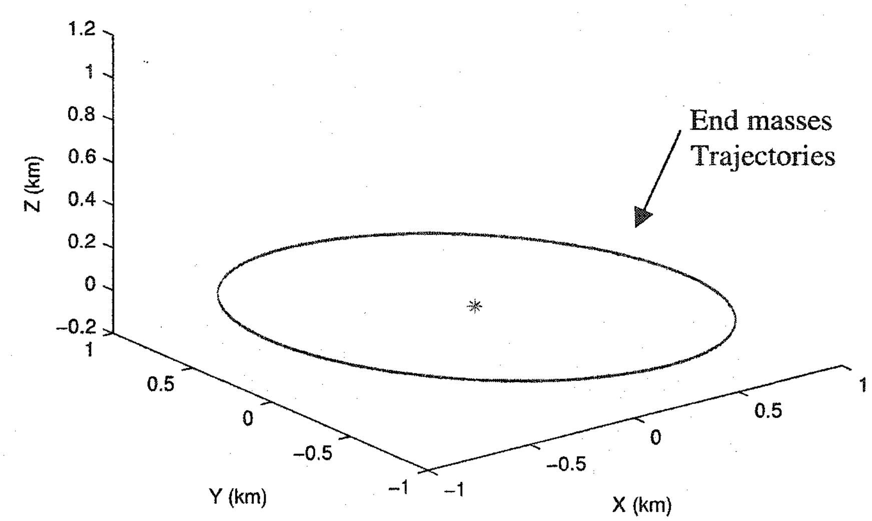

Figure 4.32 Tether Plane of Rotation, A_x=1000 km Lissajous Trajectory, $\dot{\theta}_d$ =30n

4.7 Control Effort Requirements

Finding out the control effort required is both important in terms of choosing the proper method of propulsion and in determining the amount of fuel required. As the proposed tethered system is to be located around 1.5 million km from the Earth there is no possibility of in-orbit refueling. Also important is to determine what sort of jitters the masses will encounter.

Figures 4.33 and 4.34 show the control history of the system for the baseline 10 km halo orbit case. The order of magnitude of the control accelerations is from around 10^{-9} to10^{-8} m/s^2 for in-plane motions and from 10^{-10} to 10^{-9} m/s^2 for out-of-plane motions. While it appears that almost continuous adjustments are required, small 50 hours time slice of the a_x graph (Figure 4.35) shows that it is not the case. Parent mass control inputs a_x and a_y have more or less evenly spaced periods where more inputs were required, and a_z is more or less sinusoidal. The shape of a_z comes from ω_z being forced to match ω_{xy}. Tether libration controls $a_{\theta 1}$ and $a_{\theta 2}$, have by and large evenly spaced periods where more inputs were required and $a_{\varphi 1}$, $a_{\varphi 2}$ have the a bit of a sinusoidal shape. The numerous spikes in the inputs can be attributed to various computational noises. For this small halo orbits, in-plane motion controls are a big part of the total requirement due to the unstable nature of those motions. The out-of-plane motions are oscillatory and the control system can make use of the natural dynamics of the system. As the size of the halo orbit increases for the same tether angular velocities, a_x and a_y decrease slightly while $a_{\theta 1}$ and $a_{\theta 2}$ remain roughly the same. The out-of-plane accelerations a_z, $a_{\varphi 1}$ and $a_{\varphi 2}$ increase as the control system now has to fight against the natural out-of-plane motions of the tethered system and begin to be a bigger part of the total control requirements. This can be seen in Figures 4.36-4.39. Recall from section 4.6 that control system performance is not good for A_x=100 km and A_x=1000 km halo orbits, so in reality much more efforts are needed to orientate the interferometer. While in theory it is possible to manually fine-tune the LQR controller, the results presented in this thesis is the best that the Matlab's Control Toolbox could do. Beyond this, no results can be obtained.

As was first mentioned in the previous section, increasing the desired tether spin rate does not improve the performance of the control system. Figure 4.41 shows that more effort is required to maintain the higher angular velocity compared to Figure 4.39, while the out-of-plane controls remain around the same.

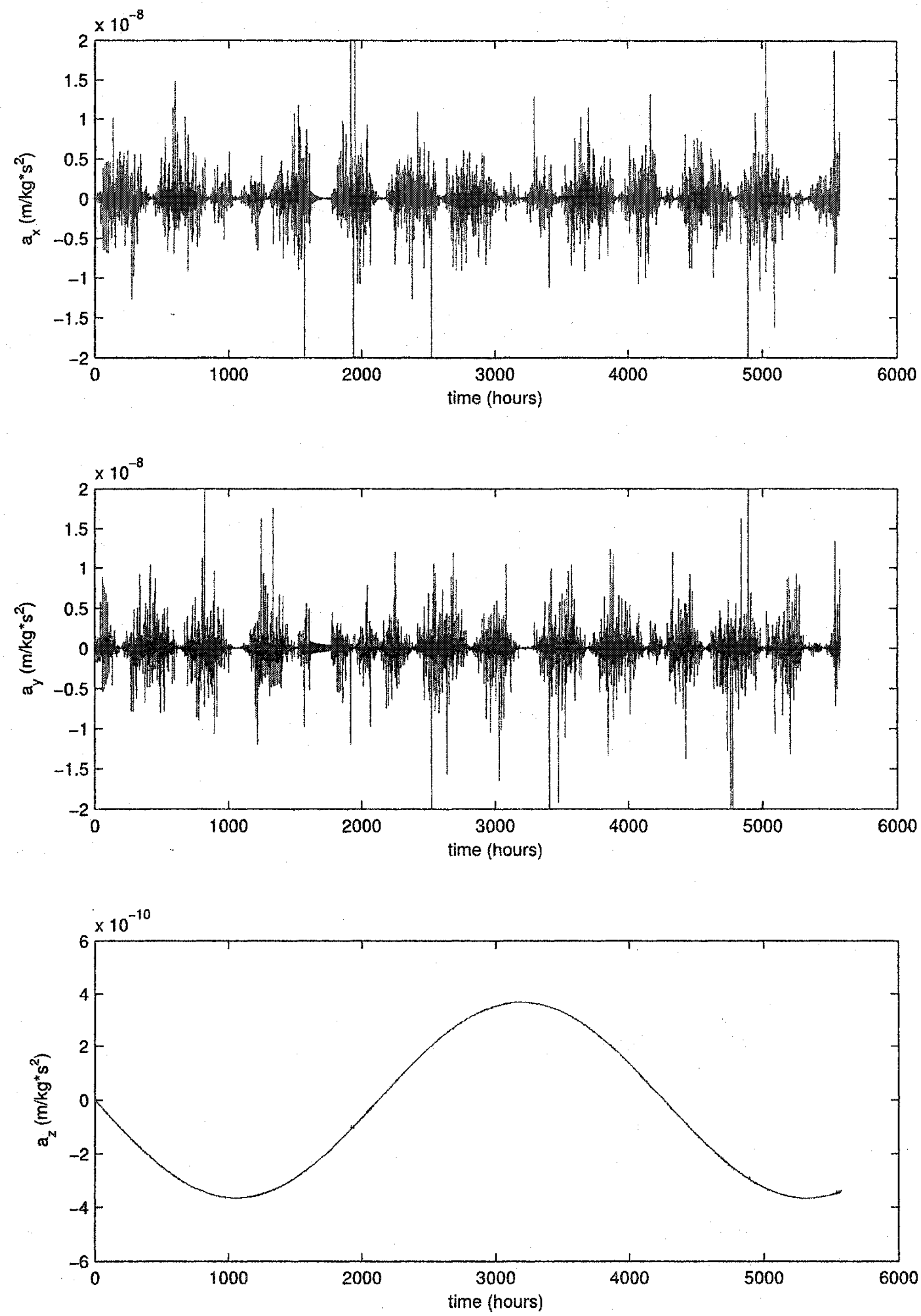

Figure 4.33 Parent Mass Control History, Baseline Case

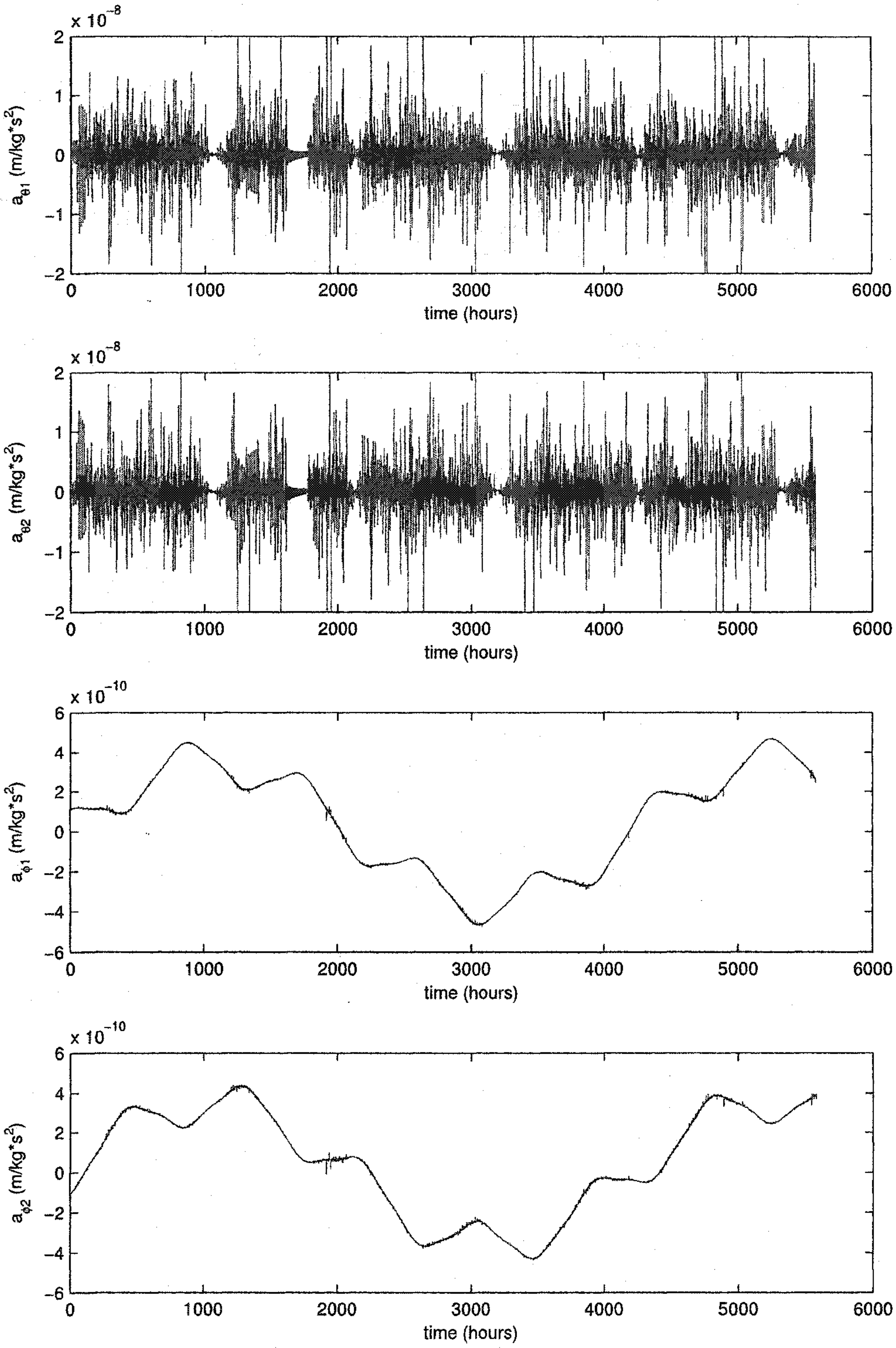

Figure 4.34 Tether Libration Control History, Baseline case

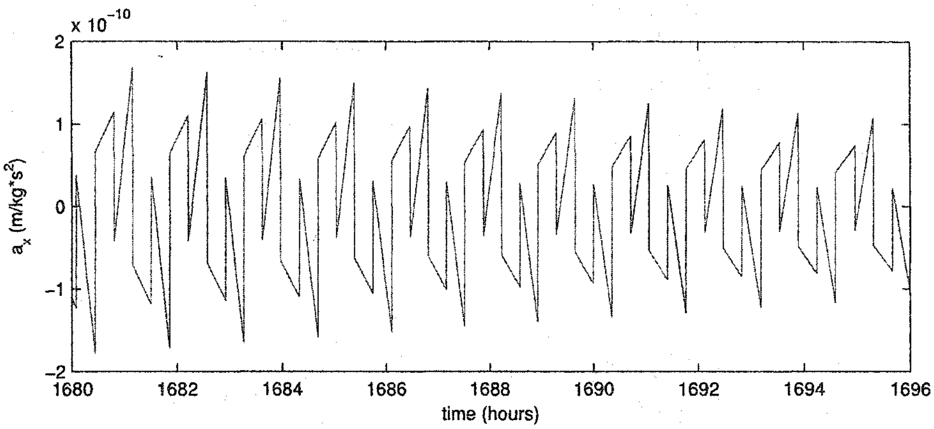

Figure 4.35 Small Time Slice of a_x

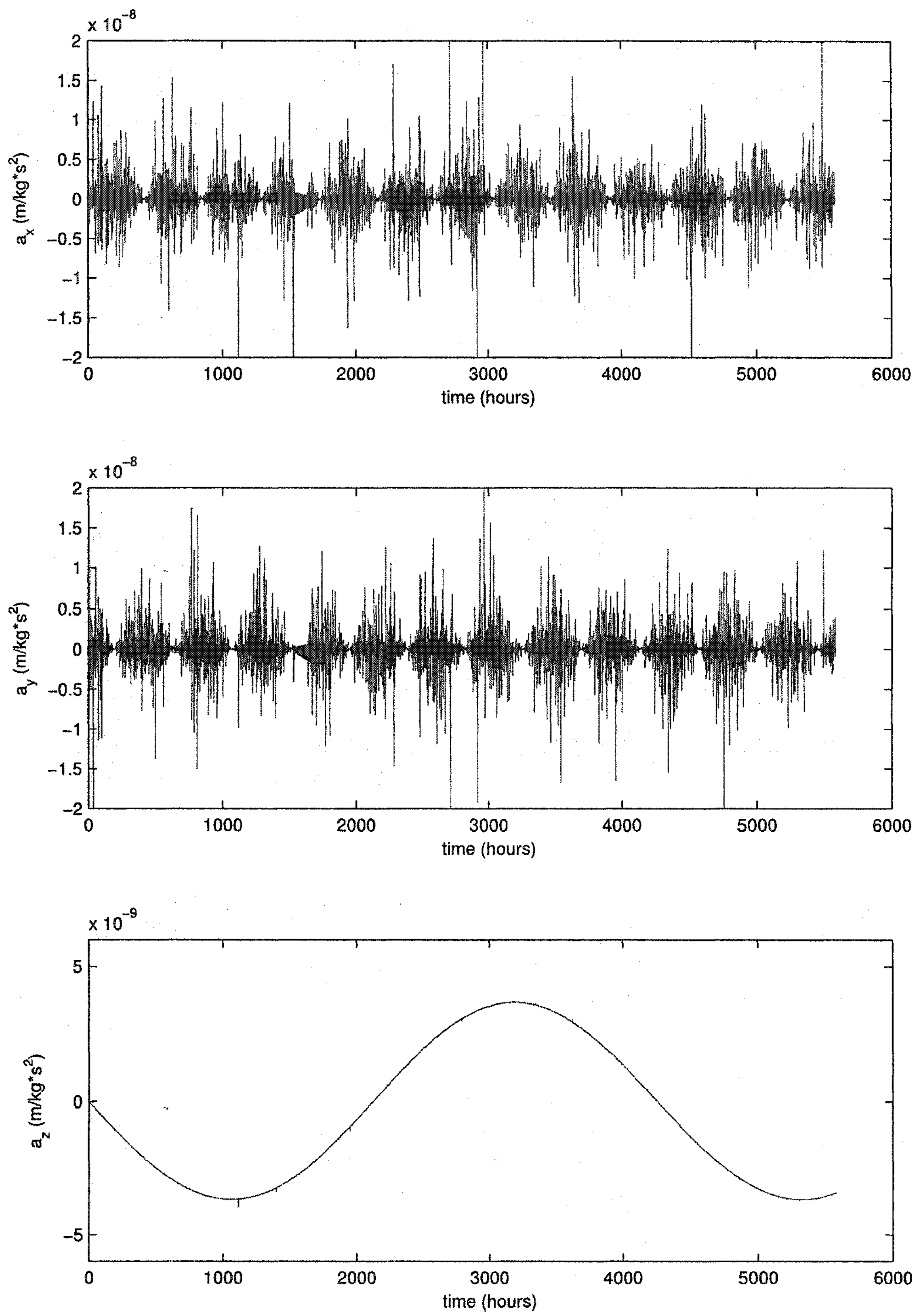

Figure 4.36 Parent Mass Control History, A_x=100km halo

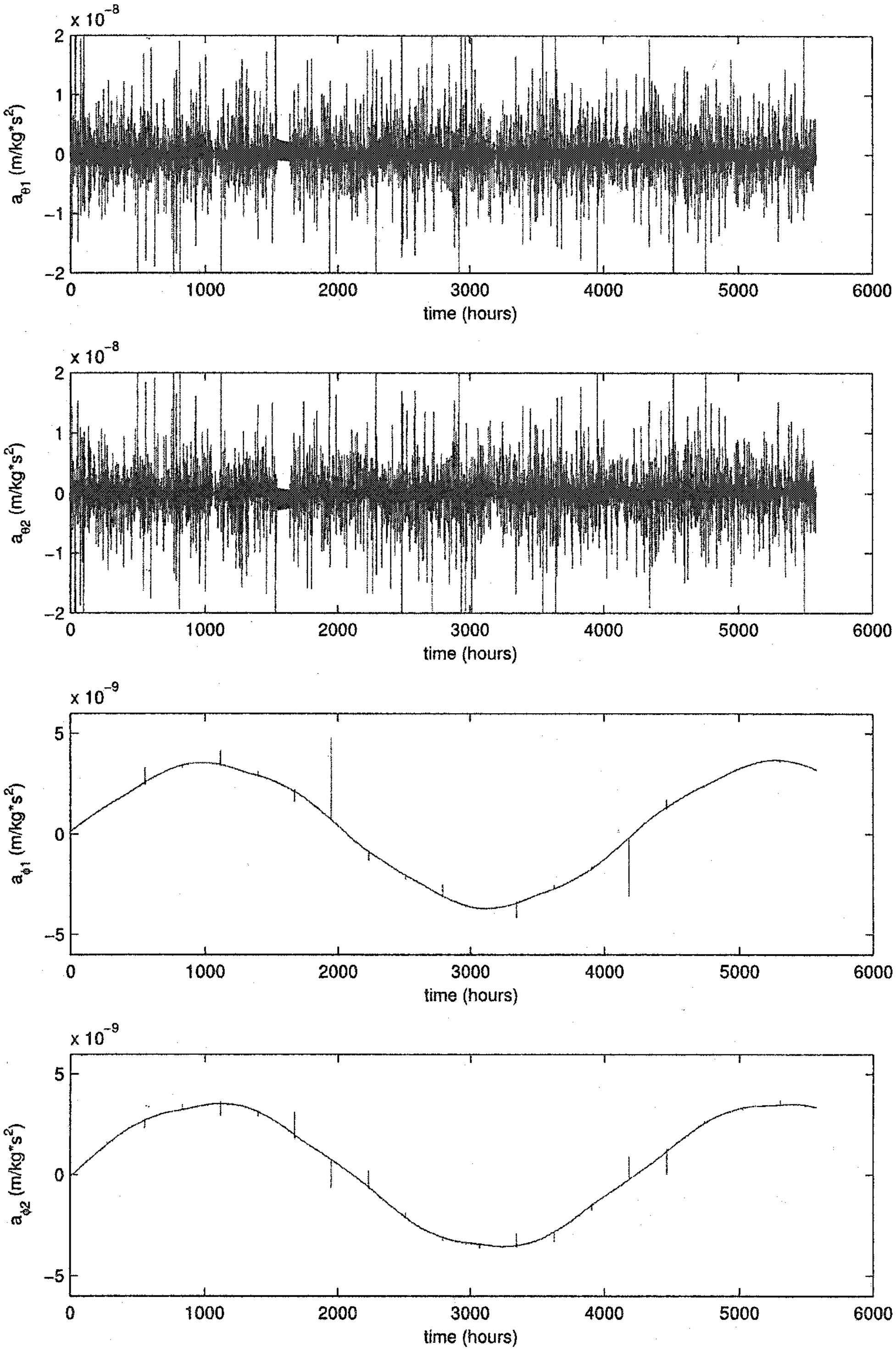

Figure 4.37 Tether Libration Control History, A_x=100 km halo

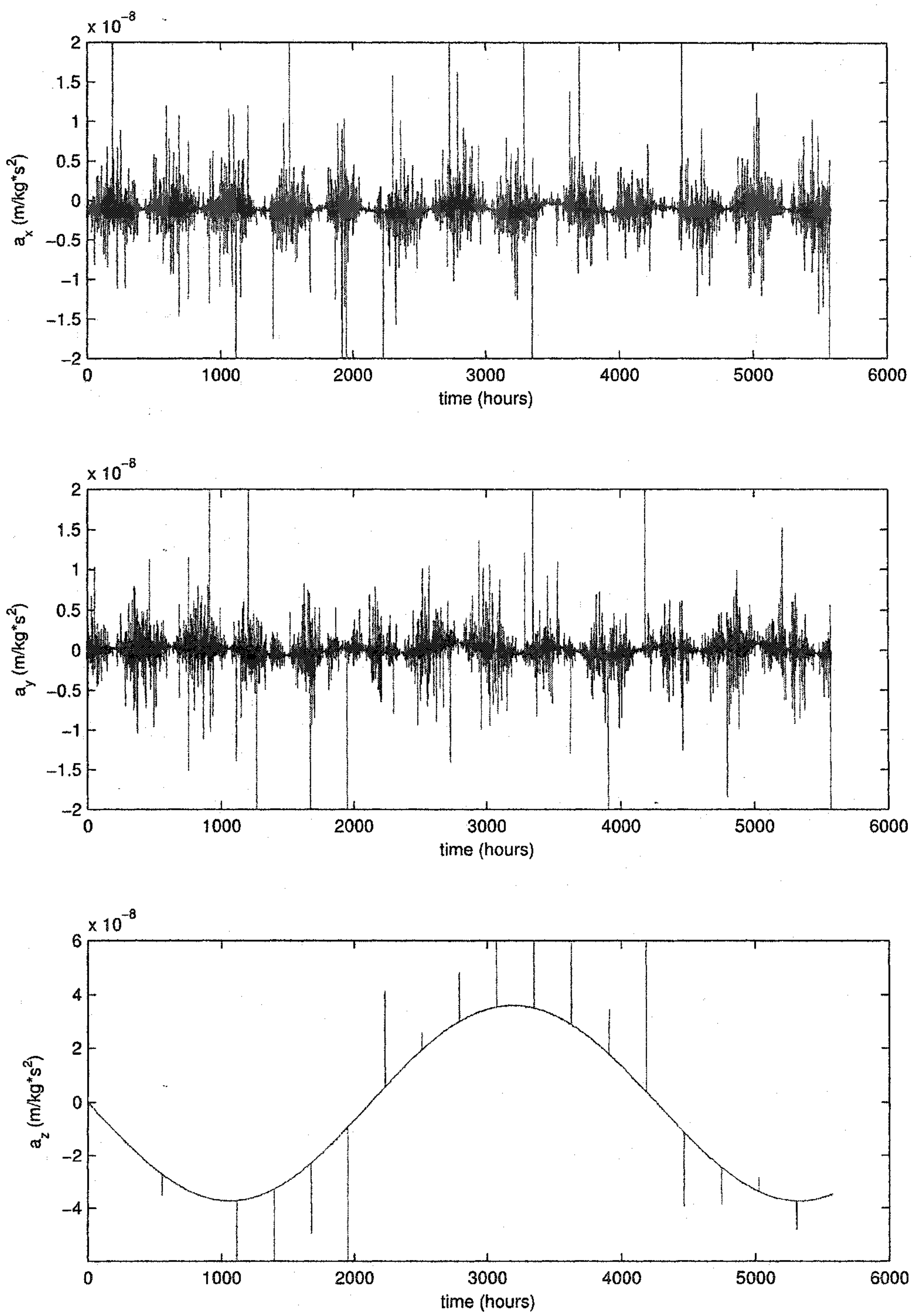

Figure 4.38 Parent Mass Control History, A_x =1000 km halo

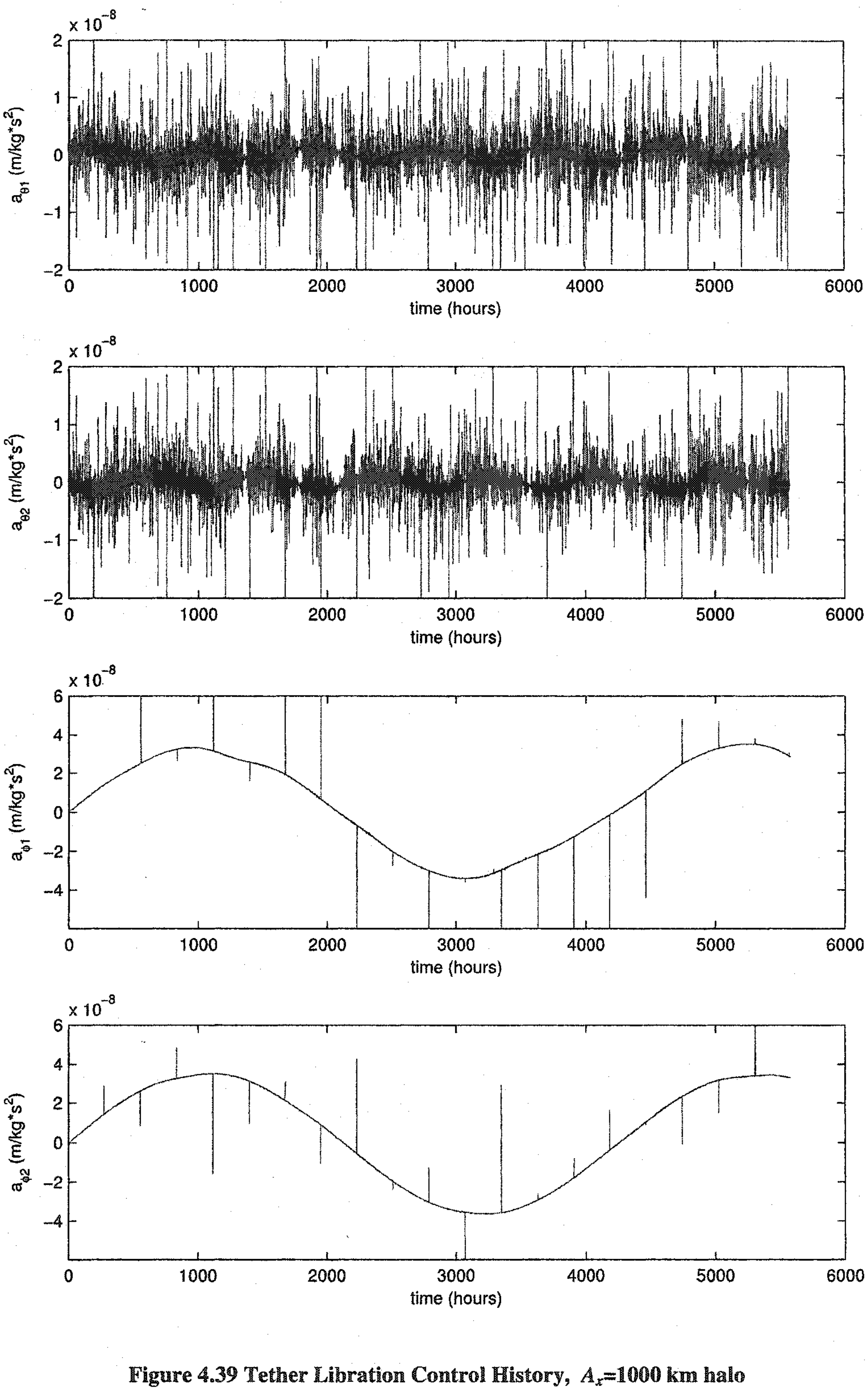

Figure 4.39 Tether Libration Control History, A_x=1000 km halo

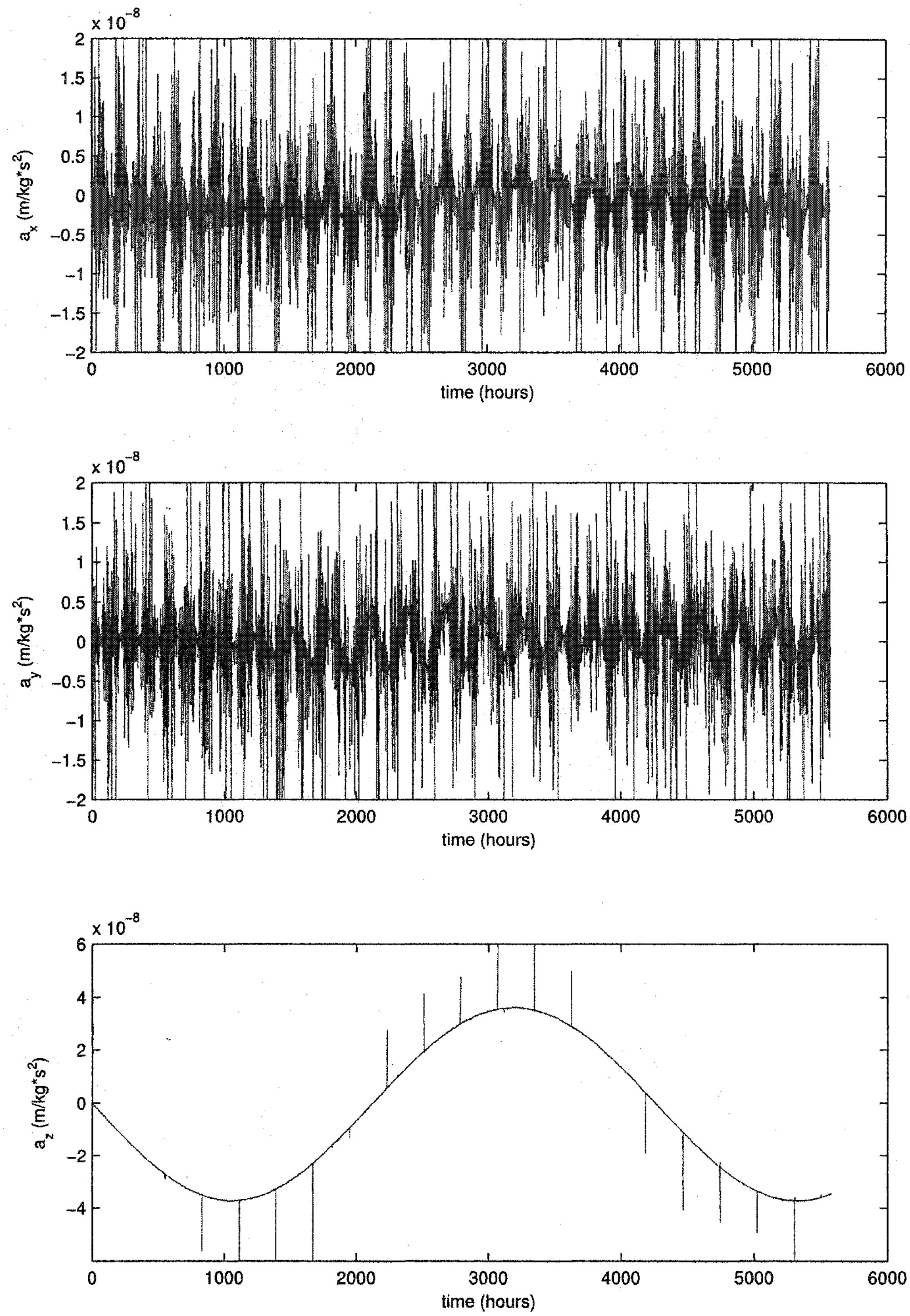

Figure 4.40 Parent Mass Control History, A_x =1000 km halo, $\dot{\theta}_d = 30n$

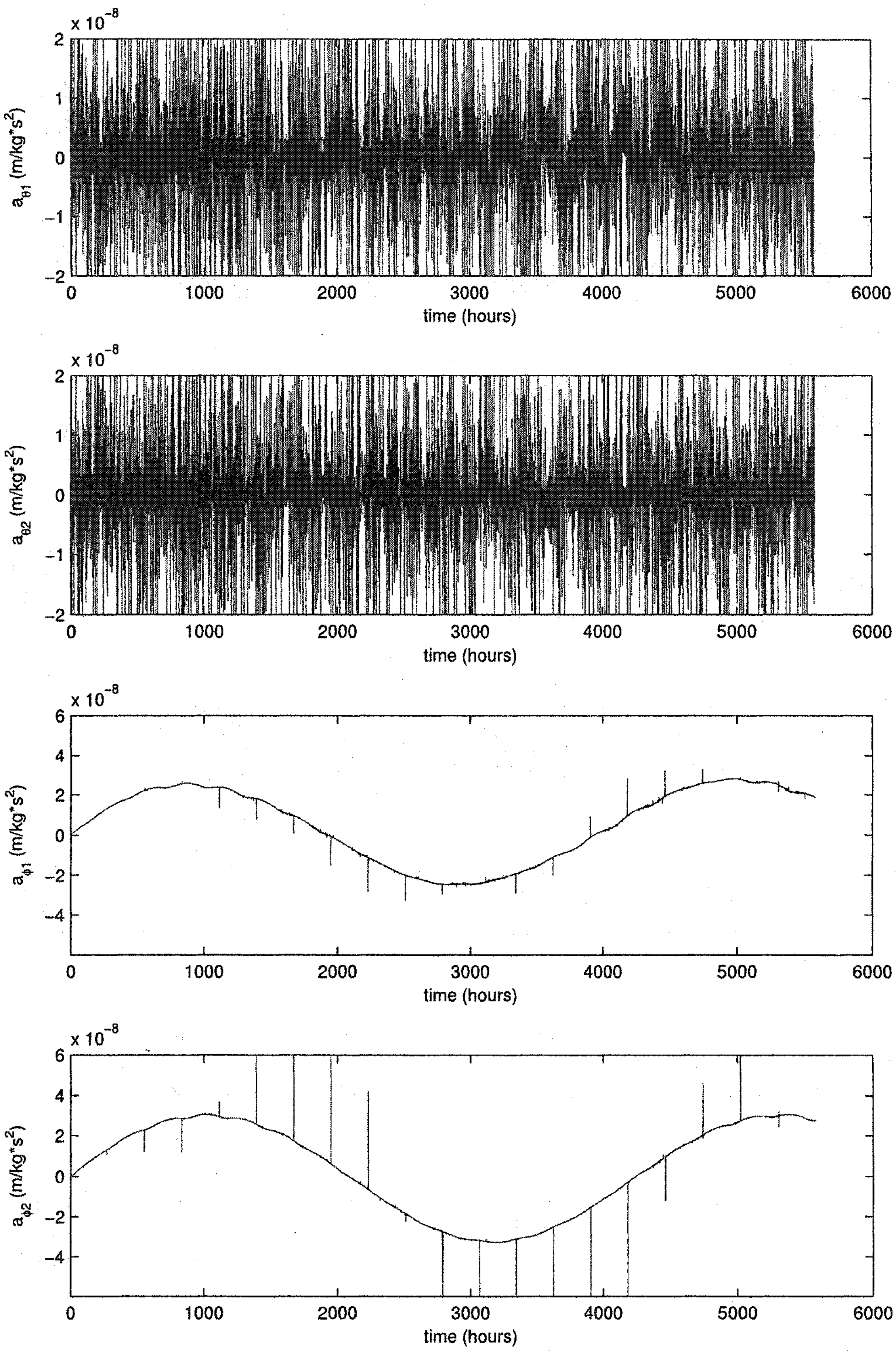

Figure 4.41 Tether Libration Control History, A_x=1000 km halo, $\dot{\theta}_d = 30n$

Letting the parent mass follow a Lissajous trajectory requires less control effort, especially for controlling out-of-plane motions. Comparing the A_x=10 km Lissajous case (Figures 4.42-4.43) to the baseline case, it is clear that less a_z is needed to keep the parent mass in the Lissajous trajectory. Also it no longer has a sinusoidal shape, instead it looks just like a_x and a_y where there are periodic bursts of activity. This is due to the parent mass control laws are more in tune with the tethered system's natural dynamics and the control system is just fine-tuning the trajectory. Control accelerations in the x and y directions are approximately the same as the baseline case. The magnitude of $a_{\theta 1}$ and $a_{\theta 2}$ are also approximately the same as the halo orbit case. $a_{\varphi 1}$ and $a_{\varphi 2}$ are very small in magnitude and have a saw-tooth shape. This is due to the fact that while the parent mass is in a Lissajous trajectory, the end masses are not as they are rotating in a specific way that has nothing to do with the Lissajous trajectory. The numerous spikes are probably due to numerical noise introduced during simulation. As A_x increases from 10 km to 1000 km, the overall control requirements increase but not as much as for the halo orbit cases. In-plane motion control accelerations are the same whether the system is in a halo or a Lissajous trajectory. The majority of the increases in total control effort comes from the out-of-plane controls. For the A_x=100 km and 1000 km cases, a_z takes on a periodic shape as the first order approximation of the Lissajous trajectory gets less accurate for larger sized trajectories.

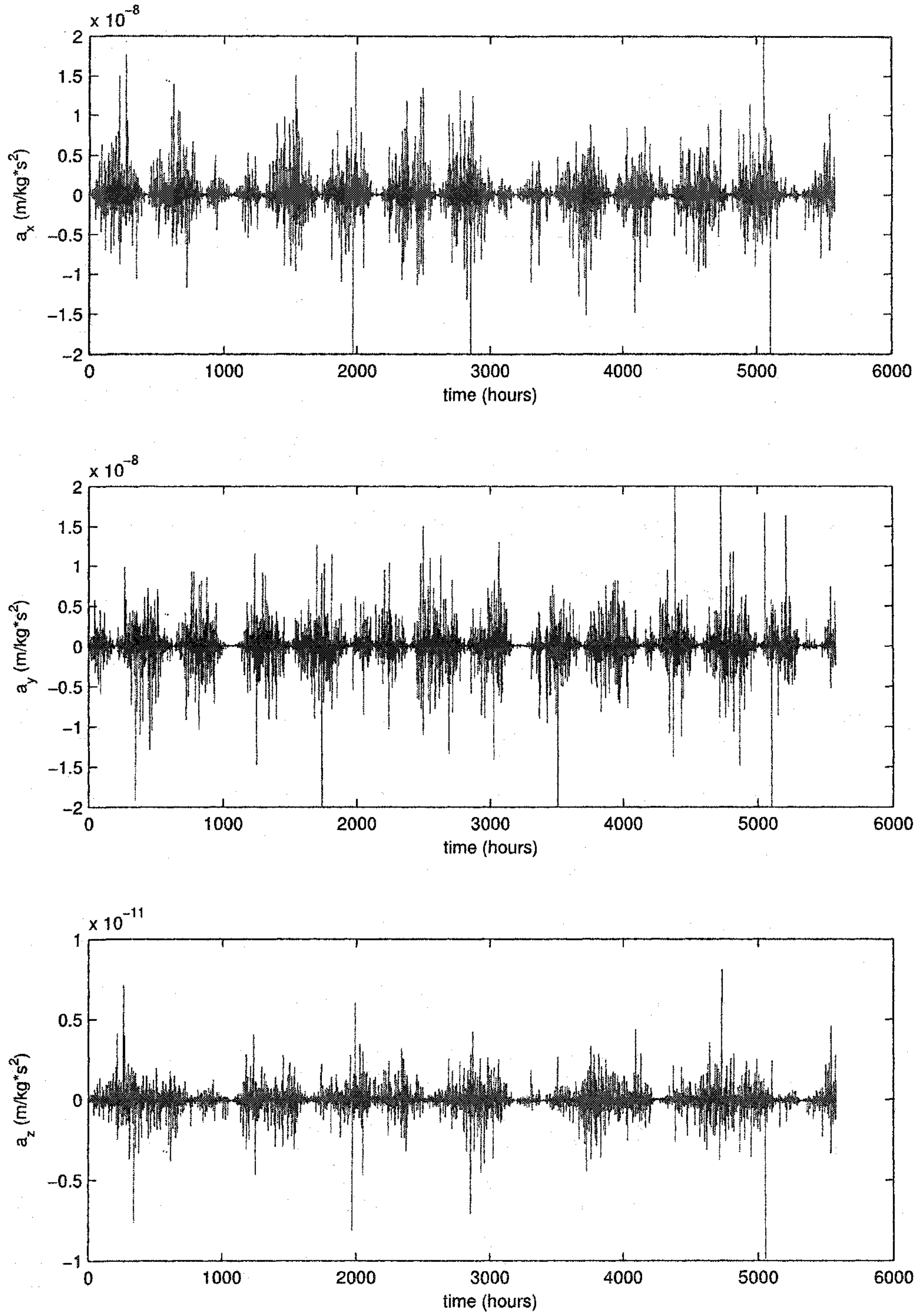

Figure 4.42 Parent Mass Control History, Ax = 10 km Lissajous

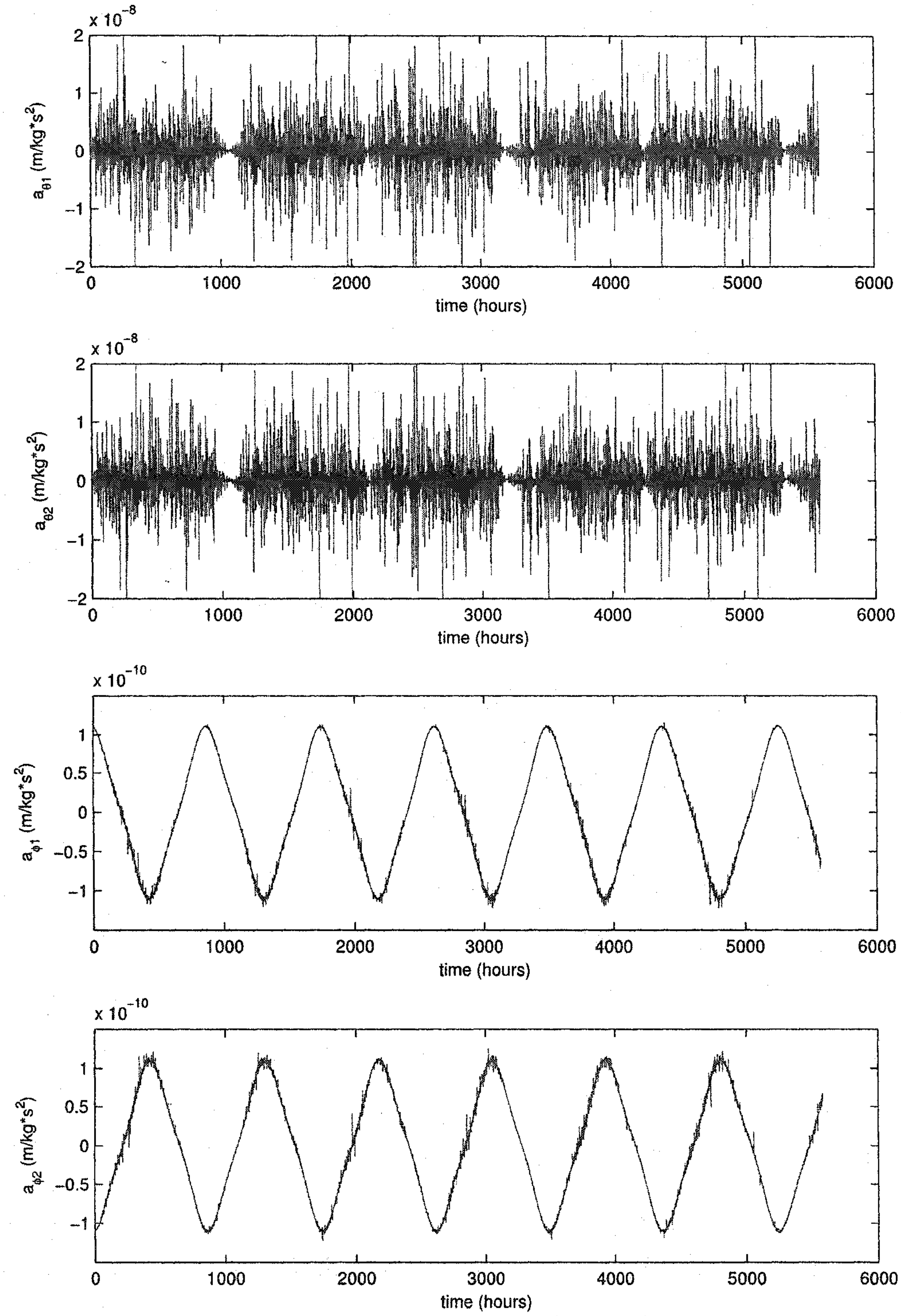

Figure 4.43 Tether Libration Control History, Ax=10 km lissajous

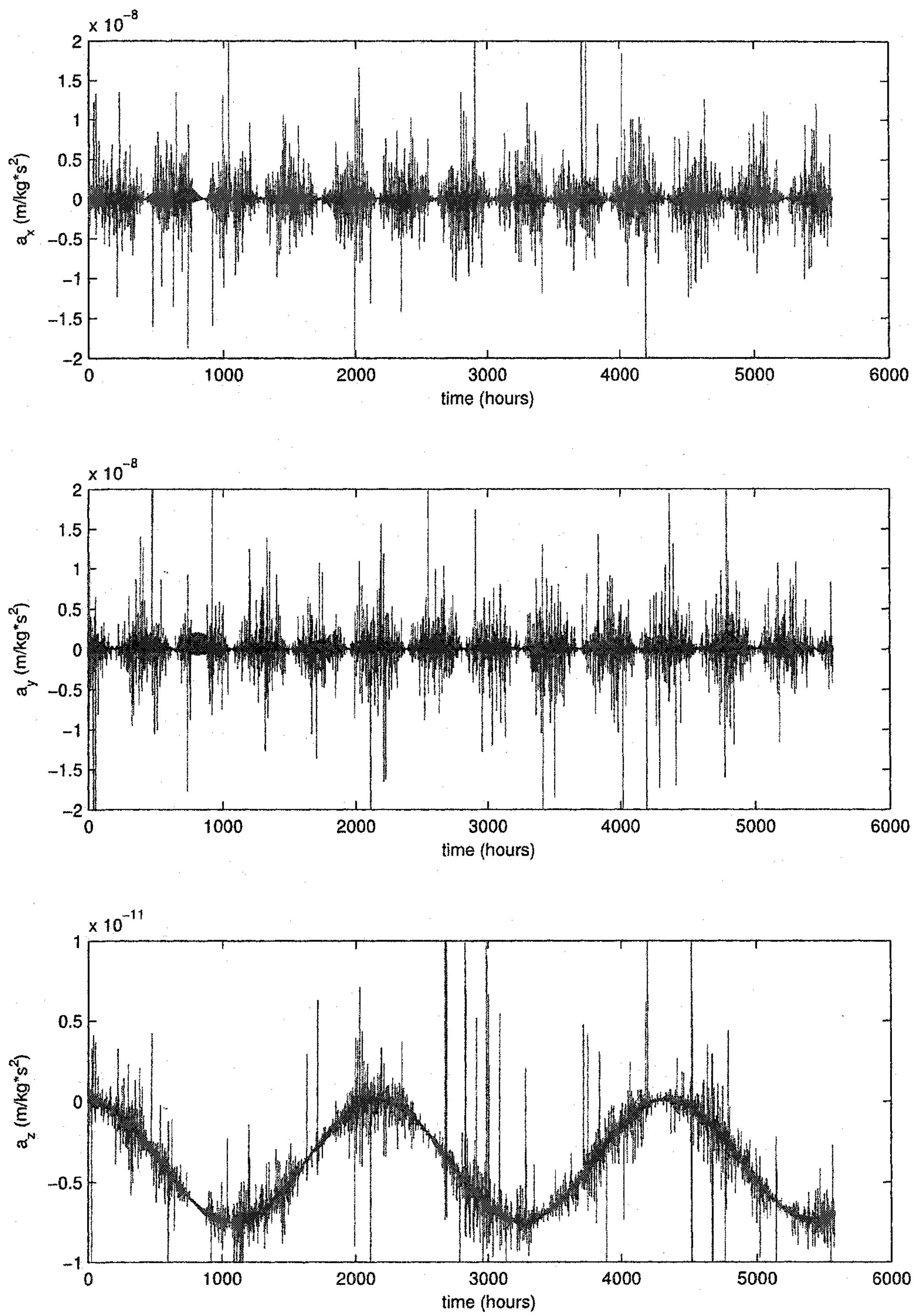

Figure 4.44 Parent Mass Control History, Ax=100 km Lissajous

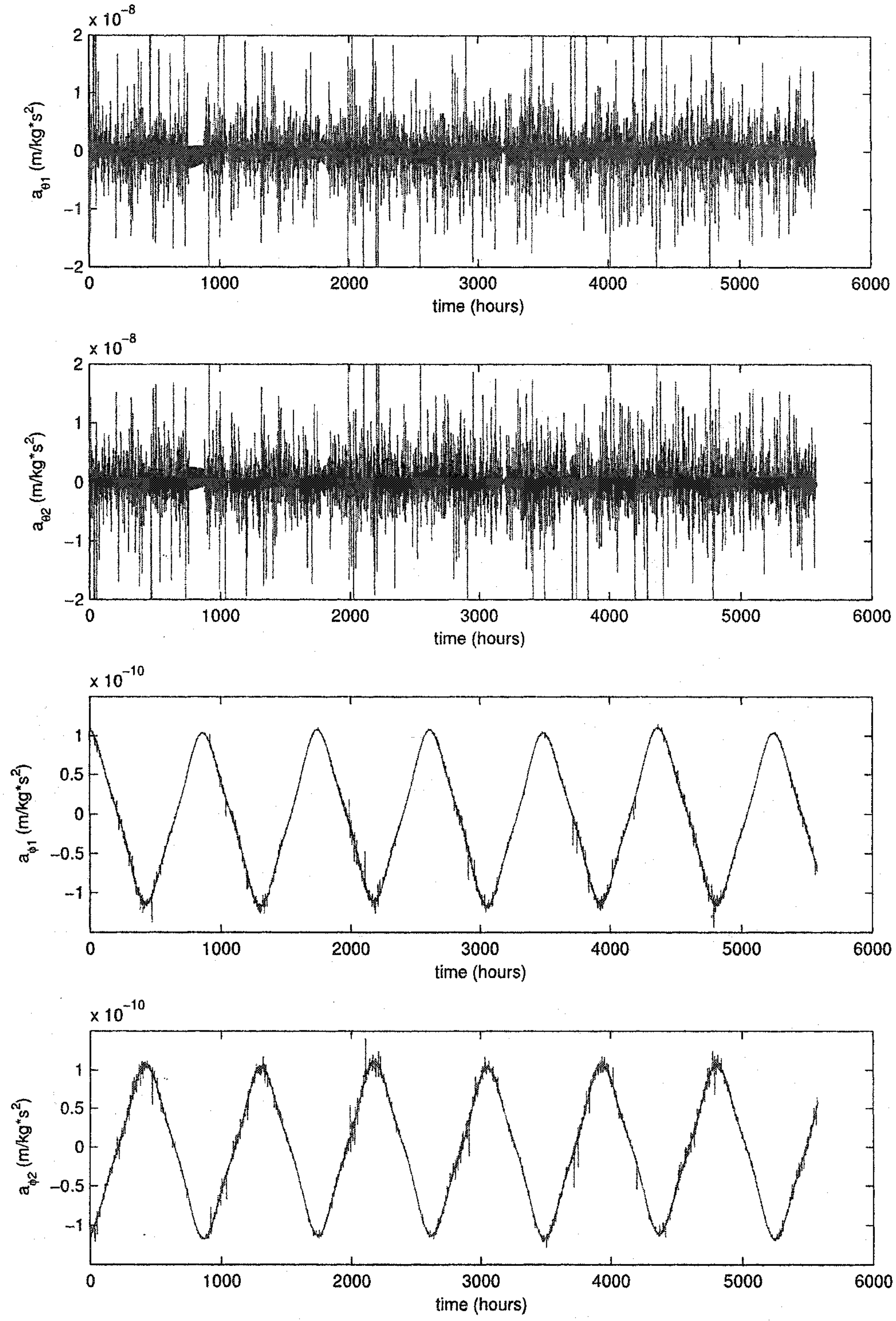

Figure 4.45 Tether Libration Control History, Ax=100 km Lissajous

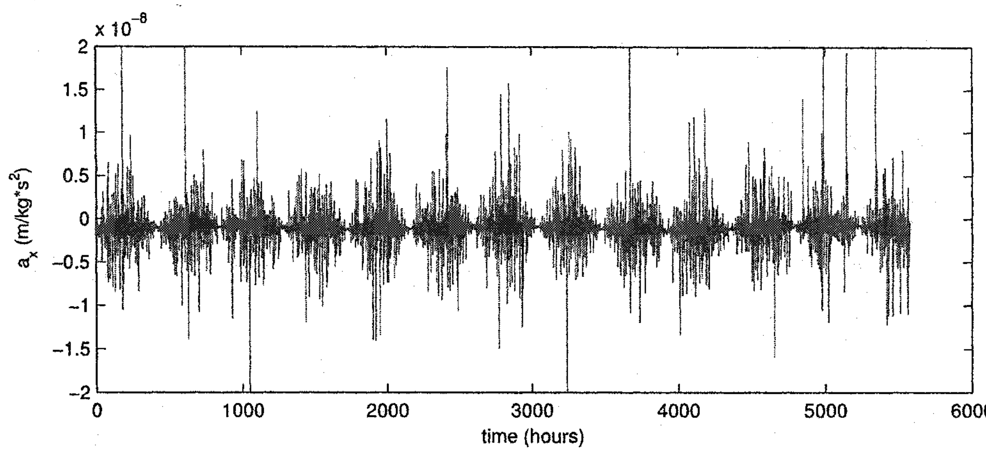

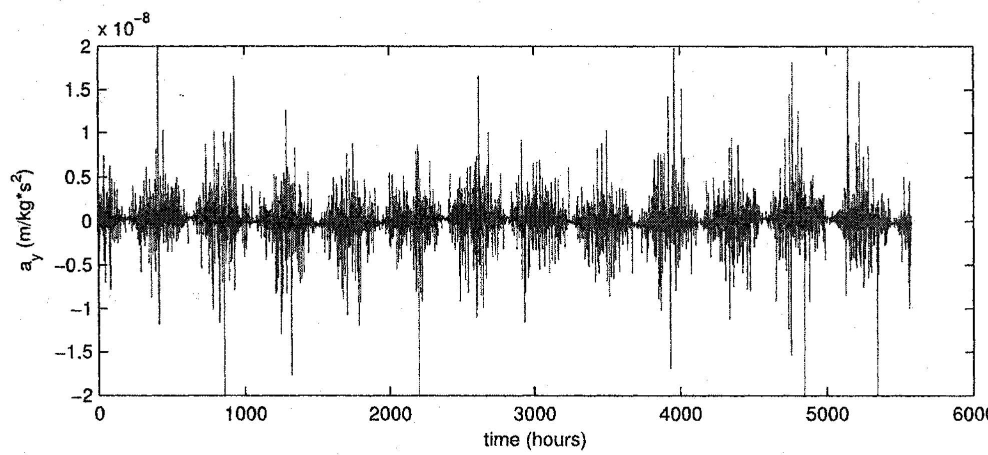

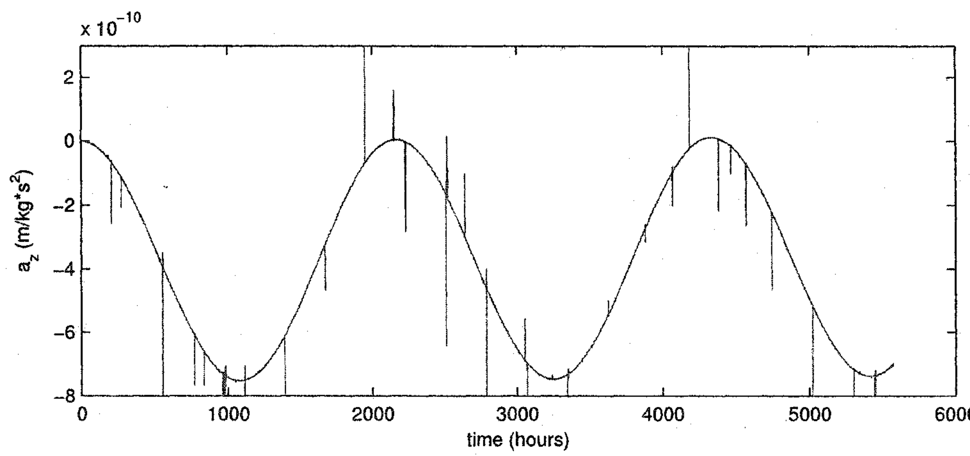

Figure 4.46 Parent Mass Control History, Ax=1000 km Lissajous

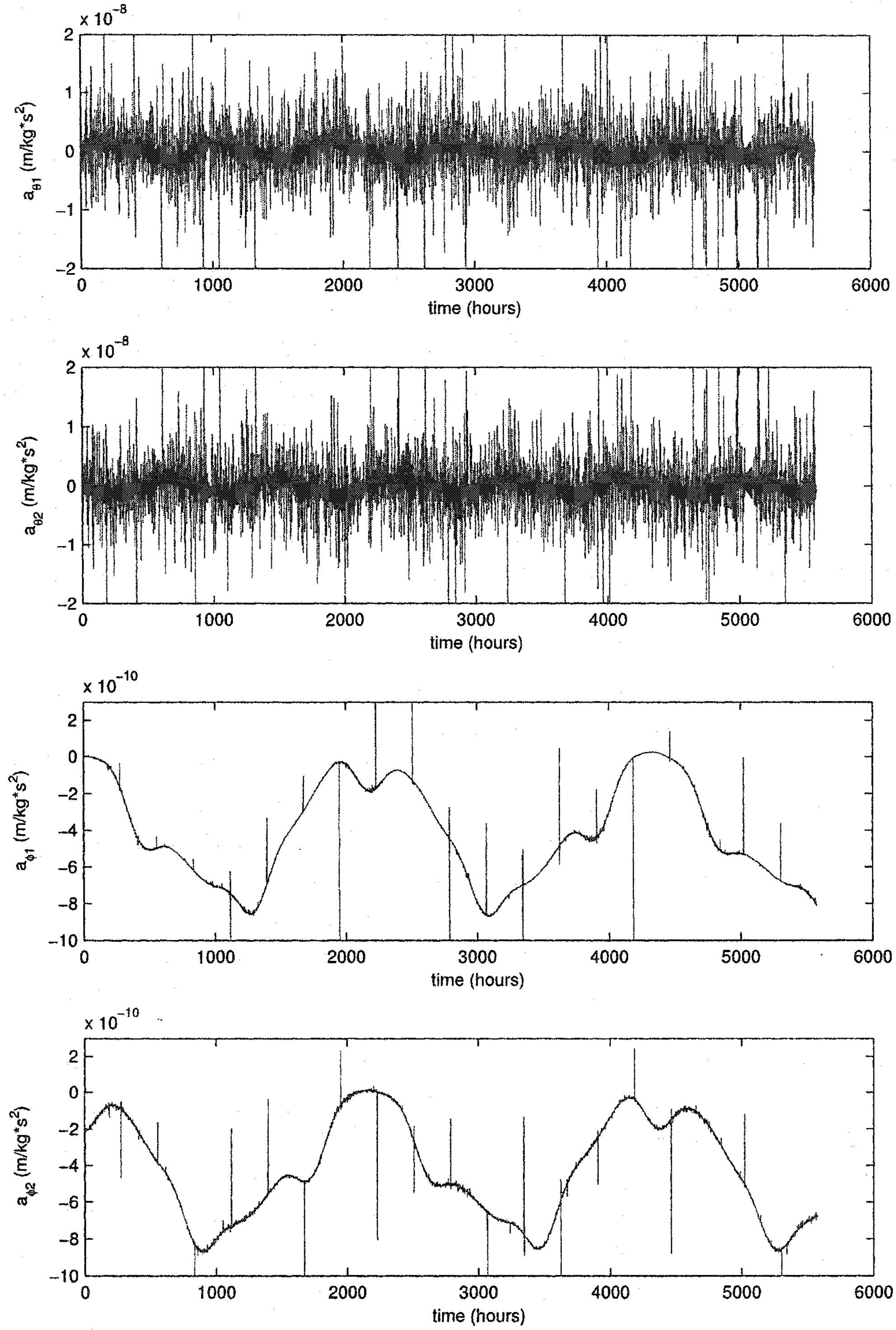

Figure 4.47 Tether Libration Control History, Ax= 1000km Lissajous

4.8 Total ΔV Cost

Integrating the control accelerations over time gives the ΔV required for that time span. Knowing this value helps the engineers pick the most appropriate method of propulsion and estimate its fuel requirements. Figure 4.48 shows the total ΔV requirements over a year as a function of A_x and tether spin rate. For small periodic orbits, the total ΔV requirements are similar for Lissajous and halo orbits, increasing from around 330 m/s to 900 m/s as spin rate increases from $10n$ to $40n$. As A_x increases for the same tether angular velocity, ΔV requirements also increase with cost growing faster for halo orbit cases than for Lissajous cases. ΔV_z, $\Delta V_{\varphi 1}$ and $\Delta V_{\varphi 2}$ increase steeply as the dimensions of the halo orbit increases. Those quantities also increase for larger Lissajous trajectories, but not nearly as fast since the command trajectory is close to the natural dynamics of a body near L_2. However the first order Lissajous approximations used here does not represent the complete picture, and even more fuel savings could be found if the tether system is following a second or even third order approximation. For the A_x=1000 km Lissajous case, total ΔV requirement for a year is about 709 m/s for $\dot{\theta}_d=10n$, rising to about 1690 m/s for $\dot{\theta}_d=40n$. For the same diameter halo orbit, total ΔV requirement for a year is about 9807 m/s for $\dot{\theta}_d=10n$ and 9187 m/s for $\dot{\theta}_d=40n$. Also of interest is that the total impulse required increases roughly in a linear fashion with tether spin rate for a particular A_x, with the exception of the largest halo orbit case where it is decreasing linearly.

The ΔV values for a three-body tethered system presented in this thesis cannot be directly compared to that of a single mass, as in addition to staying near the reference orbit, the tethered system also has to perform relative station keeping to maintain a desired orientation. The closest comparison would be to an untethered two-body system that is maintaining a constant distance between each other while staying near a reference orbit. Figure 3.1 demonstrated how quickly two unconnected mass would drift away from each other if they are displaced from L_2 in opposite directions, so the combined station keeping cost of the two-body system would be at least an order of magnitude greater than keeping a single mass near a reference orbit. However very little research to date has been done on the dynamics of a satellite constellation around a libration point.

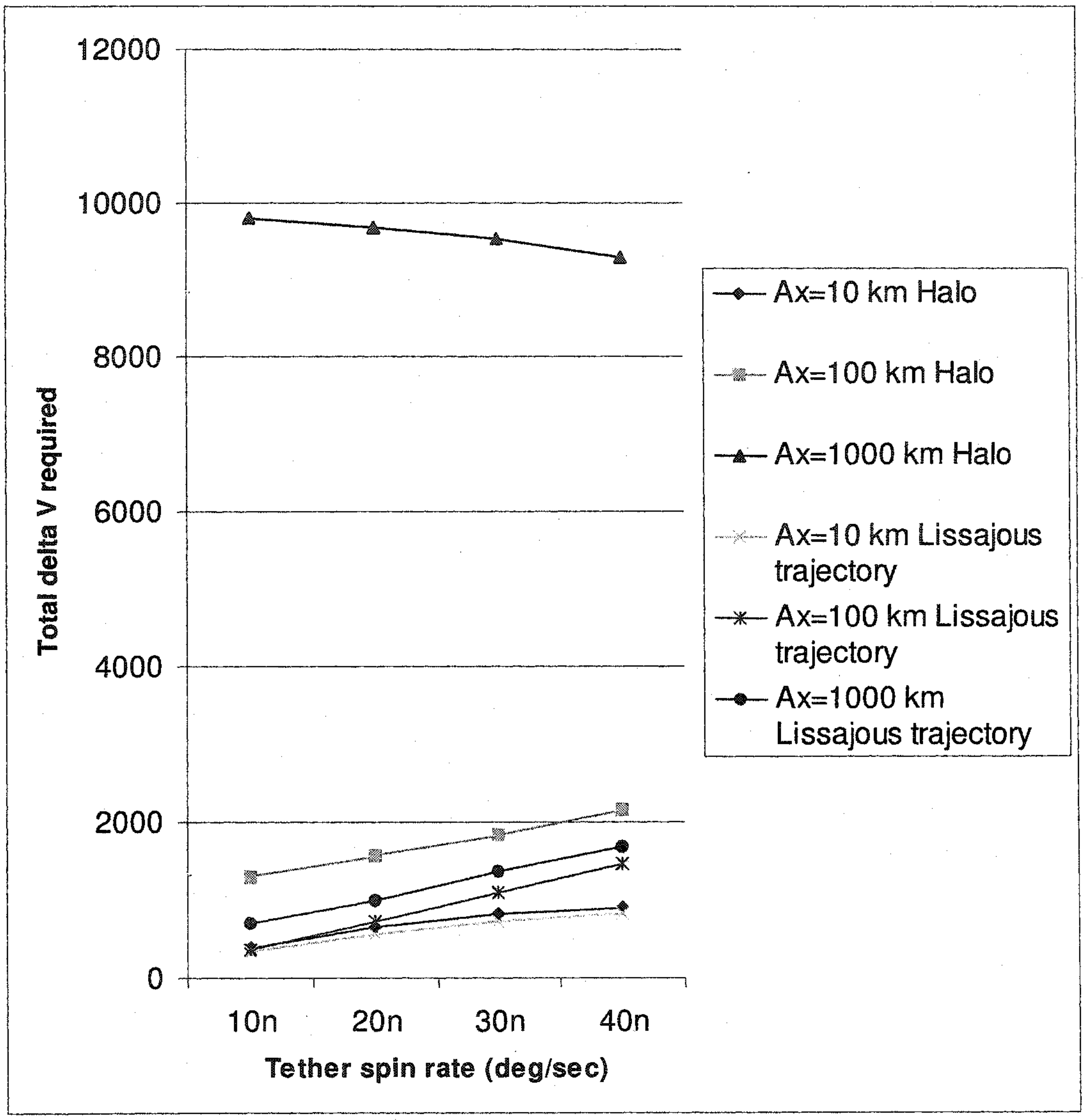

Figure 4.48 Total ΔV Cost

This chapter demonstrated that a 3-body tethered system could be controlled using a simple LQR feedback control system. The controller performed very well for small halo orbits, and got progressively worse for larger halo orbits. Results are much better if the parent mass is following a Lissajous trajectory regardless of its dimensions. While several important parameters, such as the type of orbit the parent mass will follow and the desired angular velocities, depend on the astronomical observation requirements, the numerical simulations done here show fuel expenditure can be minimized by placing the system in a Lissajous trajectory and using lower tether angular velocities while observing.

Chapter 5

CONCLUSION

5.1 Summary of Findings

In this thesis, a preliminary study of the dynamics of a multi-tethered system located near the L_2 Lagrangian point was performed. The system was assumed to be comprised of N end masses connected to a parent mass in a wheel-and-spoke configuration. The tethers are assumed to be massless, rigid and have fixed length. All the masses are considered as point masses. The equations of motion were derived using the Lagrangian approach, and an equilibrium configuration of the system was determined analytically. A linear analysis of the system revealed that the system has unstable in-plane motions and periodic motions out-of-plane.

The derived equations were implemented in a simulation software and some numerical experiments were conducted in chapter 3 to study the dynamics of the system. The parameters of the experiments are set to mimic the conditions at L_2 of the Sun-Earth system. First, the free dynamics were simulated and the results confirmed that the system has unstable in-plane dynamics. As the tethered system is to occupy a halo orbit around L_2 of the Sun-Earth system, tether librations of a rotating system, when the parent mass is occupying a halo orbit, were also examined with different initial spin rates and in halo orbits of various sizes. The numerical results showed that the amplitude of the out-of-plane librations depend on the size of the orbit as well as the rate of rotation of the system. The farther the parent mass is from L_2, the larger the amplitude. This can be reduced to a certain extent by increasing the spin rate but high angular velocities would pose their own problems. Results from these simulations showed that active control is needed for the tethered system to perform as an observatory.

In chapter 4, a control scheme was developed using the LQR method and was applied to the system. The main goal is to point the observation axis, which is perpendicular to the tether plane of rotation, at a desired direction relative to the ecliptic plane, while the parent mass is in a halo or a Lissajous trajectory. Results from the simulations showed that if the parent mass is in a halo orbit, the observation axis wobbles increasingly for larger halo orbits. Fuel consumption, measured in ΔV (m/s), also increases dramatically for large orbits. The results, both in terms of pointing accuracy and ΔV required, are much better if the parent mass is following a Lissajous trajectory. From the simulation of the controlled system, it can be concluded that a tethered system could be made to work as a space interferometer, and unless the operation of the spacecraft requires a halo orbit, life would be much easier if it is to occupy a Lissajous trajectory instead of a halo orbit.

5.2 Future work

In order to study the tether vibrations and the attitude dynamics of the parent mass and of the end masses, a more detailed model must first be developed. This model will incorporate extensible, variable length tethers along with realistic mass and inertia properties. The orbital dynamics and control of the multi-tethered system can also be explored in more detail, taking into account the elliptic motion of the primary bodies and other perturbations such as the gravitational attraction of Jupiter. There exists almost three decades of libration point mission experience and different orbit control techniques were developed, along with almost a century of academic research on the dynamics of a libration point object. These experiences can be extended to the study of multi-tethered objects.

Appendix A A method of calculating the Linear System at any arbitrary time

In order to use the LQR method to calculate the required control gains, a linear system representation of the equations of motion is required. As explained in chapter 4, a new linear system must be calculated periodically. Instead of working out in advance all the different system matrices and storing them in memory, a more efficient way is to provide the computer with a general way of calculating the linear system as required. As mentioned in chapter 4, the structure of the equations of motion is a little different from what is ordinary. The linear system can be presented as

$$\hat{\mathbf{A}}\dot{\mathbf{q}} = \hat{\mathbf{B}}\mathbf{q} + \mathbf{C} \tag{A.1}$$

where $\mathbf{q} = \left[x\,\dot{x}\,y\,\dot{y}\,z\,\dot{z}\,\theta_1\,\dot{\theta}_1\,\phi_1\,\dot{\phi}_1\,\theta_2\,\dot{\theta}_2\,\phi_2\,\dot{\phi}_2\right]^T$ and $\dot{\mathbf{q}}$ is the derivative of $\mathbf{q}$. $\hat{\mathbf{A}}$ and $\hat{\mathbf{B}}$ are 14X14 matrices where

$$\hat{\mathbf{A}} = \begin{bmatrix} 1 & 0 & 0 & 0 & 0 & 0 & 0 & 0 & 0 & 0 & 0 & 0 & 0 & 0 \\ 0 & 1 & 0 & 0 & 0 & 0 & 0 & a1 & 0 & a2 & 0 & a3 & 0 & a4 \\ 0 & 0 & 1 & 0 & 0 & 0 & 0 & 0 & 0 & 0 & 0 & 0 & 0 & 0 \\ 0 & 0 & 0 & 1 & 0 & 0 & 0 & b1 & 0 & b2 & 0 & b3 & 0 & b4 \\ 0 & 0 & 0 & 0 & 1 & 0 & 0 & 0 & 0 & 0 & 0 & 0 & 0 & 0 \\ 0 & 0 & 0 & 0 & 0 & 1 & 0 & 0 & 0 & c1 & 0 & 0 & 0 & c2 \\ 0 & 0 & 0 & 0 & 0 & 0 & 1 & 0 & 0 & 0 & 0 & 0 & 0 & 0 \\ 0 & d1 & 0 & d2 & 0 & 0 & 0 & d3 & 0 & 0 & 0 & 0 & 0 & 0 \\ 0 & 0 & 0 & 0 & 0 & 0 & 0 & 0 & 1 & 0 & 0 & 0 & 0 & 0 \\ 0 & e1 & 0 & e2 & 0 & e3 & 0 & 0 & 0 & 1 & 0 & 0 & 0 & 0 \\ 0 & 0 & 0 & 0 & 0 & 0 & 0 & 0 & 0 & 0 & 1 & 0 & 0 & 0 \\ 0 & f1 & 0 & f2 & 0 & 0 & 0 & 0 & 0 & 0 & 0 & f3 & 0 & 0 \\ 0 & 0 & 0 & 0 & 0 & 0 & 0 & 0 & 0 & 0 & 0 & 0 & 1 & 0 \\ 0 & g1 & 0 & g2 & 0 & g3 & 0 & 0 & 0 & 0 & 0 & 0 & 0 & 1 \end{bmatrix} \tag{A.2}$$

$$\hat{\mathbf{B}} = \begin{bmatrix} 0 & 1 & 0 & 0 & 0 & 0 & 0 & 0 & 0 & 0 & 0 & 0 & 0 & 0 \\ A1 & 0 & A2 & A3 & A4 & 0 & A5 & A6 & A7 & A8 & A9 & A10 & A11 & A12 \\ 0 & 0 & 0 & 1 & 0 & 0 & 0 & 0 & 0 & 0 & 0 & 0 & 0 & 0 \\ B1 & B2 & B3 & 0 & 0 & 0 & B4 & B5 & B6 & B7 & B8 & B9 & B10 & B11 \\ 0 & 0 & 0 & 0 & 0 & 1 & 0 & 0 & 0 & 0 & 0 & 0 & 0 & 0 \\ C1 & 0 & 0 & 0 & C2 & 0 & C3 & 0 & C4 & C5 & C6 & 0 & C7 & C8 \\ 0 & 0 & 0 & 0 & 0 & 0 & 0 & 1 & 0 & 0 & 0 & 0 & 0 & 0 \\ D1 & D2 & D3 & D4 & D5 & 0 & D6 & D7 & D8 & D9 & 0 & 0 & 0 & 0 \\ 0 & 0 & 0 & 0 & 0 & 0 & 0 & 0 & 0 & 1 & 0 & 0 & 0 & 0 \\ E1 & E2 & E3 & E4 & E5 & 0 & E6 & E7 & E8 & 0 & 0 & 0 & 0 & 0 \\ 0 & 0 & 0 & 0 & 0 & 0 & 0 & 0 & 0 & 0 & 0 & 1 & 0 & 0 \\ F1 & F2 & F3 & F4 & F5 & 0 & 0 & 0 & 0 & 0 & F6 & F7 & F8 & F9 \\ 0 & 0 & 0 & 0 & 0 & 0 & 0 & 0 & 0 & 0 & 0 & 0 & 0 & 1 \\ G1 & G2 & G3 & G4 & G5 & 0 & 0 & 0 & 0 & 0 & G6 & G7 & G8 & 0 \end{bmatrix} \tag{A.3}$$

$a1=-\mu_1 l_1 \sin\theta_1 \cos\phi_1$
$a2=\mu_1 l_1 \cos\theta_1 \cos\phi_1$
$a3=-\mu_2 l_2 \sin\theta_2 \sin\phi_2$
$a4=\mu_2 l_2 \cos\theta_2 \cos\phi_2$

$b1=\mu_1 l_1 \cos\theta_1 \cos\phi_1$
$b2=\mu_1 l_1 \sin\theta_1 \cos\phi_1$
$b3=\mu_2 l_2 \cos\theta_2 \cos\phi_2$
$b4=\mu_2 l_2 \sin\theta_2 \cos\phi_2$

$c1=\mu_1 l_1 \sin\phi_1$
$c2=\mu_2 l_2 \sin\phi_2$

$$d1=\frac{-\sin\theta_1 \sin\phi_1}{l_1}$$
$$d2=\frac{\cos\theta_1 \sin\phi_1}{l_1}$$
$d3=\sin^2\phi_1$

$$e1=\frac{\cos\theta_1 \cos\phi_1}{l_1}$$
$$e2=\frac{\sin\theta_1 \cos\phi_1}{l_1}$$
$$e3=\frac{-\sin\phi_1}{l_1}$$

$$f1=\frac{-\sin x\,\theta_2 \sin\phi_2}{l_2}$$
$$f2=\frac{\cos\theta_2 \sin\phi_2}{l_2}$$
$f3=\sin^2\phi_2$

$$g1=\frac{\cos\theta_2 \cos\phi_2}{l_2}$$
$$g2=\frac{\sin\theta_2 \cos\phi_2}{l_2}$$
$$g3=\frac{-\sin\phi_2}{l_2}$$

$A1 = 2B + 1 + 6C\hat{x}_p - 3C\left(\mu_1 l_1 \cos\theta_1 \sin\phi_1 + \mu_2 l_2 \cos\theta_2 \sin\phi_2\right)$

$A2 = 3C\left(2\hat{y}_p + \mu_1 l_1 \sin\theta_1 \sin\phi_1 + \mu_2 l_2 \sin\theta_2 \sin\phi_2\right)$

$A3 = 2$

$A4 = 6C\hat{z}_p - 3C\left(\mu_1 l_1 \cos\phi_1 + \mu_2 l_2 \cos\phi_2\right)$

$A5 = \mu_1 l_1 (\theta_1'' \cos\theta_1 \sin\phi_1 + \phi_1'' \sin\theta_1 \cos\phi_1 - \phi_1' \sin\theta_1 \sin\phi_1 - 2\theta_1'\phi_1' \sin\theta_1 \cos\phi_1 +$
$2\phi_1' \cos\theta_1 \cos\phi_1 - (\theta_1' + 1)^2 \sin\theta_1 \sin\phi_1 - 2B \sin\theta_1 \sin\phi_1 + 3C \sin\phi_1 (\hat{x}_p^2 + \hat{y}_p{}^2 + \hat{z}_p{}^2))$

$A6 = 2\mu_1 l_1 \cos\theta_1 (\phi_1' \cos\phi_1 + (\theta_1' + 1) \sin\phi_1)$

$A7 = \mu_1 l_1 (\theta_1'' \sin\theta_1 \cos\phi_1 + \phi_1'' \cos\theta_1 \sin\phi_1 + \phi_1'^2 \cos\theta_1 \cos\phi_1 - 2\theta_1'\phi_1' \cos\theta_1 \sin\phi_1$
$- 2\phi_1' \sin\theta_1 \sin\phi_1 + (\theta_1' + 1)^2 \cos\theta_1 \cos\phi_1 + 2B \cos\theta_1 \cos\phi_1 - 3C(\hat{x}_p \sin\theta_1 \sin\phi_1 - \hat{y}_p \sin\theta_1 \cos\phi_1$
$- \hat{z}_p \sin\phi_1))$

$A8 = 2\mu_1 l_1 \cos\phi_1 \left((\phi_1' + \theta_1')\cos\theta_1 + \sin\theta_1\right)$

$A9 = \mu_2 l_2 (\theta_2'' \cos\theta_2 \sin\phi_2 + \phi_2'' \sin\theta_2 \cos\phi_2 - \phi_2' \sin\theta_2 \sin\phi_2 - 2\theta_2'\phi_2' \sin\theta_2 \cos\phi_2 +$
$2\phi_2' \cos\theta_2 \cos\phi_2 - (\theta_2' + 1)^2 \sin\theta_2 \sin\phi_2 - 2B \sin\theta_2 \sin\phi_2 + 3C \sin\phi_2 (\hat{x}_p^2 + \hat{y}_p^2 + \hat{z}_p{}^2))$

$A10 = 2\mu_2 l_2 \cos\theta_2 (\phi_2' \cos\phi_2 + (\theta_2' + 1) \cos\theta_2 \sin\phi_2)$

$A11 = \mu_2 l_2 (\theta_2'' \sin\theta_2 \cos\phi_2 + \phi_2'' \cos\theta_2 * \sin\phi_2 + \phi_2'^2 \cos\theta_2 \cos\phi_2 - 2\theta_2'\phi_2' \cos\theta_2 \sin\phi_2 - 2\phi_2' \sin\theta_2 \sin\phi_2 +$
$(\theta_2' + 1)^2 \cos\theta_2 \cos\phi_2 + 2B \cos\theta_2 \cos\phi_2 - 3C(\hat{x}_p \sin\theta_2 \sin\phi_2 - \hat{y}_p \sin\theta_2 \cos\phi_2 - \hat{z}_p \sin\phi_2))$

$A12 = 2\mu_2 l_2 \cos\phi_2 \left((\phi_2' + \theta_2')\cos\theta_2 + \sin\theta_2\right)$

$$B1=3C(\mu_1 l_1 \sin\theta_1 \sin\phi_1 + \mu_2 l_2 \sin\theta_2 \sin\phi_2 - \hat{y}_p)$$

$$B2=-2$$

$$B3=-(B-1-3C(\hat{x}_p + \mu_1 l_1 \cos\theta_1 \sin\phi_1 + \mu_2 l_2 \cos\theta_2 \sin\phi_2))$$

$$B4=\mu_1 l_1 (\theta_1'' \sin\theta_1 \sin\phi_1 - \phi_1'' \cos\theta_1 \cos\phi_1 + \phi_1' \cos\theta_1 \sin\phi_1 + \theta_1'^2 \cos\theta_1 \sin\phi_1 + 2\theta_1'\phi_1' \sin\theta_1 \cos\phi_1$$
$$-B\cos\theta_1 \sin\phi_1 + 3Cl1\cos 2\theta_1 \sin\phi_1^2 + 3C(\hat{x}_p \cos\theta_1 \sin\phi_1 - \hat{y}_p \sin\theta_1 \sin\phi_1))$$

$$B5=\mu_1 l_1 (2((\theta_1'+1)\sin\theta_1 \sin\phi_1 - (\phi_1'+1)\cos\theta_1 \cos\phi_1))$$

$$B6=\mu_1 l_1 (\phi_1'' \sin\theta_1 \sin\phi_1 - \theta_1'' \cos\theta_1 \cos\phi_1 + \phi_1'^2 \sin\theta_1 \cos\phi_1 + \theta_1'^2 \sin\theta_1 \cos\phi_1 + 2\theta_1'\phi_1' \cos\theta_1 \sin\phi_1$$
$$-B\sin\theta_1 \cos\phi_1 + 3Cl1\sin 2\theta_1 \sin 2\phi_1 + 3C(\hat{x}_p \sin\theta_1 \cos\phi_1 + \hat{y}_p \cos\theta_1 \cos\phi_1))$$

$$B7=\mu_1 l_1 (2(\phi_1' \sin\theta_1 \sin\phi_1 + (\theta_1'+1)\cos\theta_1 \cos\phi_1))$$

$$B8=\mu_2 l_2 (\theta_2'' \sin\theta_2 \sin\phi_2 - \phi_2'' \cos\theta_2 \cos\phi_2 + \phi_2' \cos\theta_2 \sin\phi_2 + \theta_2'^2 \cos\theta_2 \sin\phi_2 + 2\theta_2'\phi_2' \sin\theta_2 \cos\phi_2$$
$$-B\cos\theta_2 \sin\phi_2 + 3Cl_2 \cos 2\theta_2 \sin\phi_2^2 + 3C(\hat{x}_p \cos\theta_2 \sin\phi_2 - \hat{y}_p \sin\theta_2 \sin\phi_2))$$

$$B9=\mu_2 l_2 (2((\theta_2'+1)\sin\theta_2 \sin\phi_2 - (\phi_2'+1)\cos\theta_2 \cos\phi_2))$$

$$B10=\mu_2 l_2 (\phi_2'' \sin\theta_2 \sin\phi_2 - \theta_2'' \cos\theta_2 \cos\phi_2 + \phi_2'^2 \sin\theta_2 \cos\phi_2 + \theta_2'^2 \sin\theta_2 \cos\phi_2 + 2\theta_2'\phi_2' \cos\theta_2 \sin\phi_2$$
$$-B\sin\theta_2 \cos\phi_2 + 3Cl2\sin 2\theta_2 \sin 2\phi_2 + 3C(\hat{x}_p \sin\theta_2 \cos\phi_2 + \hat{y}_p \cos\theta_2 \cos\phi_2))$$

$$B11=\mu_2 l_2 (2(\phi_2' \sin\theta_2 \sin\phi_2 + (\theta_2'+1)\cos\theta_2 \cos\phi_2))$$

$$C1=3C(\mu_1 l_1 \cos\phi_2 + \mu_2 l_2 \cos\phi_2 - \hat{z}_p)$$

$$C2=3C(\mu_1 l_1 \cos\theta_1 \sin\phi_2 + \mu_2 l_2 \cos\theta_2 \sin\phi_2 - \hat{x}_p) - B$$

$$C3=\mu_1 l_1 \left(\frac{3}{2} Cl_1 \sin\theta_1 \sin 2\phi_1 - \hat{z}_p \sin\theta_1 \sin\phi_1\right)$$

$$C4=\mu_1 l_1 (\phi_1'^2 \sin\phi_1 - 3C(\hat{x}_p \sin\phi_1 + \hat{z}_p \cos\theta_1 \cos\phi_1) + B\sin\phi_1 - 3Cl_1 \cos\theta_1 \cos 2\phi_1)$$

$$C5=2\mu_1 l_1 \phi_1' \cos\phi_1$$

$$C6=\mu_2 l_2 \left(\frac{3}{2} Cl_2 \sin\theta_2 \sin 2\phi_2 - \hat{z}_p \sin\theta_2 \sin\phi_2\right)$$

$$C7=\mu_2 l_2 (\phi_2'^2 \sin\phi_2 - 3C(\hat{x}_p \sin\phi_2 + \hat{z}_p \cos\theta_2 \cos\phi_2) + B\sin\phi_2 - 3Cl_2 \cos\theta_2 \cos 2\phi_2)$$

$$C8=2\mu_2 l_2 \phi_2' \cos\phi_2$$

$$D1 = \frac{9}{2} C \sin 2\theta_1 \sin \phi_1^2 + \frac{\sin \phi_2}{l_1} (3C(2\hat{x}_p \sin \theta_1 + \hat{y}_p \cos \theta_1) - (2B+1) \sin \theta_1)$$

$$D2 = \frac{-2 \cos \theta_1 \sin \phi_1}{l_1}$$

$$D3 = 3C \cos 2\theta_1 \sin \phi_1^2 - \frac{\sin \phi_1}{l_1} \left((B-1) \cos \theta_1 - 3C \left(\hat{x}_p \cos \theta_1 - \hat{y}_p \sin \theta_1 \right) \right)$$

$$D4 = \frac{-2 \sin \theta_1 \sin \phi_1}{l_1}$$

$$D5 = -3C \cos \phi_1 + \frac{\hat{z}_p \sin \theta_1 \sin \phi_1}{l_1}$$

$$D6 = \frac{\sin \phi_1}{l_1} (\hat{x}_p'' \cos \theta_1 + \hat{y}_p'' \sin \theta_1 - (2\hat{y}_p' + \hat{x}_p \cos \theta_1 + (2\hat{x}_p' + \hat{y}_p) \sin \theta_1 - B(2\hat{x}_p \cos \theta_1 - \hat{y}_p \sin \theta_1)$$
$$+ 3C(\cos \theta_1 (\hat{x}_p^2 - 0.5\hat{y}_p^2 - 0.5\hat{z}_p^2) - \hat{x}_p \hat{y}_p \sin \theta_1)) - 3 \sin \phi_1^2 ((B - 3C\hat{x}_p) \cos 2\theta_1 + 2\hat{y}_p C \sin 2\theta_1)$$

$$D7 = \phi_1' \sin 2\phi_1$$

$$D8 = \frac{\cos \phi_1}{l_1} (\hat{y}_p'' \cos \theta_1 - \hat{x}_p'' \sin \theta_1 + (2\hat{x}_p' - \hat{y}_p) \cos \theta_1 + (2\hat{y}_p' + \hat{x}_p) \sin \theta_1 + B(2\hat{x}_p \sin \theta_1 + \hat{y}_p \cos \theta_1)$$
$$- 3C(\sin \theta_1 (\hat{x}_p^2 - 0.5\hat{y}_p^2 - 0.5\hat{z}_p^2) + \hat{x}_p \hat{y}_p \cos \theta_1)) + 1.5 \sin 2\phi_1 ((B - 3C\hat{x}_p) \sin 2\theta_1 - 2C\hat{y}_p \cos 2\theta_1)$$
$$+ 3C\hat{z}_p \sin \phi_1 + \frac{\theta_1'' \sin 2\phi_1}{l_1}$$

$$D9 = (\theta_1' + 1) \sin 2\phi_1$$

$$E1=-\frac{9}{2}C\cos^2\theta_1\sin 2\phi_1+3C\hat{z}_p\sin\phi_1+\frac{\cos\phi_1}{l_1}((2B+1)\cos\theta_1+3C(2\hat{x}_p\cos\theta_1-\hat{y}_p\sin\theta_1))$$

$$E2=\frac{-2\sin\theta_1\cos\phi_1}{l_1}$$

$$E3=\frac{3}{2}C\sin 2\theta_1\sin 2\phi_1-\frac{\cos\phi_1}{l_1}((B-1)\sin\theta_1+3C(\hat{y}_p\cos\theta_1+\hat{x}_p\sin\theta_1))$$

$$E4=\frac{2\cos\theta_1\cos\phi_1}{l_1}$$

$$E5=3C\cos\theta_1\cos 2\phi_1+\sin\phi_1(B-3\hat{x}_pC)-\frac{\cos\phi_1}{l_1}(\hat{z}_p\cos\theta_1)$$

$$E6=-\frac{3}{2}(B-3C\hat{x}_p)\sin 2\theta_1\sin 2\phi_1+3C\left(\hat{y}_p\cos 2\theta_1\sin 2\phi_1-\hat{z}_p\sin\theta_1\cos 2\phi_1\right)-\frac{\cos\phi_1}{l_1}((2\hat{x}_p'-\hat{y}_p)\cos\theta_1$$
$$+(2\hat{y}_p'+\hat{x}_p)\sin\theta_1+B(2\hat{x}_p\sin\theta_1+\hat{y}_p\cos\theta_1)+3C(\sin\theta_1(\hat{x}_p{}^2-0.5\hat{y}_p{}^2-0.5\hat{z}_p{}^2)+\hat{x}_p\hat{y}_p\cos\theta_1)+\hat{x}_p''\sin\theta_1-\hat{y}_p''\cos$$

$$E7=(\theta_1'+1)\sin 2\phi_1$$

$$E8=(\theta_1'+1)^2\cos 2\phi_1+3(B-3C\hat{x}_p)\cos^2\theta_1\cos 2\phi_1+3C\hat{y}_p\sin 2\theta_1\cos 2\phi_1-6\hat{z}_pC\cos\theta_1\sin 2\phi_1+\hat{z}_p\cos\phi_1(B-3C\hat{x}_p)$$
$$+\frac{\sin\phi_1}{l_1}\left(\hat{x}_p''\cos\theta_1+\hat{y}_p''\sin\theta_1+(2\hat{x}_p'-\hat{y}_p)\sin\theta_1-(2\hat{y}_p'+\hat{x}_p)\cos\theta_1-B(2\hat{x}_p\cos\theta_1-\hat{y}_p\sin\theta_1\right)$$
$$-3C\left(\cos\theta_1(\hat{x}_p{}^2-0.5\hat{y}_p{}^2-0.5\hat{z}_p{}^2)-\hat{x}_p\hat{y}_p\sin\theta_1\right)+\frac{\hat{z}_p''\cos\phi_1}{l_1}$$

$$F1 = 4.5C\sin 2\theta_2 \sin^2\phi_2 + \frac{\sin\phi_2}{l_2}(3C(2\hat{x}_p \sin\theta_2 + \hat{y}_p \cos\theta_2) - (2B+1)\sin\theta_2)$$

$$F2 = \frac{-2\cos\theta_2 \sin\phi_2}{l_2}$$

$$F3 = 3C\cos 2\theta_2 \sin^2\phi_2 - \frac{\sin\phi_2}{l_2}((B-1)\cos\theta_2 + 3C(-\hat{x}_p\cos\theta_2 + \hat{y}_p\sin\theta_2))$$

$$F4 = \frac{-2\sin\theta_2 \sin\phi_2}{l_2}$$

$$F5 = -3C\cos\phi_2 + \frac{\hat{z}_p \sin\theta_2 \sin\phi_2}{l_2}$$

$$F6 = \frac{\sin\phi_2}{l_2}(\hat{x}_p''\cos\theta_2 + \hat{y}_p''\sin\theta_2 - (2\hat{y}_p' + \hat{x}_p)\cos\theta_2 + (2\hat{x}_p' + \hat{y}_p)\sin\theta_2 - B(2\hat{x}_p\cos\theta_2 - \hat{y}_p\sin\theta_2)$$
$$+3C(\cos\theta_2(\hat{x}_p{}^2 - 0.5\hat{y}_p{}^2 - 0.5\hat{z}_p{}^2) - \hat{x}_p\hat{y}_p\sin\theta_2)) - 3\sin^2\phi_2((B - 3C\hat{x}_p)\cos 2\theta_2 + 2\hat{y}_p C\sin 2\theta_2)$$

$$F7 = \phi_2'\sin 2\phi_2$$

$$F8 = \frac{\cos\phi_2}{l_2}(\hat{y}_p''\cos\theta_2 - \hat{x}_p''\sin\theta_2 + (2\hat{x}_p' - \hat{y}_p)\cos\theta_2 + (2\hat{y}_p' + \hat{x}_p)\sin\theta_2 + B(2\hat{x}_p\sin\theta_2 + \hat{y}_p\cos\theta_2)$$
$$-3C(\sin\theta_2(\hat{x}_p{}^2 - 0.5\hat{y}_p{}^2 - 0.5\hat{z}_p{}^2) + \hat{x}_p\hat{y}_p\cos\theta_2)) + \frac{3}{2}\sin 2\phi_2((B - 3C\hat{x}_p)\sin 2\theta_2 - 2C\hat{y}_p\cos 2\theta_2)$$
$$+3C\hat{z}_p\sin\phi_2 + \frac{\theta_2''\sin 2\phi_2}{l_2}$$

$$F9 = (\theta_2' + 1)\sin 2\phi_2$$

$$G1=-4.5C\cos^2\theta_2 \sin 2\phi_2 + 3C\hat{z}_p \sin\phi_2 + \frac{\cos\phi_2}{l_2}((2B+1)\cos\theta_2 + 3C(2\hat{x}_p \cos\theta_2 - \hat{y}_p \sin\theta_2))$$

$$G2=\frac{-2\sin\theta_2 \cos\phi_2}{l_2}$$

$$G3=\frac{3}{2}C\sin 2\theta_2 \sin 2\phi_2 - \frac{\cos\phi_2}{l_2}((B-1)\sin\theta_2 + 3C(\hat{y}_p \cos\theta_2 + \hat{x}_p \sin\theta_2))$$

$$G4=\frac{2\cos\theta_2 \cos\phi_2}{l_2}$$

$$G5=3C\cos\theta_2 \cos 2\phi_2 + \sin\phi_2 (B-3C\hat{x}_p) - \frac{\cos\phi_2}{l_2}(\hat{z}_p \cos\theta_2)$$

$$\begin{aligned}G6=&-\frac{3}{2}(B-3C\hat{x}_p)\sin 2\theta_2 \sin 2\phi_2 + 3\hat{y}_p C\cos 2\theta_2 \sin 2\phi_2 - 3\hat{z}_p C\sin\theta_2 \cos 2\phi_2 - \frac{\cos\phi_2}{l_2}((2\hat{x}_p' - \hat{y}_p)\cos\theta_2 \\ &+(2\hat{y}_p' + \hat{x}_p)\sin\theta_2 + B(2\hat{x}_p \sin\theta_2 + \hat{y}_p \cos\theta_2) + 3C(\sin\theta_2(\hat{x}_p^2 - 0.5\hat{y}_p^2 - 0.5\hat{z}_p^2) + \hat{x}_p\hat{y}_p \cos\theta_2) \\ &+\hat{x}_p'' \sin\theta_2 - \hat{y}_p'' \cos\theta_2)\end{aligned}$$

$$G7=(\theta_2'+1)\sin 2\phi_2$$

$$\begin{aligned}G8=&(\theta_2'+1)^2 \cos 2\phi_2 + 3(B-3C\hat{x}_p)\cos^2\theta_2 \cos 2\phi_2 + 3C\hat{y}_p \sin 2\theta_2 \cos 2\phi_2 - 6C\hat{z}_p \cos\theta_2 \sin 2\phi_2 + \hat{z}_p \cos\phi_2 (B-3C\hat{x} \\ &+\frac{\sin\phi_2}{l_2}(\hat{x}_p'' \cos\theta_2 + \hat{y}_p'' \sin\theta_2 + (2\hat{x}_p' - \hat{y}_p)\sin\theta_2 - (2\hat{y}_p' + \hat{x}_p)\cos\theta_2 - B(2\hat{x}_p \cos\theta_2 - \hat{y}_p \sin\theta_2) \\ &-3C(\cos\theta_2(\hat{x}_p^2 - 0.5\hat{y}_p^2 - 0.5\hat{z}_p^2) - \hat{x}_p\hat{y}_p \sin\theta_2)) + \frac{\hat{z}_p'' \cos\phi_2}{l_2}\end{aligned}$$

Using the information given above, the control system can generate $\hat{\mathbf{A}}$ and $\hat{\mathbf{B}}$ using the most recent state vector $\mathbf{q}$, hence getting the required starting point for the LQR method.

References

[1] COSMO, M. and LORENZINI, E., "Tethers in Space Handbook", Cambridge, Massachusetts, 3rd ed., 1997, prepared for NASA/MSFC by Smithsonian Astrophysical Observatory, pp. 36-60

[2] Farley, R. and Quinn, D,. "Tethered Formation Configurations: Meeting The Scientific Objectives of Large Aperture and Interferometric Science", *2001 AIAA Proceedings*, 2001-4770

[3] MOULTON, F.R., "Periodic Orbits", Carnegie Institution of Washington Publications, No 161, Washington, 1920.

[4] POINCARE, H. "Les Methodes Nouvelles de la Mecanique Celeste", Vol 1, 1892; "New Methods of Celestial Mechanics (English Translation)", Vol 13, *History of Modern Physics and Astronomy*, American Institute of Physics, 1993

[5] Clarke, A.C., " The World Behind the Moon", *The Journal of the Astronautical Sciences*, Vol 49, No. 1, January-March 2001, pp.11-22

[6] COLOMBO, G., "The Stabilization of an Artificial Satellite at the Inferior Conjunction Point of the Earth-Moon system", *Smithsonian Astrophysical Observatory Special Report*, No 80, November 1961.

[7] HOWELL, K.C. and FARQUHAR, R.W., " John Breakwell, The Restricted Problem, and Halo orbits", *Acta Astronautica*, Vol 29, No.6, 1993, pp. 485-488

[8] FARQUHAR, R.W., " The Control and Use of Libration-Point Satellites", *NASA TR R-346*, September 1970

[9] HOWELL, K.C., "Families of Orbits in the Vicinity of the Collinear Libration Points", *The Journal of the Astronautical Sciences*, Vol 49, No. 1, January-March 2001, pp. 107-125

[10] HOWELL, K.C and PERNICKA, H J., "Numerical Determination of Lissajous Trajectories in the Restricted Three Body Problem", *Celestial Mechanics*, Vol 41, Nos 1-1988, pp. 107-124.

[11] CIELASZYK, D., and WIE, B., "A New Approach to Halo Orbit Determination and Control", *Journal of Guidance, Control and Dynamics*, Vol. 19, No.2, 1996, pp. 266-273

[12] FARQUHAR, R.W., " The Flight of ISEE-3/ICE: Origins, Mission History, and a Legacy", *The Journal of the Astronautical Sciences*, Vol 49, No. 1, January-March 2001, pp. 23-73

[13] TSURUTANI, B.T, RODRIGUEZ, P. "Upstream Waves and Particles: An Overview of ISEE Results", *Journal of Geophysical Research*, Vol 86, No A6, June 1, 1981, pp. 4319-4324

[14] DOMINGO et al. "The SOHO Mission: An Overview", *Solar Physics*, Vol 162, No. 1-2, December 1995, pp. 1-37

[15] RUSSELL, C.T., NEWALDT, R.A., and Von ROSENVINGE, T.T., "The Advanced Composition Explorer Mission", *Space Science Reviews*, Vol 86, No 1-4, 1998 (Kluwer Academic Pub., Dordrencht , Netherlands).

[16] LO, M., "Genesis Mission Design", *The Journal of the Astronautical Sciences*, Vol 49, No. 1, January-March 2001, pp.169-184

[17] BURNETT, D. "The Genesis Mission: Catching Pieces of the Sun", *The Planetary Report*, Vol 18, No.2, March/April 1998, pp. 12-15

[18] RICHARDSON, D.L., "Halo-Orbit Formulation for the ISEE-3 Mission", *Journal of Guidance and Control*, Vol 3, No 6, November –December 1980, pp. 543-548.

[19] DUNHAM, D. and ROBERTS, G., "Stationkeeping Techniques for Libration Point Satellites", *The Journal of the Astronautical Sciences*, Vol 49, No. 1, January-March 2001, pp.127-144

[20] FARQUHAR, R.W., "Tether Stabilization at a Collinear Libration Point", *The Journal of the Astronautical Sciences*, Vol 49, No. 1, January-March 2001, pp.91-96

[21] GATES, S., "Multi-Tethered Space-Based Interferometers: Particle System Model", *Naval Research Laboratory Report NRL/MR/8231—01-8579*, Sept 2000

[22] Kim, M. and Hall, C.D., "Control of a Rotating Variable-Length Tethered System", 13th AAS/AIAA Space Flight Mechanics Meeting, Ponce, Puerto Rico, 9-13 February 2003

[23] MISRA, A.K, and BELLEROSE, J., "Dynamics of a Tethered System Near the Earth-Moon Lagrangian Point", *Advances in Astronomical Sciences*, Vol 109, Part 2, 2001 pp. 415-435.

[24] WIE, BONG., " Space Vehicle Dynamics and Control", AIAA Education Series, pp.250